On Mimicking Nano-particulate Behaviors of Asphaltenes in Solution and at Interfaces

by

Jeoffrey Ollinger

A thesis submitted in partial fulfillment of the requirements for the degree of

Master of Science

in

Chemical Engineering

Department of Chemical and Materials Engineering
University of Alberta

Abstract

The nature and structure of asphaltene nanoaggregates are frequently the subject of debate and speculation in the literature. The continental asphaltene nano-aggregate model, characterized by the presence of alkyl chains on their surface, and the archipelago nano-aggregate model, characterized by a diverse mix of functionalities on their outer surfaces, co-exist. In this work, these two prototypical asphaltene nanoaggregate models are probed using neutral gold-core nanoparticles with alkyl, aromatic, and alkanol functionalities on their surfaces. The nanoparticles are synthesized and characterized as part of this work. Their enthalpies of solution, and interfacial tensions reflect interactions between the organic ligands on their surface and the surrounding media. The measured values are compared with the corresponding values for Athabasca pentane asphaltenes. The solution calorimetry of asphaltenes is qualitatively represented by the gold-alkyl nanoparticles. The interfacial tension values are qualitatively represented by the gold-aromatic nanoparticles. Quantitative comparisons are precluded because the number and nature of interaction sites on asphaltene aggregates, and the possible impact of asphaltene aggregate solubility on measurements are unknown. From this preliminary exploratory study, it is clear that to mimic the behaviors of asphaltenes in solution and at interfaces, a mix of ligands on nanoparticle surfaces is required with alkyl ligands playing a primary role, and aromatic ligands playing a secondary role. N-alkanol ligands do not appear to play a significant role. The outcomes of this work support both the continental and archipelago asphaltene nanoaggregate models, and a number of lines of inquiry for future work are suggested. For example, it is not clear whether the best gold-ligand mimics for asphaltenes comprise mixes of particles with different ligands or individual particles with multiple ligands, and other

ligand types remain to be explored. Nanopaticle synthesis will pose significant challenges for these future works.

Acknowledgements

I thank my supervisor, Dr John M. Shaw, for the patience and optimism he provided during the many setbacks we encountered in the realization of this project. I am indebted to Dr Jennifer Shumaker-Parry and her group at the University of Utah, especially Mr. Art Quast. Their help with nanoparticle synthesis was key to the completion of this thesis.

I am very grateful to Ms. Mildred Becerra and Ms. Linda Kaert, who provided so much help in the laboratory and with university matters.

I thank Dr. Hongbo Zeng, for letting us use his IFT facility and Dr Mohammad Reza Poopari for his help in the process. Also, My sincere thanks to Dr. Anqiang He and Dr. Dimitre Karpuzov from the University of Alberta NANOFAB for their help with particle characterization.

I also thank all of my colleagues, especially Amin Pourmohammadbagher for his help with nanoparticles synthesis and calorimetric measurements and Bobby Uyanwune and Ramanish Singh for their help with IFT measurements.

I owe my deepest gratitude to my parents and siblings for their love and support, without which I would have never found the strength to pursue this work.

TABLE OF CONTENTS

List of figures

List of Tables

Nomenclature

$(Et_3P)AuCl$	Chlorotriethylphosphine Gold(I)
$(PPh_3)AuCl$	Chlorotriphenylphosphine Gold(I)
9-BBN	9-Borabicyclo[3.3.1]nonane
Amu	Atomic Mass Unit
BTB	Borane Tert-Butylamine
C_p	Heat Capacity at constant pressure
CVD	Chemical Vapor deposition
DIW	Deionized water
EDX	Energy-Dispersive X-Ray spectroscopy
FTICR-MS	Fourier Transform Ion Cyclotron Resonance Mass Spectrometry
FTIR	Fourier Transform Infrared Spectroscopy
G	Standard gravity 9.82 m/s^2
Gold-Ar	Gold nanoparticles synthesized with biphenyl-4-thiol
Gold-C_{12}	Gold nanoparticles synthesized with dodecanethiol
Gold-C_8	Gold nanoparticles synthesized with octanethiol
Gold-OH	Gold nanoparticles synthesized with 11 mercapto 1 undecanol
Gold-TPP	Gold nanoparticles synthesized with Triphenylphosphine
$H(AuCl_4)$	Chloroauric acid
Heptol x/y	Volumic mixture of x (heptane) to y (toluene)
HPLC grade	High Pressure Liquid Chromotagraphy
ICP-Ms	Inductively Coupled Plasma Mass Spectrometry
IFT	Interfacial tension
M	Mass in kg

$NaBH_4$	Sodium Borohydride
NMR	Nuclear magnetic resonance
R	Radius in m
S/TEM	Scanning Transmission Electron Microscopy
SANS	Small-Angle Neutron Scattering
SAXS	Small-Angle X-Ray Scattering
TEM	Transmission Electron Microscopy
THF	Tetrahydrofuran
TOA	TriOctylAmine
TOAB	TetraOctylAmmonium Bromide
TPP	Triphenylphosphine
Uv-Vis	Ultraviolet-Visible Spectroscopy
XANES	X-Ray Absorption Near End Structure
XPS	X-Ray Photoelectron Spectroscopy
B	Shape factor used by the IFT apparatus
Γ	Interfacial tension in mN/m
P	Density in kg/m^3

Chapter 1: Introduction

1.1 What are asphaltenes?

Asphaltenes are a poorly defined class of self-assembling and surface active molecules present in crude oils. Their mass fraction in light and conventional oils is low but numerous production, transport and refining problems from plugging to catalyst deactivation are attributed to them. The worst problems appear to be associated with crudes with only trace asphaltene contents. The Asphaltene fraction of heavy oils and bitumen can exceed 20% of the total crude [1.1] and for these materials, extraction of the economic value of this significant fraction of the resources is a priority because asphaltenes do not appear to pose significant production problems despite their higher mass fraction. For heavy oils, asphaltenes pose refining challenges (deasphalting) and equipment fouling problems. The number of asphaltenes-related papers published every year keeps increasing [1.2]. Asphaltenes are responsible for the high viscosity of heavy oil and bitumen [1.3], [1.4] and they play an important role in the stabilization of water in crude oil emulsions [1.5], [1.6]. Their tendency to self-aggregate and to adsorb on surfaces are issues in all production [1.7] and refining processes. The change in pressure that occurs during the depletion of reservoirs can lead to asphaltene flocculation and deposition, which can trigger obstruction in wells or reservoir rock [1.8]. Flocculation and deposition also arise in pipelines [1.9] and during refining [1.10]. The technical uncertainties and economic risks associated with asphaltenes remain significant.

Basic properties, such as the mean molar mass and representative molecular structure(s) of this class of molecules continue to be debated in the literature. For example, different methods provide contrasting results with the same sample for mean asphaltene aggregate size – from 1000 to 100000 amu [1.11] Mean molecular mass ranges are equally broad- from 400 to more than 1500 amu in recent publications [1.12] [1.13]. In addition to variations by method of measurement, results, such as their mass fraction and elemental composition, vary depending on the provenance and even the preparation of asphaltenes from the same samples. Illustrative elemental compositions

for Athabasca bitumen and asphaltenes obtained from this resource are shown in Table 1. Asphaltenes comprise carbon and hydrogen, and tend to be enriched in heteroatomic species (Oxygen, Nitrogen, Sulfur, Nickel and Vanadium relative to the parent resource) [1.14], [1.15].

Table 1.1 Chemical analysis of Athabasca bitumen and its asphaltene content [1.15][1] [1.16][2].

	Bitumen	**Asphaltenes**
C(wt%)[1]	82.8	80.7
H(wt%)[1]	10.4	8
N(wt%)[1]	1.6	1
S(wt%)[1]	4.8	8.3
O(wt%)[1]	1.8	2.1
H/C (atomic)[1]	1.5	1.2
Fraction(wt%)[1]	-	15.59
Aromaticity(%)[2]	-	37% of carbon 8% of hydrogen

Classic experimental characterization techniques such as UV-Vis or FTIR underscore the presence of aromatics rings in the asphaltenes molecules, along with alkanes chains, and the presence of S, N, O substituted groups [1.15]. FTICR-MS provides additional detail regarding the elemental composition and molar mass of asphaltenes [1.17] [1.18]. Naphthenic motifs would appear to be missed in typical analyses [1.19]. Two contrasting average molecular models continue to coexist in the literature for the description of the principal structures of asphaltene molecules. A representation of the “island” or ‘’continental” structure vs the “archipelago” structure is shown in Figure 1.1.

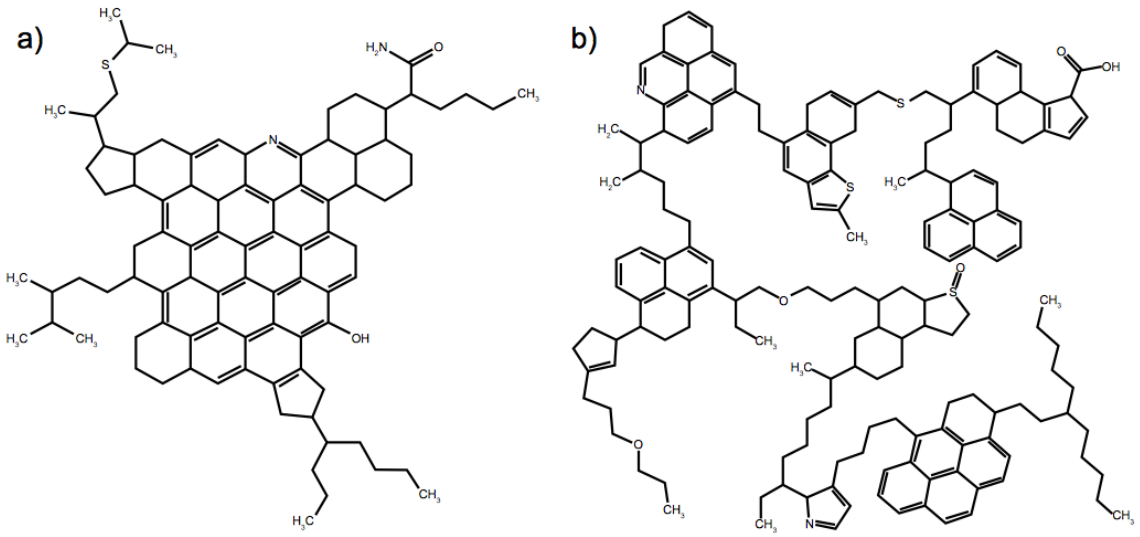

Figure 1.1: a) Continental/Island model for asphaltenes structure b) Archipelago model [1.20].

The differences between these average molecular prototypes are important because, perceived reaction chemistries during refining and perceived aggregation mechanisms differ greatly. For the island model, aggregation would appear to be driven by Pi-Pi stacking interactions complimented by steric repulsion. For the archipelago model, the spatial mix of attractive and repulsive interactions would be due to the presence of heteroatom interactions, hydrogen bonding and possibly entanglement. The literature continues to be split with evidence pointing toward the island structural model [1.21], especially Laser Desorption Ionization Mass Spectrometry [1.22] and time-resolved fluorescence depletion measurements [1.23]. Theoretical considerations [1.24] and experimental work related to the pyrolysis and coking of asphaltenes [1.25] identify small alkane and aromatic motifs that underscore the presence of molecules with an archipelago structure. Ongoing development and improvements to the FTICR-MS technique are contributing to this debate as new classes and subclasses of compounds are identified [1.26].

Irrespective of the perspective one has on the average nature/structure/size of asphaltene molecules, they do form small and tightly bound aggregates at ppm level concentrations (50 to 200mg/L) in solvents including toluene [1.27], [1.28]. Small angle X-Ray scattering (SAXS) and small angle neutron scattering (SANS) [1.29], [1.30]

indicate that 2 nm aggregates that by definition comprise a few molecules are present at these low concentrations.

As with average molecule structure, the literature on nanoaggregation is also split. From the island molecular model literature, the reasons asphaltenes aggregate, is the attractive Pi-Pi stacking of aromatics cores. Aggregation is limited by the repulsion of aliphatic chains [1.31]. The size of this nanoaggregates and the aggregation numbers were first predicted by Yen and then revisited by Mullins et al. [1.21], [1.23]. Figure 1.2 presents an overview of the island aggregation scheme where molecules form nanoaggregates, and nanoaggregates form "flocs" or clusters at higher concentrations depending on the details of the surrounding medium [1.32] [1.33], [1.34]. Clusters tend to form at the 1 to 10 g/L concentration level and 4 nm to 30 nm diameters have been reported [1.35], [1.36]. For the island model the distinction between nanoaggregates and clusters is important because the chemistry and kinetics of flocculation are not governed by the same phenomena as the formation of nanoaggregates [1.37]. At low concentration, a diffusion-limited aggregation that supposes pure attraction between the particles is assumed. At higher asphaltenes concentration, a reaction-limited aggregation is anticipated which implies a change in the external structures of clusters. The mechanism of aggregation proposed by the Yen-Model relies on attraction between aromatic motifs balanced by repulsion between alkanes chains. While the presence of Pi-Pi stacking interaction and steric repulsion is acknowledged broadly in the literature, their relative importance is debated.

For the Archipelago model, the mechanisms for nanoaggregation are not well defined but it is thought that heteroatoms and the diversity of the molecular structures present permit aggregation among molecules [1.38]. For example, a supramolecular assembly model proposed by Gray et al. [1.39] indicates the importance of acid-base interactions, metal complexes and hydrogen bonding. This model arose in order to explain the surface activity and the porosity of aggregates. A scheme can be found in Figure 1.3. The distinction between nanoaggregation and flocculation is not delineated within this modeling framework.

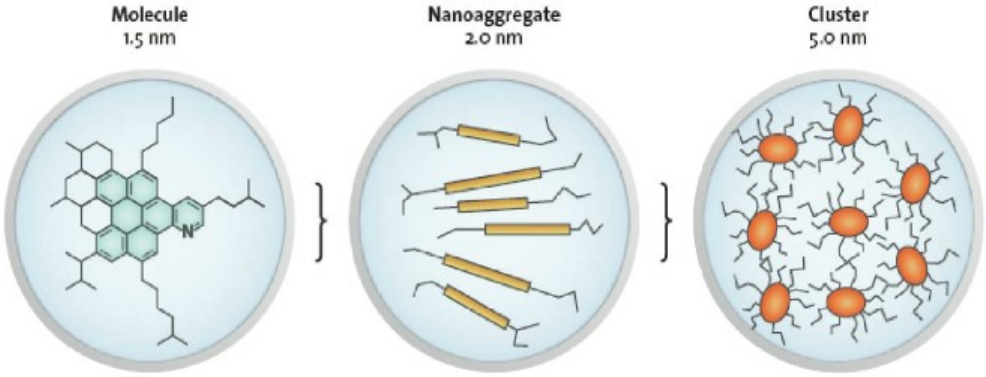

Figure 1.2: The modified Yen-Mullins model [1.23]

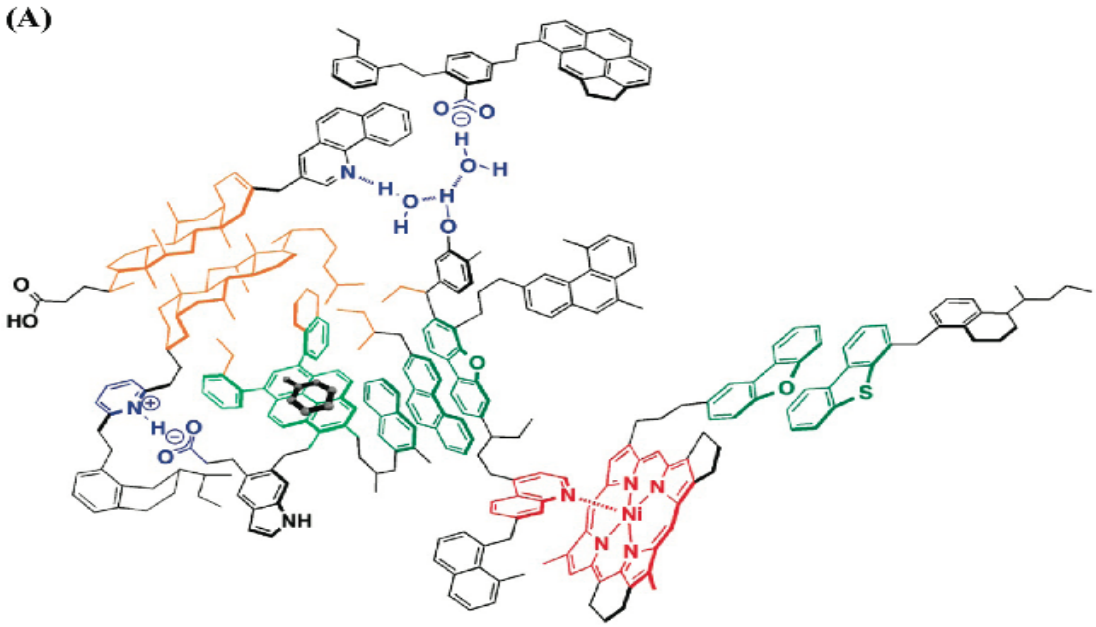

Figure 1.3: Supramolecular assembly for asphaltenes molecules. Metal complex (Red), Pi-PI stacking (green and grey), Hydrogen bonding (blue), Hydrophobic pocket (Yellow) [1.39].

The link between either of these aggregation mechanisms and triggers that lead to the formation of flocs and deposits is unclear. Pressure or temperature variations or variations of the local chemical composition in the crude oil alter the stability of asphaltenes nanoaggregates and affect aggregation kinetics [1.40], [1.41] in certain parts of the phase diagram. At pressures near the bubble pressure, fluids are prone to flocculation [1.42], [1.43]. The reverse process, disaggregation of flocs, or large aggregates is also a subject of debate [1.44], with data suggesting that partial reversibility adjacent to conditions where flocs form is possible [1.45] but the use of chemical

treatments is frequently found to be necessary [1.46]. An easy and inexpensive way to disperse asphaltene flocs would be of tremendous help for the oil industry.

1.2 Thesis Objectives and overview

From this brief overview, it is clear that there is tremendous uncertainty related to the fundamental properties and behaviors of asphaltenes as molecules and nanoaggregates, and with respect to the propagation and termination mechanisms leading to cluster and floc formation in particular. Only one part of this uncertainty is addressed in this work. The details of the internal structure and composition of nanoaggregates formed at low concentration are hypothesized to be irrelevant to cluster/floc formation. Interactions among nanoaggregates are hypothesized to be dictated by molecular motifs at or protruding from nanoaggregate surfaces. Simple physical models for asphaltene nanoaggregates comprising gold nanoparticles to which alkyl, primary alcohol, and alkyl aromatic organic ligands are attached are prepared. Their solution calorimetry and interfacial properties in diverse solvents and at diverse interfaces are then compared with the properties of asphaltenes both qualitatively and quantitatively to shed light on the surface properties of asphaltene nanoaggregates and hence on probable cluster and floc formation mechanisms and on their interfacial behavior. The objective of the work is to identify a robust mimic for asphaltene behavior based on these nanoparticles.

The balance of the thesis comprises:

Chapter 2 - a literature review that justifies the selection of potential nanoparticle mimics. The solution calorimetry of asphaltenes in specific solvents, and the interfacial tensions of asphaltenes at diverse interfaces, is also reviewed.

Chapter 3 - the recipes for the synthesis of gold-based nanoparticles. These recipes can be deceptively difficult to apply in practice, and a collaborative approach was adopted to prepare some of them. Experimental setups used to compare the behaviors of asphaltenes and the functionalized gold nanoparticles are also described.

Chapter 4 – the characterization results for the gold core nanoparticles, including their size and surface composition. The solution calorimetric and interfacial tension data for asphaltenes and gold core nanoparticles are also presented and discussed.

Chapter 5 – key findings, perspectives gained, and potential future work are presented.

Chapter 2: Literature Review

Asphaltenes, the most polar and aromatic components of crude oil self-associate, form aggregates and the aggregates floc. Floc formation depends on asphaltene concentration, the composition of the surrounding medium and temperature and pressure. Therefore the study of asphaltenes aggregates is important, the most interesting part being the study of their surface properties in order to understand what phenomena lead to flocculation and how aggregates or flocs stabilize water in oil emulsions. For this reason, colloids covered with molecular scale ligands possessing a specific functional group that is expected to be present on asphaltene aggregate surfaces were synthesized and their properties measured and compared with those of asphaltenes in this work. Such selectivity is a promising way to isolate key properties and interactions among the many possible interactions that may be present in asphaltene + diluent mixtures and by extension in live oil mixtures. The colloids chosen are functionalized gold nanoparticles. As the synthesis and functionalization of these nanoparticles are the first steps, background on nanoscience and nanoparticles are briefly reviewed along with pertinent literature on colloid behaviors at liquid-liquid interfaces, and their enthalpic interactions with solvents. Asphaltene behaviors in comparable environments are also reviewed.

2.1 Nanoscience and nanoparticles

2.1.1 Introduction

Nanoparticle science is a recent and explosively active field of physics, based on peer-reviewed publication and patent activity (Figure 2.1)[2.1]. Nanoparticles are ultra small particles of arbitrary shape with a leading dimension less than ~ 100 nm. Due to their size, they possess very large surface area to volume ratios. For example, the surface to volume ratio of a sphere is proportional to $\frac{M}{R}$ where M the mass of the sphere, and R is the radius. 1kg of 1mm nanoparticles possesses the same surface area as 5 mg of 5 nm particles. Quantum effects are often more important than Newtonian mechanics effects

[2.2]. Interactions between particles are not dictated by gravitational effects, but by electromagnetic interactions, Van der Waals forces and other interactions commonly associated with molecules. The most well-known quantum effect is called surface plasmon resonance [2.3]. It can be described as the excitation of the electron cloud of the nanoparticles by phonons of a wavelength larger than the size of this nanoparticle. This results in a peak for absorption at certain wavelengths. For instance 5 nm gold nanoparticles are typically red under visible light and UV-visible spectroscopy can therefore be used to check their approximate size rapidly. Other sizes and shapes lead to other colors because the wavelengths absorbed are not the same [2.4]. This optical effect is now used in the field of biosensing [2.5].

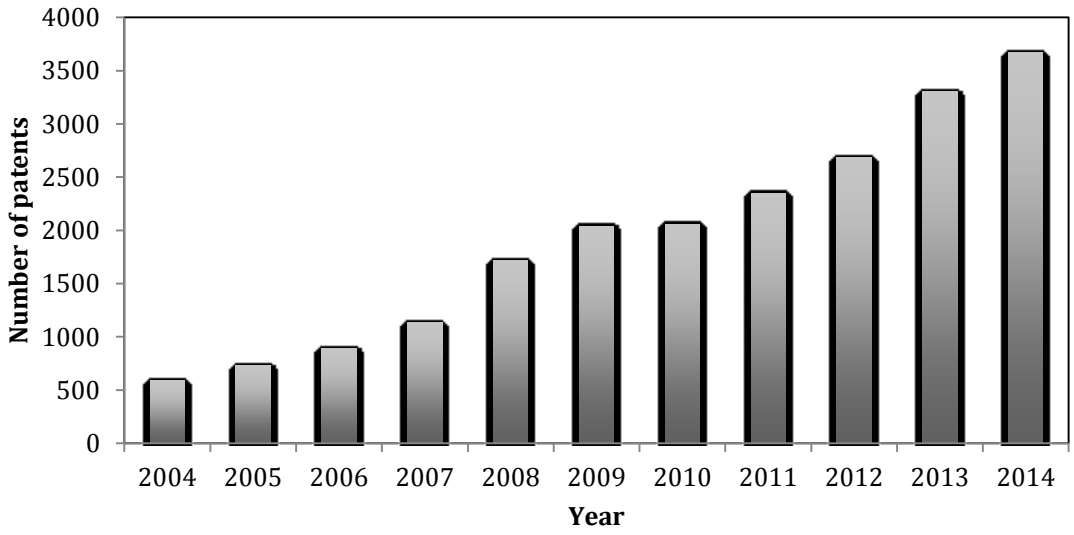

Figure 2.1: Number of patents published per year using Web of Science with the key words patent and nanoparticles [2.1].

As a lot of nanoparticles are made with metals, like aluminum or copper, an increase in the thermal conductivity of nanofluids that contain them is expected [2.6] and heat transfer between liquid + nanoparticles mixtures and other surfaces is posited to be higher than for a liquid. If true, micro-devices for heat transfer could be made for application in nuclear power systems, space exploration and electronic cooling [2.7] to cite a few examples. However, such effects are frequently exaggerated [2.8] and the need for new studies and the development of new models in this area has been underscored [2.5], [2.9].

Particle size also plays a role in electrical conductivity. Bulk carbon is an insulator, but the opposite has been found for carbon nanotubes, where the properties of helicity and purity can turn carbon into a semiconductor/conductor [2.10] or even attain supraconductivity [2.11]. Metals are usually conductors due to their cloud of free electrons but the phenomenon of quantum confinement in small nanoparticles (<10 nm) is today used to create nano semiconductors [2.12]. Based on these new properties, the creation of solar cells with a broad range of wavelength absorption can be made by controlling the size and the shape of the nanoparticles [2.13].

These applications would not have been identified without particle synthesis methods that permit the control of the size, shape and surface properties of nanoparticles. Nano sized objects can be created by mechanical milling [2.14], where a macroscopic or microscopic powder is added into a high-energy mill and reduced to nano size objects under plastic deformation. Rotation speed, temperature and the Young's modulus impact the size and shape of the materials produced by this method. With this approach it is often hard to have good dispersity and size control for the particles and additional processes are needed to obtain particles with narrowly defined properties [2.15]. A Bottom-up Approach is more common for the synthesis of nanoparticles on a small scale, particularly where greater control on particle size and functionalization is needed. For instance, chemical vapor deposition (CVD) can be used to create nanoparticles or nanofilms [2.6]. Another method is the chemical reduction of a metallic salt, delivering metallic ions in solution. Once reduced, the metallic ion can encounter other atoms and form nano-crystals [2.17]. Depending on the nature of the nanoparticles, different strategies to stop the growth of nanoparticles can be adopted. The main advantage of the Bottom-up approach is better control over different parameters of the nanoparticles and this approach was adopted for the present study even though it is both technically challenging and expensive to apply, and only small batches of particles can be prepared at a time.

2.1.2 Gold nanoparticles

Electrically neutral gold core nanoparticles were chosen as a base to explore and mimic the surface and solution properties of asphaltene aggregates. The most ancient known example of the application of gold nanoparticles is found in the famous Lycurgus cup, dated from the 4th century CE. The red color of this glass was only explained by Faraday [2.18] in 1857 and today is understood through the principle of surface Plasmon resonance. Even if the synthesis of gold colloids is ancient, significant effort has gone into understanding how to control all the aspects of the preparation process. Scalability, shape, size, polydispersity, lifetime and stability in different solvents are just some of the details that must be mastered when it comes to the synthesis of gold nanoparticles. Even though detailed "recipes" and procedures are available in the literature, aspects of the preparation work continue to rely on artisanal like understanding to ensure consistent outcomes. It is for this reason that in the completion of this work assistance was sought from Prof. Jennifer Shumaker-Perry at the University of Utah. She and her research team are experts in preparation of functionalized gold nanoparticles.

The most common approach for gold colloid synthesis is the bottom-up approach where a reducing agent is used to separate gold atoms salts. Some examples of these salts are shown in Figure 2.2.

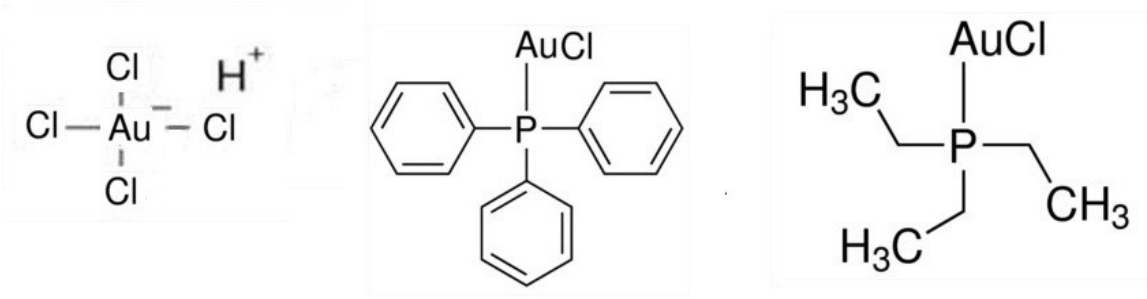

Figure 2.2: Example of gold Salts. *Left*: $H(AuCl_4)$ oxidation state of gold III *Center:* $P(Ph_3)AuCl$ oxidation state of gold I *Right:* $(Et_3P)AuCl$ oxidation state gold I

The release of Au3+ ions into a solution is believed to be followed first by reduction to Au+ ions by the reducing agent. Then a disproportionation reaction between 3 Au+ ions occurs, releasing one Au3+ and two Au(0) that become the sources for the

growth of the particles [2.19]. Further growth of the particles is pursued by disproportionation reaction of Au+ ions on the surfaces of the particles. The first step does not occur if the natural state of oxidation of the gold atom in the salt is already one, and the quantity of the reducing agent must be reduced to obtain the same nanoparticle outcomes. The Au atoms act as seeds for the growth of nanoparticles. Therefore, the reducing agent power has a direct impact on the rate of the reaction and the properties of nanoparticles produced as it controls the number of seeds present. Once the nucleation of the particles has started, the challenge is to control and to stop their growth, which determines their final mean size and the size distribution.

The Turkevish/Frens method [2.20], [2.21], also known as the citrate process, was the first method used to create gold nanoparticles in water. In this method, H[AuCl4] is mixed with Sodium citrate in distilled water. The ratio between these two reagents determines the size and the polydispersity of the colloids produced [2.22]. The electromagnetic forces around the particles halt their growth. Indeed, the weak interaction between citrate and the particles creates a charged surface that will lead, according to the Stern theory, to an ionic double layer that prevents further aggregation. The schematic of these layers is presented in Figure 2.3.

Synthetizing nanoparticles in organic solvents present other challenges. The most well known method is the one of Brust [2.23], where the reducing agent NaBH4 is mixed with chlorauric acid $H[AuCl_4]$ in water. Tetraoctylammonium bromide (TOAB) is a phase transfer agent and a weak stabilizer that allows particles to migrate into the added toluene phase. Once transferred, a strongly binding stabilizer, typically a thiol, is necessary to prevent the gold nanoparticles from combining. The bond nature between gold and sulfur is quite complex and is considered to be covalent and electrostatic [2.24] with a negative energy of formation [2.25]. Competition between growth of nanoparticles and the absorption of thiol impacts the final size of particles, by preventing further growth. Compounds with thiol groups are used as a basis for the creation of stable functionalized gold nanoparticles of nominally fixed size.

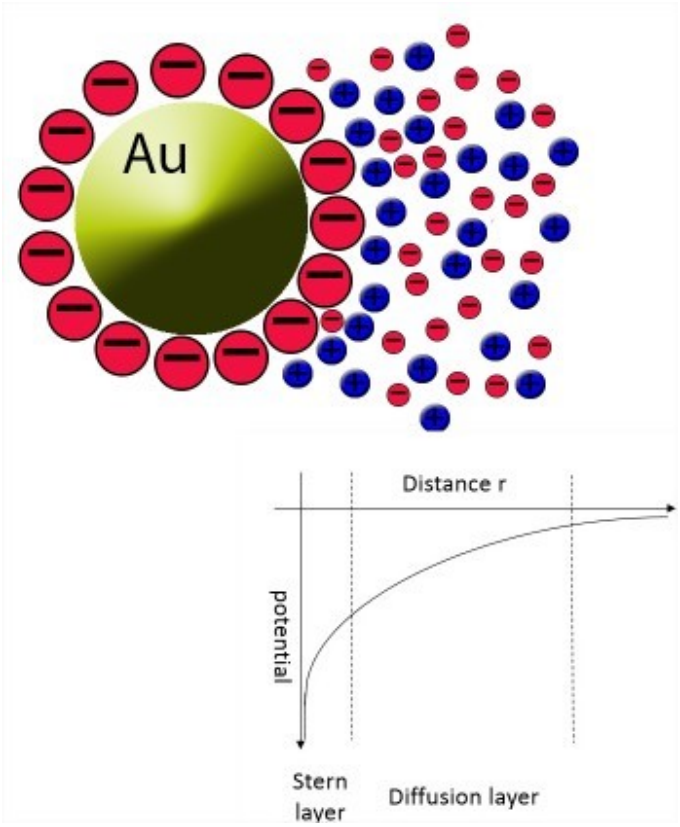

Figure 2.3: *Top*: Scheme of a gold nanoparticle medium interface for the Turkevich Method. The first layer of negative ions comprises citrate ions. A protective layer of water ions called the Stern layer therefore drives the surrounding medium to equilibrium and prevents the interaction of particles. *Bottom:* Decrease of the potential due to the presence of the electromagnetic layers.

These two bottom up approaches are illustrative and have spawned numerous recipes for nanoparticle preparation [2.26] [2.27] [2.28] [2.29] [2.30]. The goal here is to identify simple, safe and scalable ways to make gold nanoparticles of controlled size, with a narrow size distribution, and with divers thiols to yield particles with different surface properties. Particle synthesis is very sensitive to global composition and timing. For instance, the power and the concentration of the reducing agent affect the number of seed particles. The temperature and the strength of the binding agent affect the size of the particles, by determining the equilibrium between further growth and the binding on particles. The homogeneity of the solution affects the polydispersity of the particles. The purity of the reagents affects the purity and nature of the products. Recipes provide only

a starting point for experiential learning. Nanoparticle synthesis method testing and outcome evaluation are addressed in Chapter 3.

2.2 Surface/Interfacial tension

Surface/interfacial tension is defined as the energy required to increase the surface/interfacial area with vapor/another liquid of a liquid by one unit at fixed volume. To understand this need for energy, we must look at the nano scale. Molecules on the surface of a drop do not have the same energy as those in bulk liquid. Fewer molecules of the same kind are present around them. Thus, surface molecules tend to adhere more strongly to their neighbors, giving rise to an inward force that pulls them toward the interior. To create additional surface this force must be overcome. Surface tension (gas/liquid) and interfacial tension (liquid/liquid) values are impacted by the adhesion forces between molecules, the repulsive force between the two phases and the presence of species, such as nanoparticles, that can accumulate at interfaces.

Fine drops of water are stable in water in heavy oil emulsions. In enhanced oil recovery processes, this is a favorable property as it improves sweep efficiency hence improving yields of oil from sectors of a reservoir. During refining, water in oil emulsions can reduce the efficiency of individual refining processes as well as damage process units through increased corrosion. Understanding mechanisms that stabilize and destabilize such interfaces is a core competence in the oil industry. One illustrative demulsification example suffices. Demulsification is a two-stage process [2.31]. First drops of the dispersed medium come into contact with each other without merging, by sedimenting or creaming depending on the density difference with the continuous phase, or by flocculating if the attractive force among the drops is high, as shown in Figure 2.4. Typically, a combination of these processes occurs. By lowering the viscosity of the continuous phase or by applying a controlled shear rate, the speed of these demulsification processes is increased [2.32]. As the density of bitumen is close to the density of water [2.33], flocculation is the dominant phenomenon. Second, drops must coalesce. As the interfaces of the two drops are in contact at a molecular level, a channel can form between drops leading to the formation of a larger drop as described in Figure 2.5. Because the interfacial area is reduced each time two drops coalesce, the final stage

is the presence of two separated phases. Low surface/interfacial tension, steric hindrance or elasticity of the interface can slow demulsification or stabilize an emulsion.

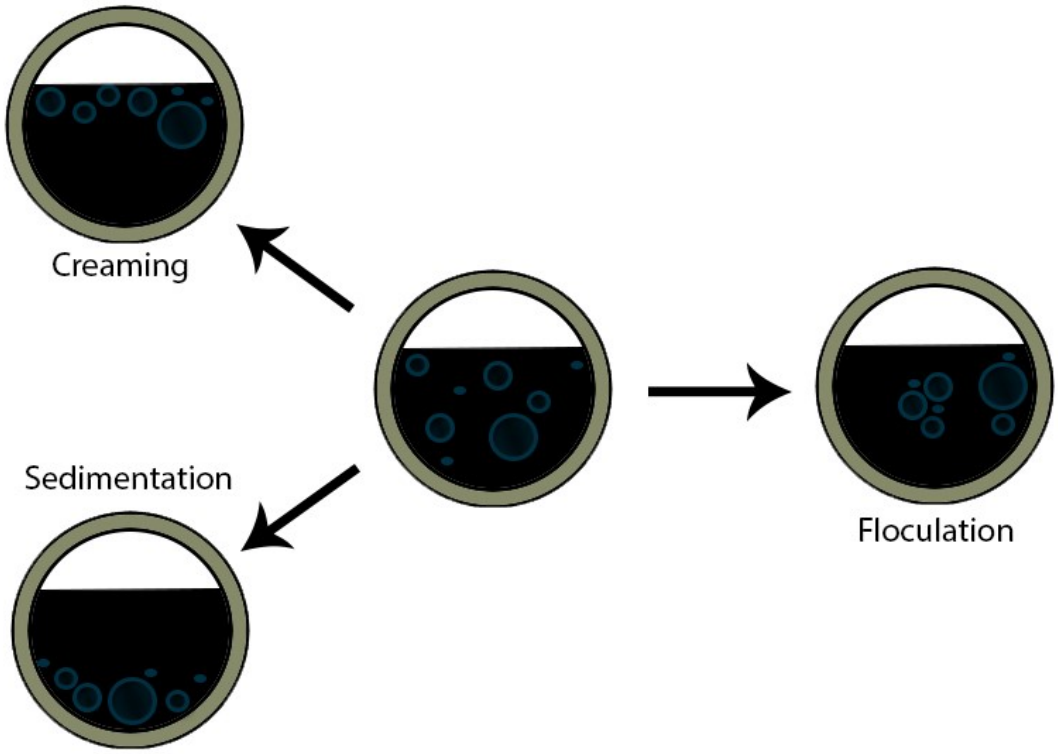

Figure 2.4: Mechanisms that can lead to the gathering of droplets in emulsions. In the case of sedimentation or creaming, water is easier to remove because of the proximity of the droplets.

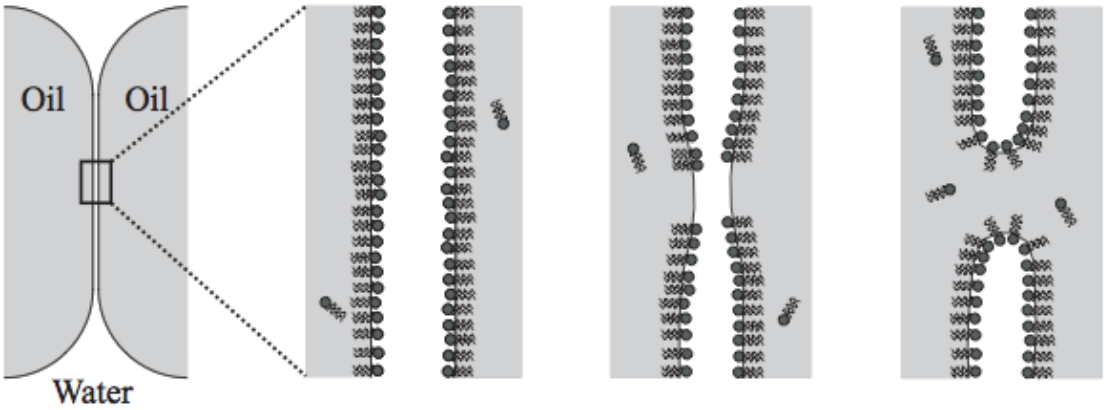

Figure 2.5: Scheme showing the coalescence of two drops of oil in an oil in water emulsion. A brief local change in surface density can lead to coalescence. Image from reference 2.31.

In crude oils, and especially heavy oils, the emulsion of water can lead to a lot of issues. This water can come from two sources. The first one is the contamination of the well by the surroundings materials [2.34], water that have been trapped with the oil since the beginning. The second is the addition of water during production or surface processing. For instance, steam can be injected to heat a reservoir, to reduce the viscosity of an oil, and to facilitate transport [2.35]. Also, emulsions of water can be purposely produced in order to remove chloride residue or other salts that can cause corrosion and reducing the productivity of a refinery [2.36]. Even so, in refineries, pH must be controlled to reduce equipment and pipe work corrosion, and sludge deposition must be monitored [2.37].

Emulsions are not stable by their nature and over time, they tend to demulsify. However, for an industry as demanding as the petroleum industry, the time scale must be as short as possible in order to maintain productivity. Many methods have been developed to speed the separation of water from oils. Examples range from standard thermal or microwave heating [2.38]; to surfactant addition [2.39], [2.40]; to the use of ionic liquids, coupled with microwaves [2.39]; to dilution with light hydrocarbons [2.41]; and membrane separation [2.42] [2.43]. No universal demulsifiers or processes have been identified. The origin of the oil, and their individual contaminants from fine solids or clays [2.444] to asphaltenes play important roles in the stabilization of emulsions [2.45].

As this work focuses on mimics for asphaltene aggregates, only the impacts of asphaltenes at interfaces are reviewed in detail. Wu [2.46] took a close look at the way water drops evolve in a mixture of bitumen and heptol and found two different regimes, depending on asphaltenes solubility. At high content in bitumen, water drops in bitumen remain spherical during expansion and contraction (Figure 2.6). Particles on the interface are found to be a mix of asphaltenes, resins and other oil contents. At high dilution, or at high content in heptol, only asphaltenes are found on the interface and drops deformation during expansion and contraction. The precipitation/flocculation of asphaltenes is thought to change the properties of the interface.

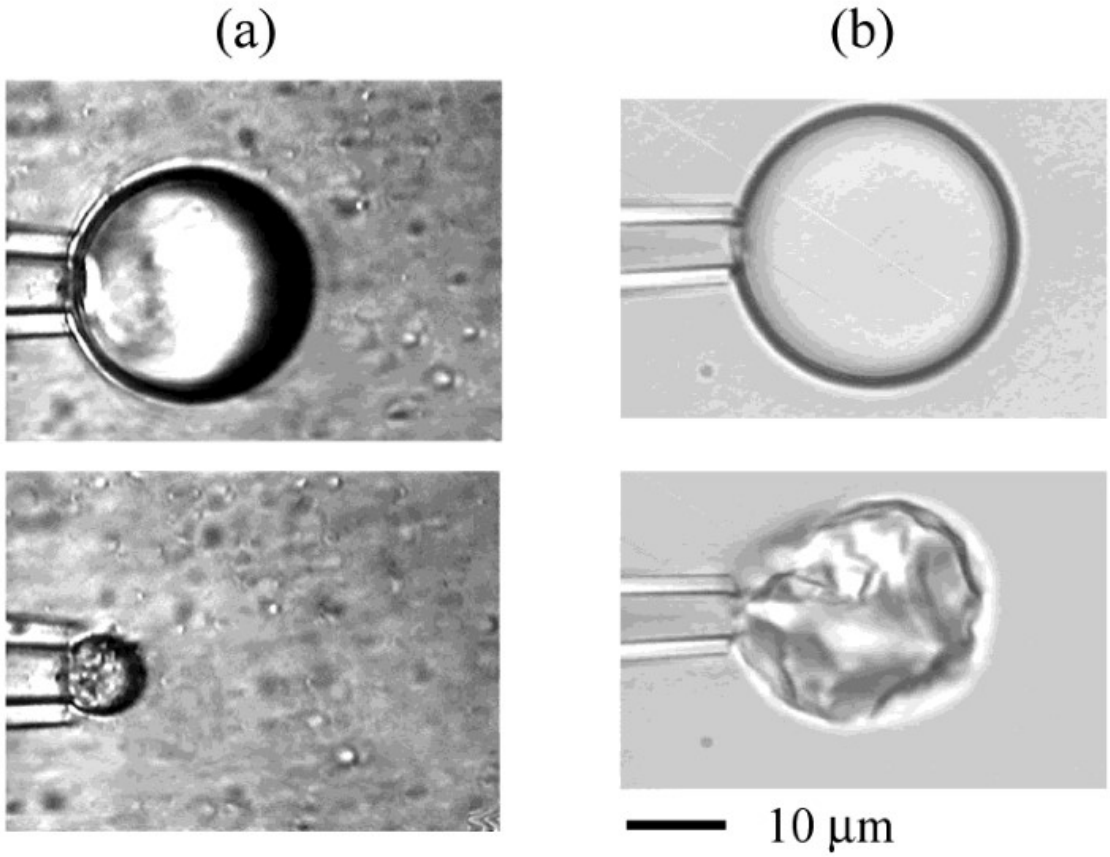

Figure 2.6: Dynamic bitumen water interface behavior (a) The bitumen content is high in the drop, and the shape of the drop remains spherical upon contraction. (b) The content in heptol is high, therefore asphaltenes precipitate and the surface of the drop change. Contraction changes the shape of the drop. Image from reference 2.46.

Czarnecki et al. [2.47] confirmed this using Langmuir Trough experiments with asphaltene rich mixtures and solvents. In good solvents where asphaltenes are only nanoaggreated, the oil film is drained readily. In a solvent known to make asphaltenes precipitate/floc the film drainage is resisted. The creation of a rigid film on the surface of the oil can be responsible for two anti coalescence mechanisms. The first one is related to a Bingham yield stress, making the surface rigid for small stress values and the second one is due to steric hindrance that prevents drop coalescence.

While these mechanisms describe the possible roles of asphaltene nanoaggregates/flocs in emulsion stabilization, their direct adsorption on surfaces is

controversial. Some models describe their presence as macromolecular interaction with monomeric asphaltenes adsorbed on the surface [2.48]. This perspective is increasingly untenable, as asphaltenes have been shown to aggregate even in good solvents at ppm level concentrations. Nanoaggregate and floc behaviors opposed to molecular behaviors are more consistent with the recent data and theory. Even a cursory look at the proposed structures of asphaltene molecules on Figure 2.7 shows us that they are unlike classic surfactants with a clear division between hydrophilic and hydrophobic parts. Yet they are found at interfaces [2.49]. The presence of polar and nonpolar functionalities is a reason for their interfacial activity, but the low frequency and distributed nature of these functionalities does not explain the high surface activity of asphaltenes [2.50]. It was suspected that aromatic rings and alkyl motifs played a role in interface stabilization, by sterically hindering drop coalescence. However, only a small fraction of asphaltenes appears to be responsible for stabilizing emulsions. For example, ultra centrifuged mixtures of bitumen + water show lower interface stability with water than emulsions formed initially, even though only a small fraction of the asphaltenes is removed with the first water wash [2.51].

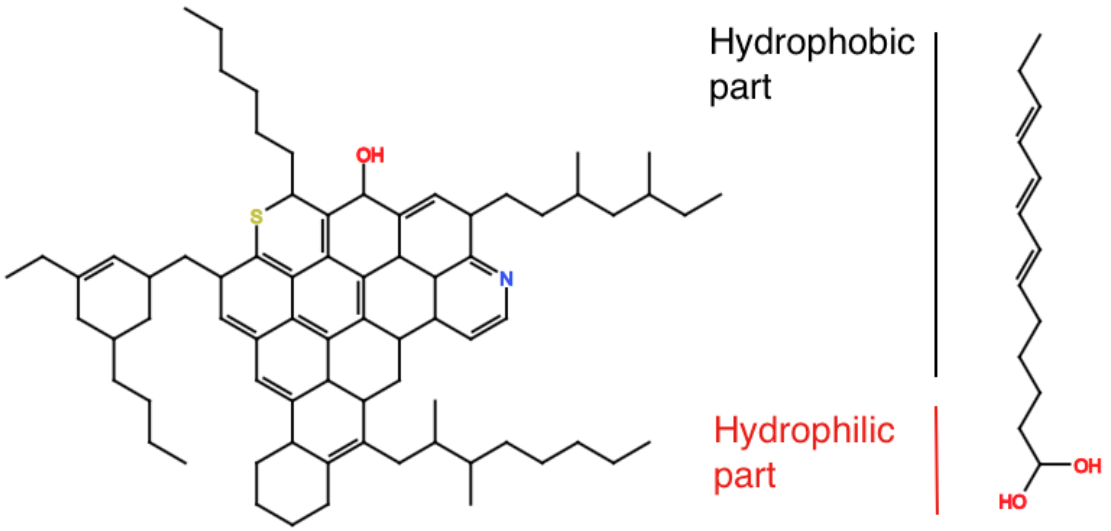

Figure 2.7: *Left:* Possible asphaltene structure. *Right:* Amphiphilic molecule with a net distinction between hydrophobic and hydrophilic parts.

Regardless of their molecular structure and their state of aggregation, the way asphaltenes act at an interface can be easily monitored as shown in Figure 2.8, where interfacial tension outcomes between a synthetic oil and water obtained for ppm levels of asphaltenes added to the synthetic oil are shown. The interfacial tension is a function of asphaltene content and approaches a steady state value with time. The adsorption of asphaltenes at interfaces is slow. In many cases even after 60h, steady state is not attained. This suggests that the interface is dynamic with a slow exchange process [2.52] and an arrangement of thicker and multiple layers around the drops as asphaltenes interact with each other [2.53].

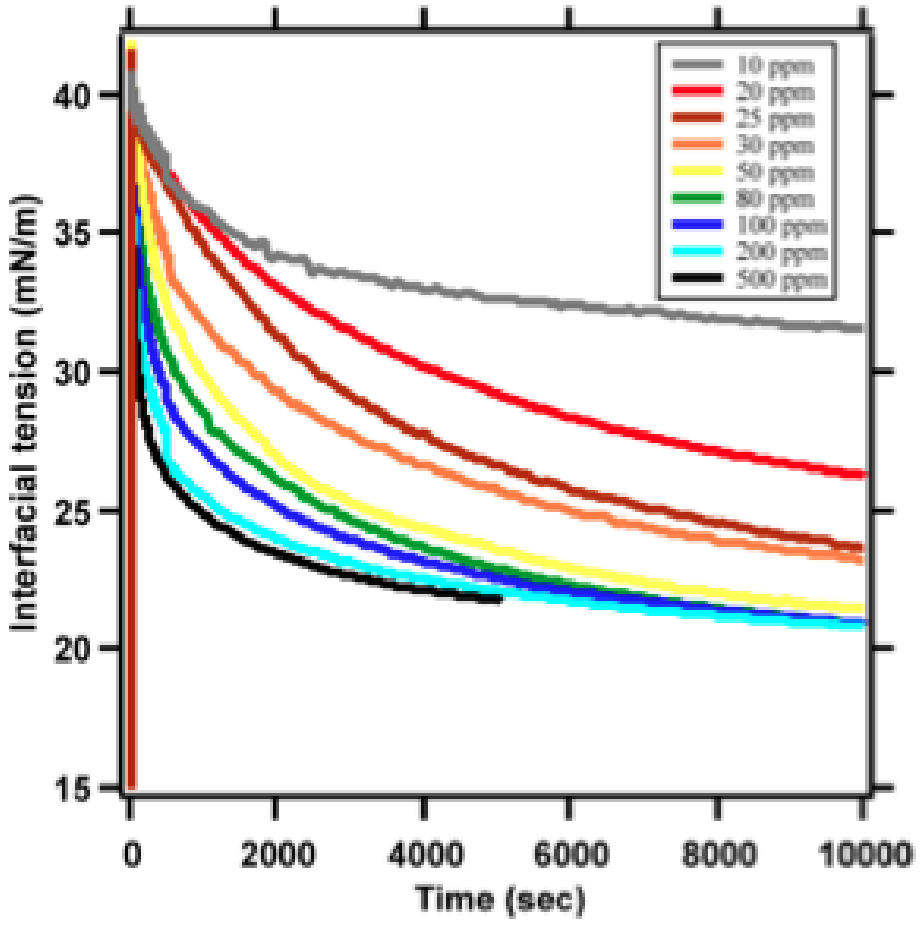

Figure 2.8: Evolution of interfacial tension of asphaltenes in synthetic oil (Newbies 2002) [2.50].

At first, the interfacial tension of the drop decreases really fast and is due to a diffusion-controlled adsorption on the surface. Figure 2.9 shows the extracted plot over

$\sqrt{t}$. We can notice a linear relation between these two components for low asphaltene concentrations. For higher concentrations, a nonlinear relation is observed, suggesting a change in the coefficient of diffusion and therefore the size of the species adsorbing on the surface.

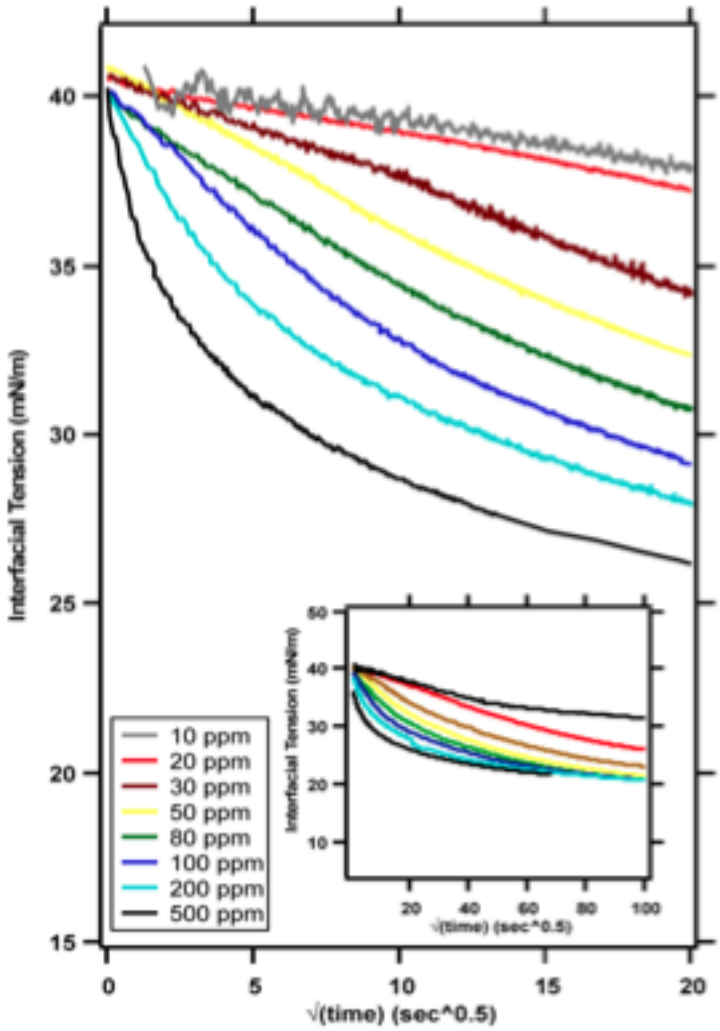

Figure 2.9: Diffusion mechanism identification for asphaltenes at a nexbase 2002/\deionized water interface. (Graph from reference 2.50)

Starting at a surface coverage of ~ 35%, bulk diffusion controlled adsorption is replaced by surface coverage diffusion [2.52]. An asymptotic limit of 85% is found for surface coverage which is similar to the random close packing of disks on a surface. [2.54]

The dynamics of asphaltenes on interfacial tension differ from classical surfactants. First the way they stabilize emulsions is different and can depend of their state of aggregation, which can differ from one oil to another. Second, the age of the emulsions is an important criterion as they become more stable over time. This is why more needs to be learned about which components or functional groups in asphaltenes are responsible for their observed behaviors. Some researchers have already called for better ways to use demulsifiers [2.46]. Better understanding of these issues could lead to new techniques to mitigate the effects they introduce. It is expected that nanoparticles with specific functionalities on their surface can play an important role in hypothesis testing.

2.3 Behaviors of Asphaltenes in Diluents

Because they are defined as a solubility class, and as the use of diluents is common in industry (to decrease oil viscosity [2.55], to destabilize emulsions), understanding the phase behavior of asphaltenes in organic media is important. Asphaltene aggregate size can vary with temperature and pressure. While it is easy to determine the presence of a solid phase, by visual inspection or centrifugation, the detection of colloids, and their state of aggregation is more complex. Further, there is a wide range of states accessible to asphaltenes, depending on the conditions they are placed in. Thinking of asphaltenes as being either soluble species or aggregates neglects the possibility of having different states of aggregation and different portions of the asphaltenes in different states depending on the temperature and the surrounding chemical environment [2.56]. Nikooyeh [2.57] reviewed simple theoretical models based on molecular solubility and colloidal behaviors that have been used to describe the physical and phase states of asphaltenes in diluents and showed that they have had only limited success. These models are typically used to correlate and not to predict asphaltene behaviors in diluents and native crude oils.

Experimental measurements on the state of aggregation of asphaltenes have been carried out [2.58-2.61] as noted in chapter one. These experiments provide insights regarding the scale of aggregation and the nature of the asphaltene-asphaltene interactions, but do not give direct measures of the interaction between asphaltenes and

the surrounding media. Enthalpy of solution measurements do give information about the changes of state and the interactions that species undergo when combined with other species. Two calorimetric measurements, solution calorimetry at near infinite dilution and titration calorimetry are used commonly. In titration calorimetry the entire range of solute and diluent compositions is surveyed. Studies about asphaltenes precipitation [2.62] or association [2.63] and also characterizing their subtractions [2.64] have been carried out using titration calorimetry. In solution calorimetry, milligrams of solute are added to grams of solvent providing summative information regarding dissolution and solute-solvent interaction at low solute concentrations. Zhang [2.65] and Nikooyeh [2.66] confirmed some behaviors of asphaltene + diluent mixtures, and Nikooyeh [2.67] challenged the application of regular solution theory to asphaltene + diluent behavior.

By comparing the calorimetric behavior of well-defined gold+ligand nanoparticles with asphaltene behaviors in a range of diluents, hypotheses regarding the roles of functional groups in asphaltene aggregation behaviours/solvent interactions can be tested. For example, are alkane, hydroxyl or aromatic groups primarily responsible for asphaltene diluent interaction? Testing and comparing interactions with diverse diluents affords the possibility of understanding whether or not one type of interaction is a better mimic for asphaltene behaviors and whether or not controls for asphaltene behaviours can be identified.

Chapter 3: Experimental

3.1 Ligand Selection for the gold nanoparticles

Asphaltenes possess a range of chemical functionalities. They have a carbon skeleton that includes a mix of alkane chains and aromatic groups. From NMR and Raman spectroscopy measurements, 50% to 60% of the carbon is aromatic [3.1], [3.2]. The heteroatoms O, S and N possess different functionalities depending on where they are found in the carbon backbone. For example, nitrogen is mostly found among aromatic or cyclic carbons as pyrrolic or pyridinic nitrogen [3.3] [3.4]. Amine type functional groups are largely absent. For sulfur, XANES measurements show that sulfur is present predominantly as thiophenes, followed by sulfides or sulfoxides [3.6] depending on the maturity of the oil [3.5]. For oxygen, phenolic OH groups are predominant [3.8], but small fractions of Carboxyl and ketone groups are also present. NMR measurements suggest that between 4 and 8 oxygen functional groups are typically found in an asphaltene molecules [3.7]. These functional groups that may appear on the surfaces of asphaltene aggregates are shown in Figure 3.1. Other functionalities known to be present include porphyrin rings [3.9] but these are present in very low mass fractions because vanadium and nickel contents are measured in ppm, even in asphaltenes [3.10].

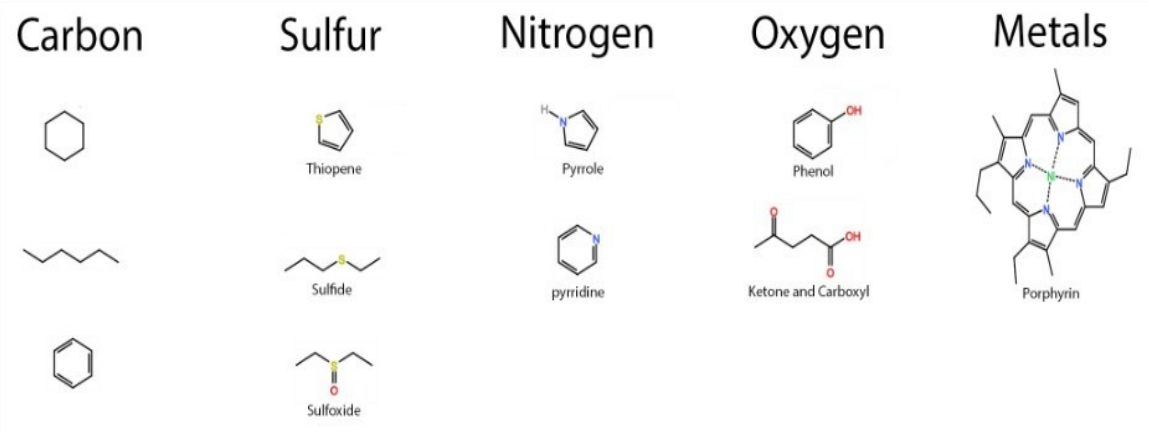

Figure 3.1: Possible functional groups appearing on asphaltene aggregate surfaces.

The strategy to functionalize gold nanoparticles is based on the gold-sulfur bond. This dictates the presence of thiol functionalities at the particle surface. The feasibility of preparing gold nanoparticles with specific ligands imposes additional constraints. The island molecular prototype, with C_8-C_{12} alkane chains [3.11] hypothesized to be present on the exterior surface of aggregates, and the archipelago molecular prototype, with diverse functionalities hypothesized to be present on the exterior surface of aggregates, provide a framework for the final selection of ligands from the feasible options. These compromises led to the following selections:

Gold-alkane nanoparticles were synthesized using octanethiol and dodecaethiol.

Gold-aromatic nanoparticles were synthesized using biphenyl-4-thiol. An alkylethiol-phenyl was not available for alternate preparations.

Gold-hydroxyl nanoparticles were synthesized using 11-Hydroxy-1-undecanethiol. An alkylethiol-phenol was not available for alternate preparations.

Planned syntheses of carboxylic and imidazole functionalized nanoparticles proved unsuccessful and along with nanoparticles including sulfur containing end groups (not part of the original scope), work on these categories of nanoparticles was left for future work. The synthesized and planned gold-ligand particles are illustrated in Figure 3.2.

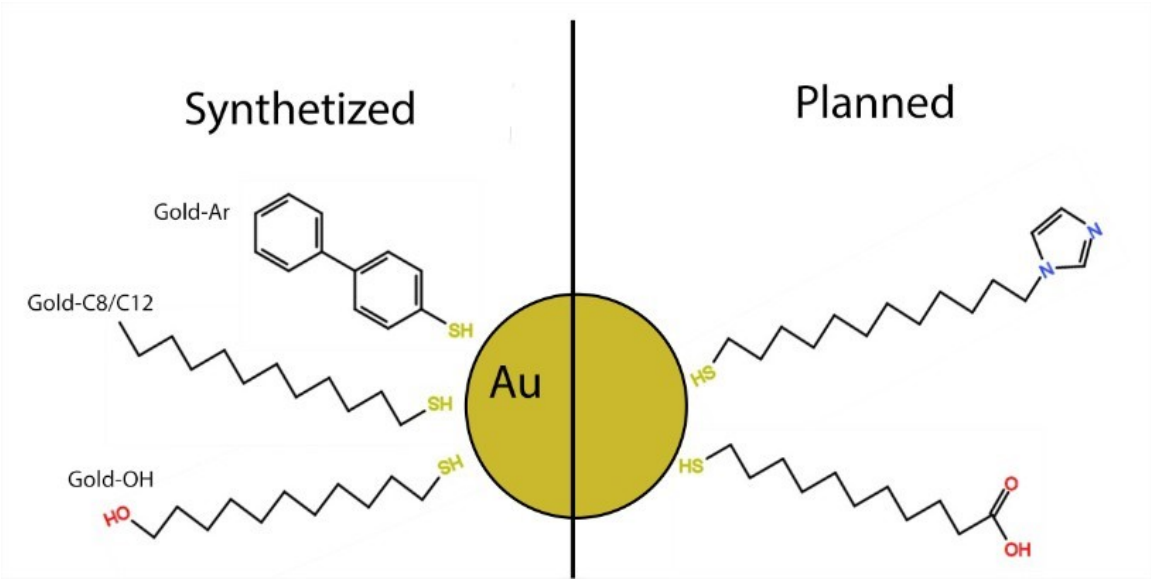

Figure 3.2: Summary of the gold nanoparticles synthetized and planned. The right on the graph represent the particles with *Top:* Aromatic ligands (gold-Ar) *Centre:* Alkanes ligands (gold-C_8/C_{12}) *Bottom:* Alcohol ligands (gold-OH).

3.2 Gold nanoparticles synthesis

3.2.1 Synthesis of Octanethiol/Dodecanethiol nanoparticles.

The synthesis of the octanethiol and dodecanethiol gold nanoparticles was largely inspired a procedure in Zeng et al. [3.12]. The main change implemented was the use of toluene instead of benzene as the reaction medium. Toluene is easier and safer to handle than benzene.

In a brand new 200 mL glass vial 100mL of toluene and 2.174g (25mmol) of borane tert-butylamine (BTB) were added. The vial was then sonicated for 10 minutes. Meanwhile, 100 mL of toluene was added to a 400mL glass vial followed by addition of 1.25mL of dodecanethiol and 1.236g (2.5mmol) of chloro(triphenylphosphine)gold(I) (P[Ph3]AuCl). The vial was stirred under medium shear for 5 minutes and was then put into a 55°C water bath for 5 minutes. The reducing solution was then added using a 50mL burette at ~ 1mL/s. After 25 minutes of reaction, the dark red solution was removed from the bath and cooled at ambient temperature for 25 minutes. Then, 200 mL of ethanol was added, turning the dispersed solution into a totally black solution with

bigger particles inside. The solution was refrigerated for 24hours, and then centrifuged at 2000g for 10 minutes. The remaining solid was sonicated and centrifuged twice in a 1:1 ratio of toluene/ethanol under the same conditions in order to remove the remaining reagents.

The black solid obtained could then be mixed with toluene or n-alkanes in order to observe the characteristic dispersion of nanoparticles. The sizes of the particles were checked by TEM and UV-Vis spectroscopy. The proper coating of the ligands was checked by comparison with titration calorimetry and FTIR measurements for gold-C_{12} nanoparticles purchased form Sigma-Aldrich. The characterization and measurement results are presented in Chapter 4.

Remarks

Successful synthesis of these nanoparticles is much more challenging than indicated by the literature. There is as much art as science involved. The many parameters that must be taken into account and mastered provide numerous sources for errors and contamination. Before successful trials with this synthesis method were achieved, alternate synthesis methods were attempted without success [3.13]. Some approaches were very good on a tiny scale but it was not possible to scale up the synthesis so that samples large enough for sample property determination, calorimetry and interfacial tension measurements could be performed. Typically, strong reducing agents are used. These reagents create reaction paths that determine particle size and surface quality that are hard to control and that are sensitive to all experimental details including how reagents are introduced. Even for the method presented above, many attempts were needed to achieve a success rate of less than ~50%. Trace contaminants (metallic residue or dust) can lead to total failure of an experiment. Careful cleaning of every item with aqua regia is essential. Measurement of the surface composition of particles produced is equally important. At one point, a method that produced good particles (size, dispersion) based on TEM measurements and possessed an appropriate solubility were obtained and used in experiments. However, a quick comparison using FTIR, with gold-C_8 Nanoparticles purchased from Sigma underscored the presence of contamination on the particle surfaces that negated the measurements. Readers are advised to take extra care of

the purity of all chemicals and reagents and to use a weak reducing agent in order to obtain good reproducibility. As gold can form bonds with common atoms (nitrogen, phosphorus and of course sulfur) chemical analysis of particle surfaces should be performed with each batch of particles produced.

Making small batches of dispersed particles proved to be easy. Preparing particles as reusable powders proved harder. Centrifugation was the preferred choice for this but a mix of solvents was needed that made the particles aggregate. Without aggregation, forces of ~ 100 000g are required to separate 5nm gold particles.

3.2.2 Synthesis of Hydroxyl functionalized gold nanoparticles.

The synthesis of hydroxyl-functionalized nanoparticles was performed at the University of Utah in Salt Lake City between April and June 2015 during a visit to the laboratory of Professor Shumaker-Parry. She and her team have published numerous papers about the synthesis of nanomaterials and about gold nanoparticles in particular. The purpose of the trip was to learn the synthesis of different gold nanoparticles and get some advice about the previous experiences with nanomaterials and analytical chemistry. The synthesis of these particles follows their published work [3.14] and laboratory norms, and was performed under their supervision.

First a new 1L Erlenmeyer to be used for the synthesis of the particles was washed with piranha solution in order to remove organic contaminants from the surface of the glass. The inside glass surface was then silanized for 24 hours to render it hydrophobic. This procedure improved the efficiency of the synthesis because the strong hydrophilic behaviors of gold-OH nanoparticles lead them to stick to the glass when synthesized in a partially hydrophobic solvent. Between batches the Erlenmeyer flask and a stir bar were washed for 30 minutes in fresh Aqua Regia in order to remove metallic contaminants that could ruin the reaction by serving as a nucleation site for gold atoms.

After that, 800mL of acetonitrile and 200mL of toluene were added to the erlenmeyer and stirred to produce a homogeneous solution. 1.6 mmol (0.544 grams) of chlorotriethylphosphine Gold and then 16 mmol (1.76 grams) of 11-Mercapto-1-undecanol were then dissolved in the solution and stirred for 20 minutes. The solution was thereupon immerged into a 60°C water bath for 10 minutes. Next, addition of 10mL of 0.5 M of 9-BBN and 0,2 mL of Tryocetyleamine (TOA) lead to a dark red coloration of the solution for the first two minutes of reaction, followed by the discoloration of the solution and the formation of large black particles. Indeed, the coating of the nanoparticles by the hydrophilic ligand pushed them to aggregate in a hydrophobic environment. The solution was left in the water bath for a total of 20 minutes and then cooled at room temperature for 30 minutes. After this, the slurry was placed in a fridge overnight to permit particles to sediment. Most of the solvent was decanted and the rest was removed by centrifugation. Then the particles were washed with the same solvent mixture that was used for the synthesis. The process was repeated four times, yielding ~ 100 mg of black powder. Mixing this powder with ethanol or methanol gave a red color characteristic to a dispersion of nanoparticles. Stored in the fridge, no sedimentation was observed for these mixtures after two weeks. The characterization of the particles was performed using TEM, XPS, FTIR and UV-Vis.

3.2.3 Synthesis of biphenyl functionalized gold nanoparticles.

Synthesis of nanoparticles with biphenyl ligands, using direct reduction of gold salts did not work. Sulfur bonds were absent in the XPS characterization results. However, synthesis was achieved by ligand exchange based on particles previously stabilized with a phosphorus ligand that has a weaker interaction than the sulfur-gold interaction [3.15] [3.16].

The first step of the synthesis process was the synthesis of triphenylphosphine-stabilized nanoparticles (gold-TPP). A 6L Erlenmeyer was washed with aqua regia and filed with a mixture of 4:1 toluene to acetonitrile at room temperature. Then, 2.04g of $(Et_3P)AuCl$ was added, along with 9.345g of triphenylphosphine. This mixture was

stirred for 1 hour. The addition of 10mL of 0,5M 9-BBN in THF followed. The reaction slowly turned the mixture from yellow to cloudy brown. 1 Liter of nanofiltered water was added and the solution turned purple black upon stirring. As water was not miscible, strong mixing was used. At the end, the whole solution was rotovapped and the solid washed in hexane twice at 7000 rpm. For the exchange step, the solid was dispersed in 3 Liters of methylene chloride to give a dark purple solution. A 1:1 mass ratio of 4-Byphenilthiol to gold nanoparticles was injected in the solution, which was then stirred for 24 hours. After this, the solution was filtered to remove large aggregates. The solution was then placed in a rotovap and washed twice with hexane at 7000 rpm. The black solid dispersed in toluene and was characterized using FTIR, UV-Vis, TEM and XPS measurements.

The synthesis described above resulted in larger particles than obtained with the classical method [3.11] used by Professor Shumaker-Parry's group for the synthesis of gold with triphenylphosphine (gold-TPP) (~ 4nm vs ~ 2nm). While this outcome was desirable large aggregates were produced as well, an undesirable outcome. Direct centrifugation, instead of water addition was also tried but resulted in even bigger aggregates for the gold-TPP particles. Very large particles, visible on naked eye, could not be re-dispersed for the ligand exchange step. Poor solution homogeneity in the 6L Erlenmeyer or repeated centrifugation could explain the presence of these macroaggregates.

3.3 Gold nanoparticle characterization.

3.3.1 Size characterization

The most direct way to characterize the size of particles is to look at them under a microscope. As the size of the particles is in the nanometer range, a transmission electronic microscope (TEM) was used. The measurements were carried with a CM20 FEG operated at 200kV at the nanofab of the University of Alberta) and with a JEOL 1400 Plus TEM operated at 120kV at the University of Utah. Solid nanoparticle samples were dispersed in a solvent. A concentration 0.05mg/mL or less is recommended to

avoid multilayer of particles in TEM images. A drop of ≈2μL was put on a TEM grid and dried under atmospheric conditions. Toluene was used for gold-C_8/C_{12} and gold-Ar and ethanol for gold-OH. As nanoparticles are driven by Brownian motion, no variation in particle size measurements was observed based on subsamples taken from two different elevations in the dispersion (top/bottom of the vial).

As gold nanoparticles exhibit the plasmon resonance phenomenon [3.17], UV-Vis spectrophotometry is also useful to monitor the size of particles and their behaviors in solvents. Monodispersed 5 nm gold nanoparticles have an absorbency peak at ≈ 520 nm. Dispersions appear red in colour. For theses measurements, gold nanoparticles were dispersed in the same solvents used for TEM measurements and placed in a Varian Carey 50 UV-Vis spectrometer that registers absorption signals at one nanometer intervals between 800nm and 350nm. Pure solvent spectra were also measured and subtracted from the nanoparticle dispersion signal.

3.3.2 Surface ligand characterization

Three surface characterization techniques, Fourier-Transform-Infrared-Spectroscopy (FTIR), X-Ray photoelectron spectroscopy (XPS) and Scanning Transmission Electronic Microscope (STEM) were used to characterize the surfaces of particles. Where possible, outcomes were compared with commercial particles of the same type. Where this was not possible, comparisons were made with the ligands.

Fourier-Transform-Infrared-Spectroscopy (FTIR) experiments were performed in order to identify functional groups present in samples. This technique is based on the characteristic excitation of chemical bonds when they are exposed to a known wavelength of photons with a specific intensity. The energy absorbed for each wavelength is registered and used to draw a spectrum that can be linked to chemical bonds. The experiments were carried out on Erkin Elmer Spectrum 100 with DiffusIR attachment from PIKE at the university of Utah (from 4000cm^{-1} to 600cm^{-1}) and on a FTIR spectrometer nicolet from Thermo Instruments at the university of Alberta from 4000cm^{-1} to 500cm^{-1}. The wave number step was one cm^{-1} in both cases. For each

experiment, nanoparticles or ligand was mixed with KBr powder and placed in the instrument. Pure KBr acts as an internal standard and background.

X-Ray photoelectron spectroscopy (XPS) is a characterization technique where the kinetic energy of electrons that escape from a surface bombarded by x-rays is measured at high vacuum. The binding energy of electrons is element specific and it is possible to determine which elements are present and to measure their relative abundance from the numbers of ejected electrons with specific energies. Measurements were carried out at the University of Utah with a Kratos Axis Ultra DLD system. Monochromatic Al K alpha X-Rays were used (1486.6 eV), with a power of 150 W. Around 10 mg of nanoparticles were placed on a carbon pellet and put under vacuum 24 hours before measurements. High resolution spectra for carbon, gold, sulfur and phosphorus provided controls.

A high resolution JEOL 2800 Scanning Transmission Electronic Microscope (STEM) at the University of Utah, equipped of an energy-Dispersive X-ray (EDX) spectrophotometer was used to characterize and to map element distributions at the nanoscale. Each element possesses a set of peaks in an X-Ray emission spectrum, and these are linked to specific physical locations on sample surfaces during scanning. Sample preparation is the same as for TEM measurements. Unlike classic TEM analysis, the beam is focused on the sample, which makes the need for good grid quality as burn and deformation of the grid can occur.

3.4 Nanoparticle property measurements.

3.4.1 Interfacial tension (IFT) measurements

Interfacial tension measurements were performed using the well-known pendant-drop method (Ramé-Hart goniometer model 250) and the results were obtained with the software "Advanced DROPimage" from the same company. In this method, a drop of an immiscible liquid is dispensed with a needle inside an optical quartz cell filled with the second liquid. The shape of the needle depends on the relative density of the droplet compared to the dispersed phase. Then a CCD camera captures an image of the drop and the software, makes use of the Young-Laplace Equation:

$$\gamma = \frac{\Delta\rho * g * R}{\beta} \quad \text{Equation 3.1}$$

to determine the interfacial tension. In equation 3.1, γ is the interfacial tension in Nm^{-1}, Δρ the density difference between the two phases, g the gravity constant, R the radius at the apex of the drop and β the shape factor. The radius R and the shape factor β are determined by the DROPimage software [3.18]. Drops with volumes in the range of 20 to 30μL are used. Interfacial tension values are calculated every 2 seconds over an interval of 2000s or less if the volume variation with time is too significant to obtain meaningful measures of γ. As the mutual solubilities of water and hydrocarbons are low (e.g. the Solubility of toluene in water is 0.052% at 25°C and the Solubility of water in toluene 0.033% at 25°C) impacts of composition variation with time on IFT measurements is ignored.

Nanoparticle dispersions were prepared fresh before each measurement. Between 0.5mg and 10mg of nanoparticles were weighed and dispersed in 10 mL of solvent. The solutions were then sonicated for 15 minutes and the measurements were carried out as fast as possible in order to mitigate impacts of aggregation over time noted in specific cases (e.g.:, asphaltenes and gold-Ar in heptol 3/1 and pure heptane). Measurement repeatability and reproducibility are discussed in Chapter 4.

3.4.2 Solution Calorimetry measurements

Isothermal solution calorimetry measurements were performed with a TAM III thermostat and a TAM precision solution calorimeter from TA Instruments. The data were collected and analyzed using the software package SolCal from the same company. The thermostat assures a precision of +/- 0.0001°C and the precision solution calorimeter is considered semi-adiabatic, with temperature fluctuation inferior to 10μ°C per 5 minutes. The thermister monitors temperature fluctuations of 1μ°C which correspond roughly to an energy change of 1mJ.

In this work, 25 mg of nanoparticles are weighed and inserted in a 1.1ml SolCal crushing ampoule. The ampoule is then put in the 25mL vial of the calorimeter, carefully and accurately filled with the desired solvent. The whole assembly, shown in Figure 3.3,

is then placed in the TAM III thermostat and the temperature offset (difference between the bath and the calorimeter) is measured. At this time, a 500-rpm rotation device is activated in the calorimeter in order to ensure dispersion of the sample once the ampoule is broken. When the temperature offset is below 150mK, a first baseline is taken until the variation of the temperature over time is below 10µ°C/5mins. Then a 1J calibration spike is applied and a second baseline obtained. At that point the ampoule is crushed and the temperature change is monitored. After the recording of the signal, a new 1J spike is applied and a third baseline is obtained. The first 1J spike is used to calibrate the response of the system and therefore quantify the response to breaking the ampule. The difference between the second and the third baseline, registered after each 1J spike is used to compare the heat capacity Cp of the sample before and after the addition of the solute.

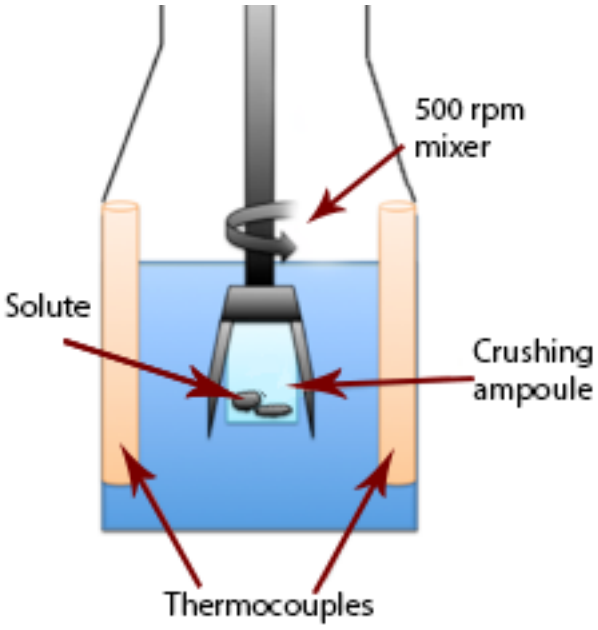

Figure 3.3: Schematic of the solution precision calorimeter

Chapter 4: Results and discussion

4.1 Characterization results.

4.1.1 Nanoparticle Size characterization

TEM measurements

TEM images were obtained for gold-C_8/C_{12} (Figure 4.1), gold-OH,(Figure 4.2) and gold-Ar (Figure 4.3) nanoparticles. The mean size and the size distribution of the particles were analyzed with the software ImageJ. For the gold-C_8/C_{12} nanoparticles a mean size of 5.3 nm with a standard deviation of 0.7 nm was found. The corresponding values for gold-OH particles are 4 nm and 2.3 nm and for gold-Ar particles 3.8nm and 2.1 nm. For the gold-Ar particles it was necessary to eliminate the impacts of large clusters (Figure 4.3) sometimes found in TEM images for gold-Ar particles. The origin of the clusters is not clear. They may arise from Pi-Pi stacking among particles during drying or from sintering of gold atoms on adjacent particle surfaces. At ~ 100 mg/L, gold-Ar particle sedimentation was not observed after one week, but at ~ 1000 mg/L aggregates, dispersible by sonication, could be found on the bottom of the vial after few days.

UV-Vis Spectra

Although the nano-particles possess a similar mean size and size distribution, suspensions of the three particles appear differently to the naked eye. Gold-C_8/C_{12} particles in toluene and gold-OH particles in ethanol appear red but gold-Ar particles appear purple. This difference is quantified in the UV-Vis measurements shown in Figure 4.4. Gold-OH and gold-C_{12} nano-particles have a maximum absorbance at ~ 510 nm. The principal peak for gold-Ar particles is shifted to a higher value of 539 nm and two minor peaks appear between 700nm and 800nm. As gold-Ar particles have the same mean size as the other two types of particles, they would appear red in solution if they were monodispersed. Two mechanisms can explain the absorbance difference: if particle spacing is small enough, then the absorbance peak for equal sized particles shifts to the right [4.1]; if larger particles are present, additional peaks are expected. Based on the

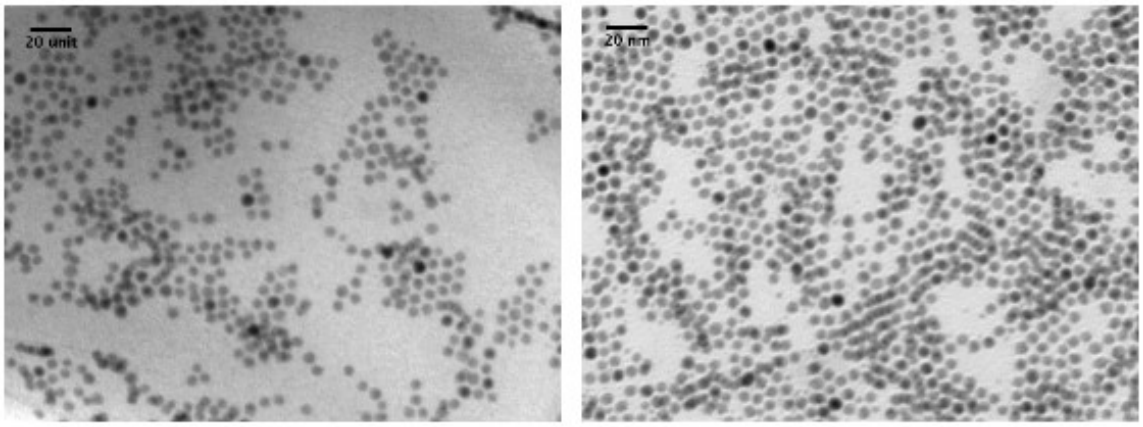

Figure 4.1: TEM images of synthetized Gold-C_{12} carried out on a CM20 FEG and dried from toluene.

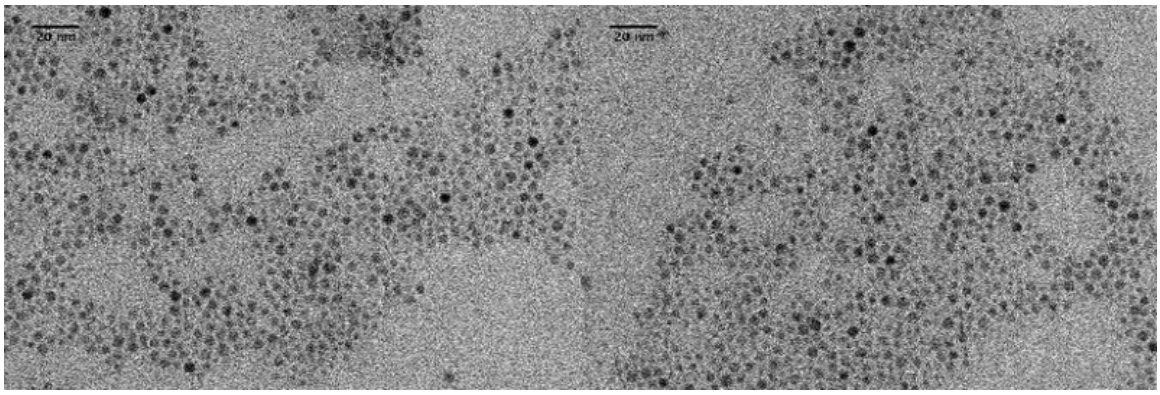

Figure 4.2 TEM images of synthesized gold-OH carried out a JEOL 1400 Plus and dried from ethanol.

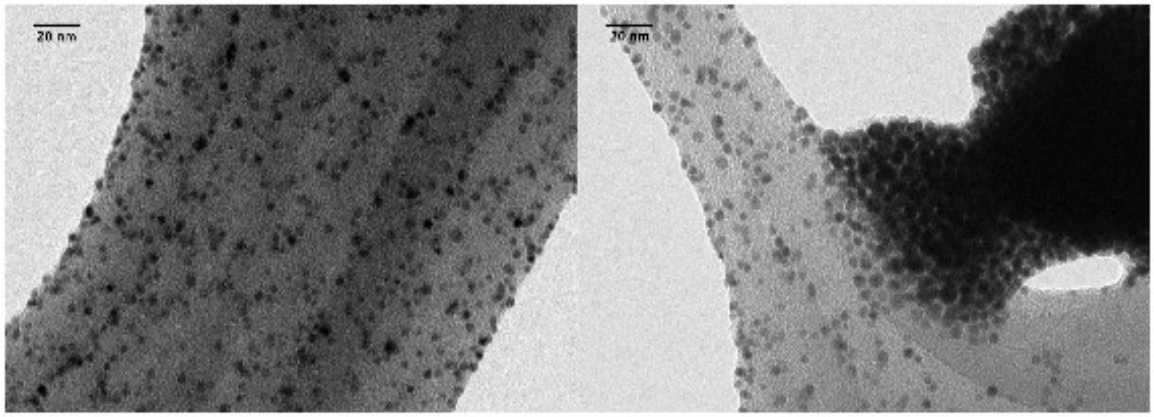

Figure 4.3: TEM images of synthesized gold-Ar carried a JEOL 1400 Plus and dried from toluene.

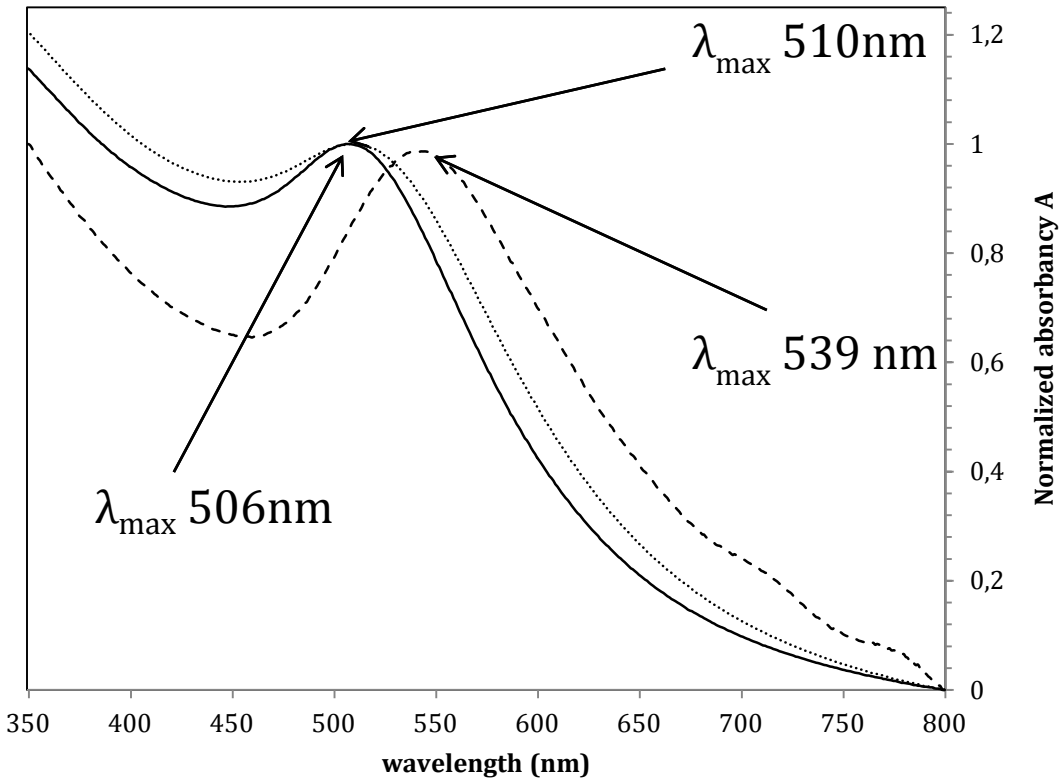

Figure 4.4: UV-Vis Spectra of synthesized gold nanoparticles. Straight-line gold-OH in ethanol λmax= 510nm. Doted-line gold-C_{12} in toluene λmax= 506 nm. Dashed-line gold-Ar in toluene λmax= 539nm.

TEM images, the shift in the principal peak is attributed to the proximity of particles. Both TEM and UV-Vis contribute to an assessment of the physical properties of particles.

4.1.2 Surface properties

FTIR measurements

FTIR results for the gold nanoparticles are presented on Figure 4.5 (gold-C_8), Figure 4.6 (gold-OH) and Figure 4.7 (gold-Ar). Regions of interest are highlighted and used to compare the properties of the particles. The yellow region (3000 cm^{-1}-2800 cm^{-1}) describes the presence of linear saturated carbons in the sample. The peaks seen in this

region correspond to symmetric and asymmetric CH_2/CH_3 stretching bands. Measurements for both synthesized and purchased gold-C_8 nanoparticles are presented in Figure 4.5. Their spectra are qualitatively and quantitatively similar in this and in other respects. For the gold-OH particles, Figure 4.6, only two peaks are seen in this wave number range because the ligand, 11-mercaptoundecanol, does not possess a terminal CH_3 group. The terminal OH-group appears in the red region (3500 cm^{-1}-3200 cm^{-1}). For the gold-Ar particles, a small signal in the 3000 cm^{-1}-2800 cm^{-1} wave number range, Figure 4.7a and Figure 4.7b, suggests that there is residual TPP (Triphenylphosphine) the first ligand used to the synthesis of gold-Ar) or an external contaminant present. FTIR does not permit more detailed analysis or investigation. The thiol bond (≈ 2600 cm^{-1}) present in the ligand starting material, Figure 4.6b and Figure 4.7b is absent from the spectra of the particles, indicating a change in the bond nature for sulfur. Aromatic carbon peaks (3200cm^{-1} -3000cm^{-1} and ≈1500cm^{-1}) are visible in Figure 4.7a,b and c because both TPP and biphenyl-4-thiol include aromatic carbon. The three peaks around 800cm^{-1} are present in both the gold-Ar particles and in the ligand biphenyl-4-thiol.

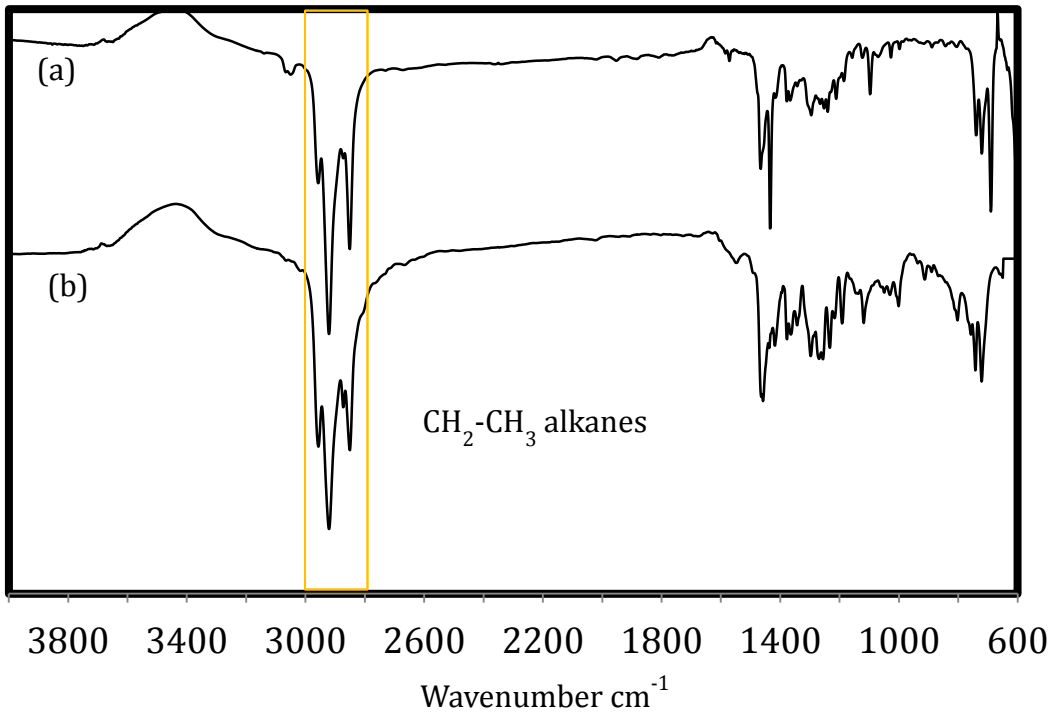

Figure 4.5: FTIR spectra of (a) synthetized nanoparticles (gold-C8) and of (b) Sigma-Aldrich nanoparticles.

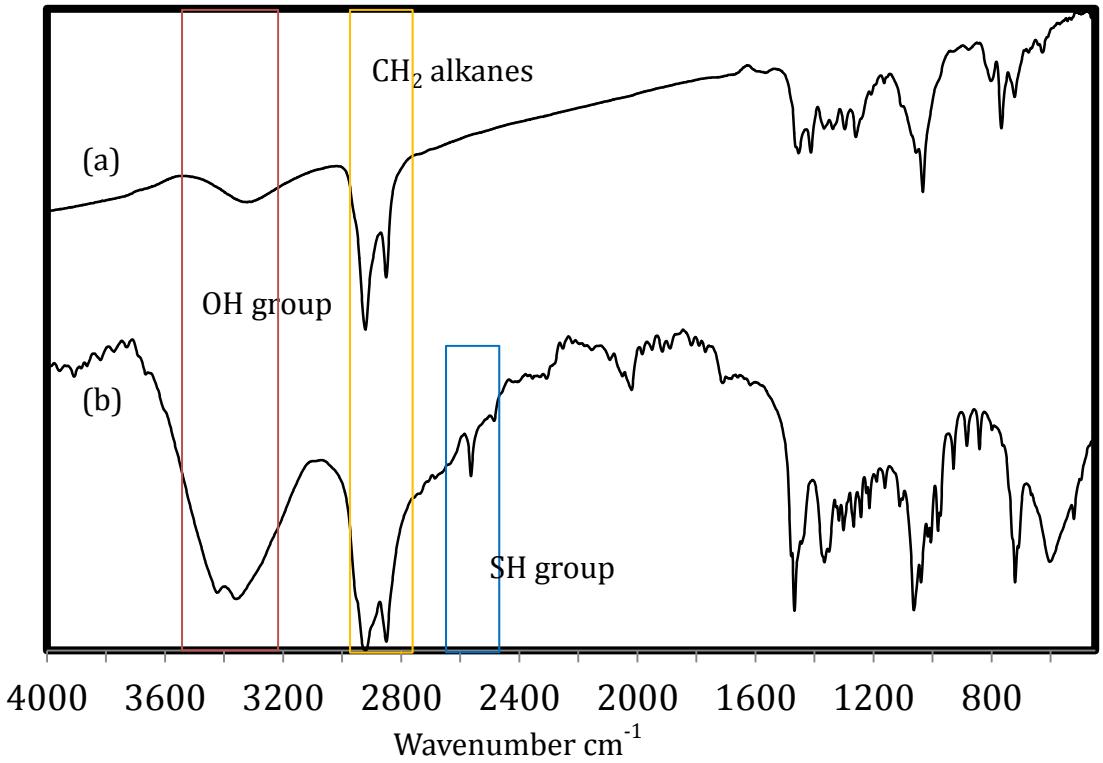

Figure 4.6: (a) FTIR spectra of the synthesized gold-OH (b) FTIR spectra of 11-mercaptoundecanol (ligand).

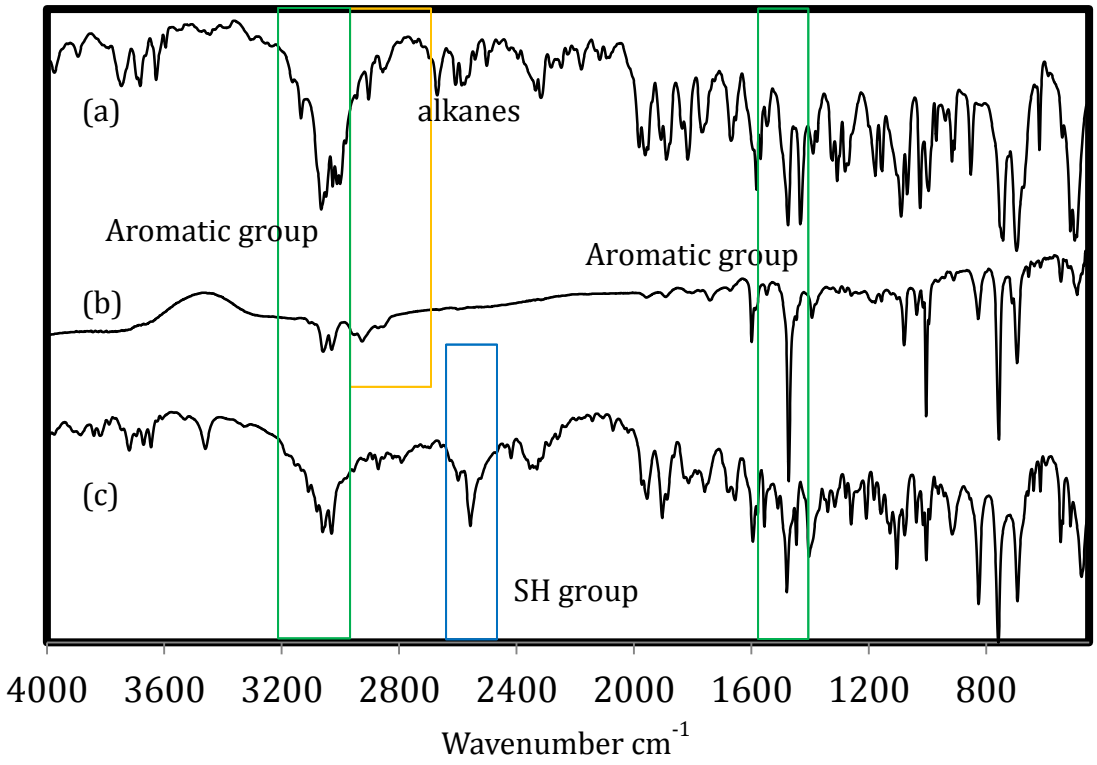

Figure 4.7: FTIR spectra of (a) triphenylphospine, (b) synthesized gold-Ar and (c) biphenyl-4-thiol.

XPS measurements

High-resolution XPS measurements for gold, sulfur, phosphorus and carbon are presented in Figure 4.8 for gold-OH nanoparticles, in Figure 4.9 for gold-Ar nanoparticles and in Figure 4.10 for gold-C_{12} nanoparticles. For the gold-OH nanoparticles, the relative atomic concentrations are, 84.8% for gold, 3.7% for phosphorus and 11.5% for sulfur. The ratio for gold atoms to bonding atoms is 5.57, giving an overall coverage of 58%. The rest of the surface is covered by gold atoms only. The covered surface is made of 24.3% of phosphorus and 75.7% of sulfur. A mix of ligands on the surface is to be expected as the gold salt has triethylphosphine in it. The surface comprises a mix of 11-mercaptoundecanol and triethylphosphine, which results in a ratio of approximately one to one alcohol to alkane as each phosphorus atom have 3

ethyl chains attached to it. The length of the desired undecanol ligand compared to the length of triethylphosphine, the relative ratio between sulfur and phosphorus and the dispersive behavior of the particles in alcohol compared to pure alkanes is sufficient to attribute much of the behavior of these particles to the presence of the OH group.

Phosphorus is not detected on the surface of gold-Ar nanoparticles, as shown in Figure 4.9. The gold to sulfur atomic ratio is 5.23 (a surface coverage around 59%). The absence of phosphorus on the surface indicates the absence of triphenylphosphine (ligand used before the exchange). This outcome illustrates the efficiency of the ligand exchange process because the phosphorus is removed in favor of the second ligand. No information is provided about the contaminants present between $3000cm^{-1}$-$2800cm^{-1}$, their origin is unknown at this time.

XPS measurements were also performed for gold-C_{12} nanoparticles and a gold to sulfur ratio of 15.3:1 was found, corresponding to an overall surface coverage of 29%. Phosphorus is also not detected on the surface of the gold-C_{12} nanoparticles. The difference between gold-OH and gold-C_{12} nanoparticles in terms of sulfur contamination is very likely to be explained by the force of the reducing agent, which is stronger for gold-C_{12} than for gold-OH nanoparticles. If not contaminated by another material visible on FTIR or XPS, the gold-C_{12} nanoparticles are covered only by dodecanethiol and the rest of the surface comprises gold atoms.

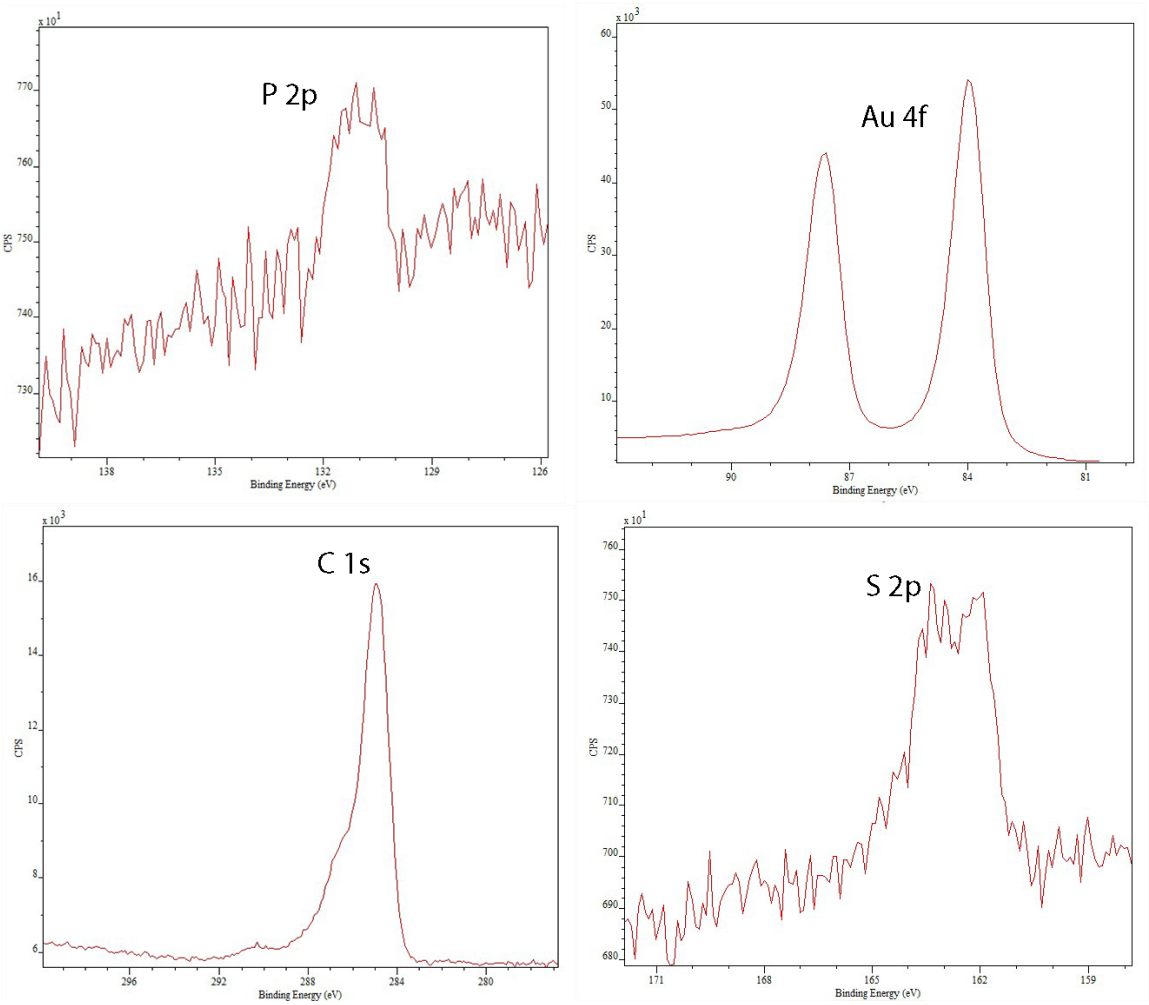

Figure 4.8: High resolution XPS spectra of the gold-OH nanoparticles for the region associated to carbon, gold, sulfur and phosphorus.

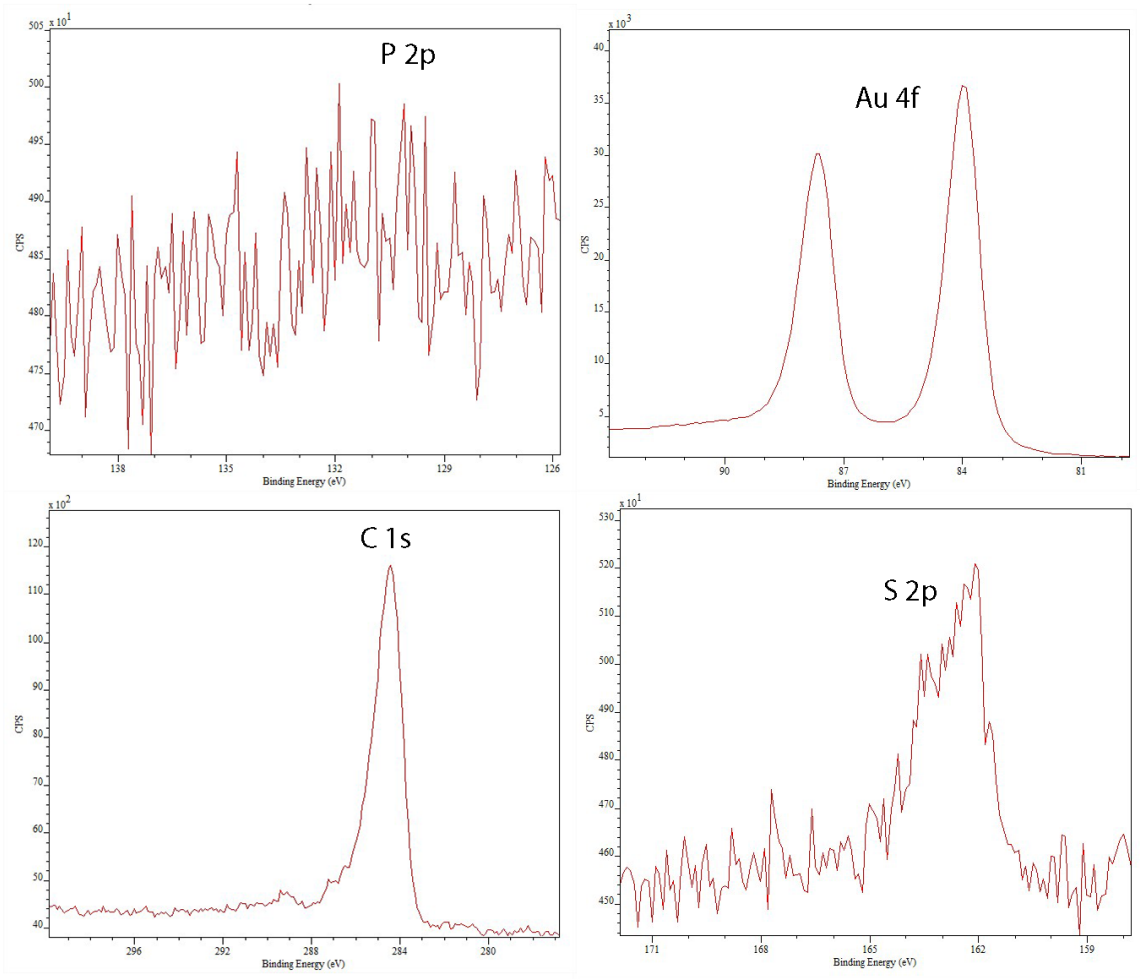

Figure 4.9: High resolution XPS spectra of the gold-Ar nanoparticles for the region associated to carbon, gold, sulfur and phosphorus.

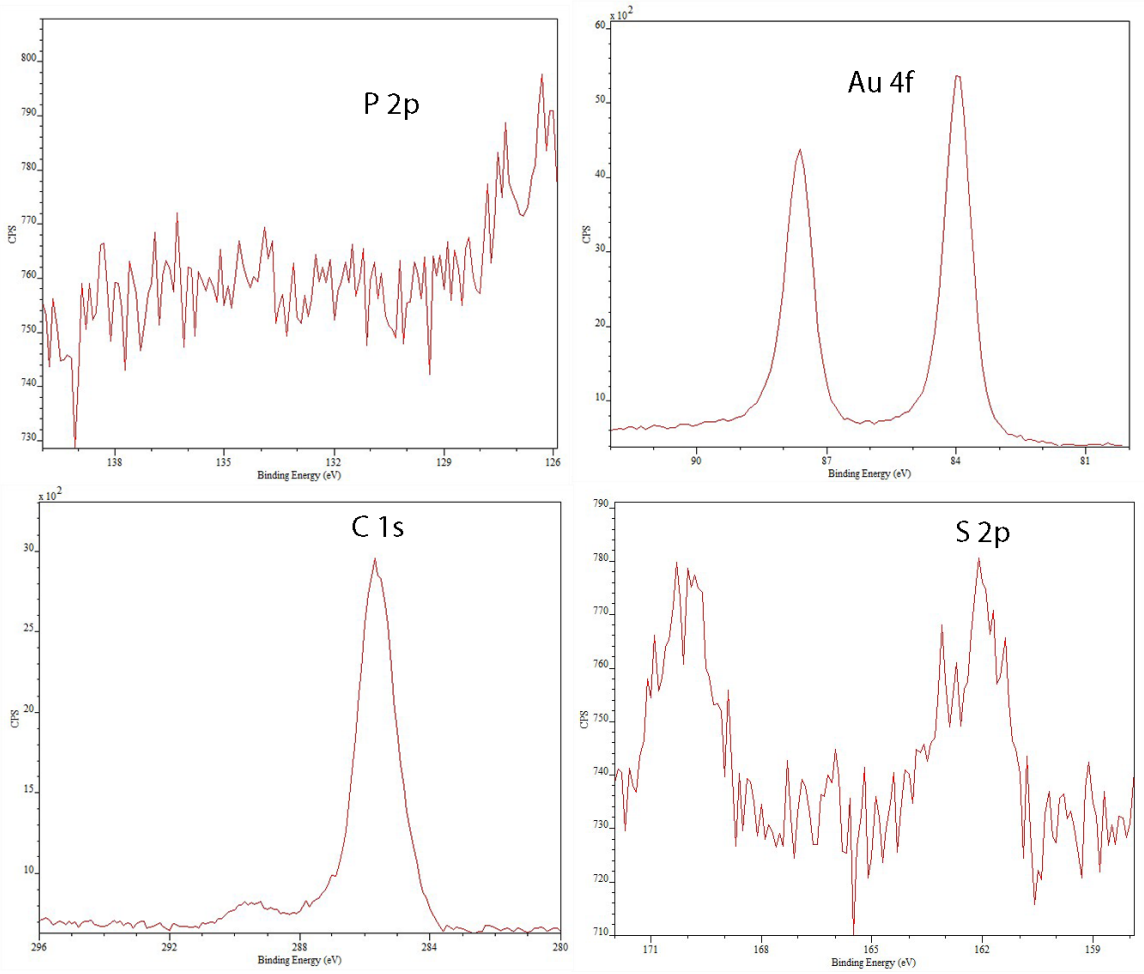

Figure 4.10: High resolution XPS spectra of the gold-C_{12} nanoparticles for the region associated to carbon, gold, sulfur and phosphorus.

S/TEM measurements

S/TEM results for the gold-OH and the gold-Ar nanoparticles are shown in Figure 4.11 and Figure 4.12 respectively. The SEM images of the particles and the maps showing high concentrations of gold and sulfur overlap, as expected, and confirm the presence of sulfur on the particle surfaces.

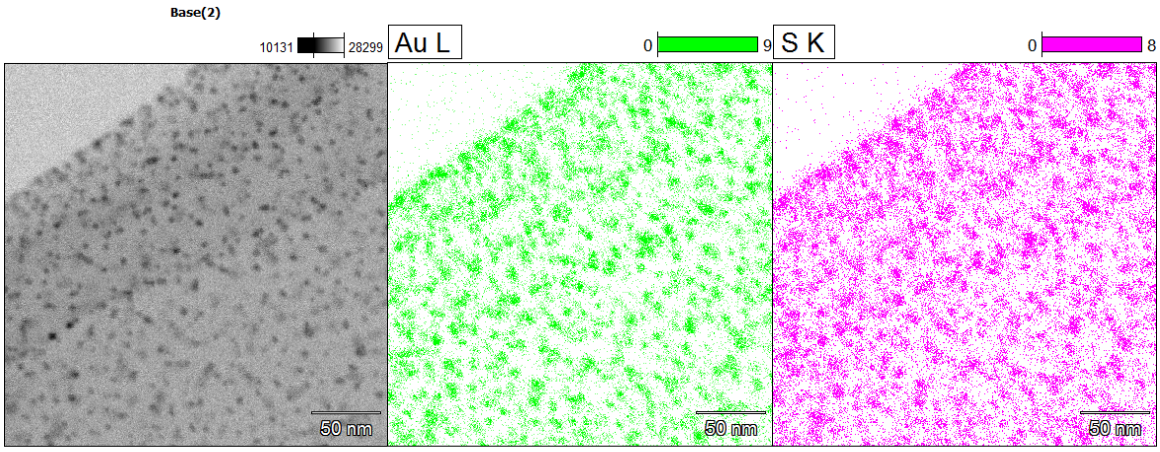

Figure 4.11 S/TEM results for the gold-OH particles showing, left: an SEM image, centre: a gold map, right: a sulfur map.

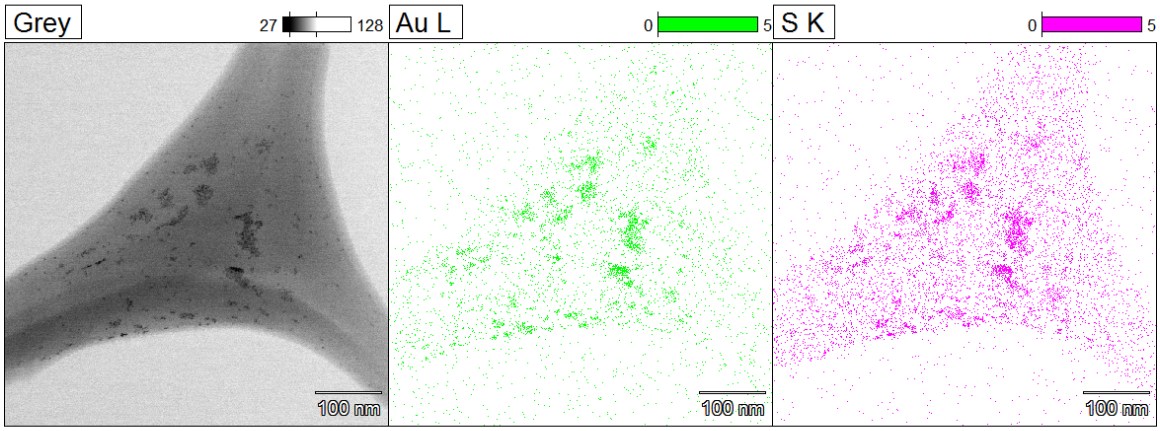

Figure 4.12 S/TEM results for the gold-Ar particles showing, left: an SEM image, centre: a gold map, right: a sulfur map.

4.2 Calorimetric measurements

Solution calorimetry of nanoparticles

Solution calorimetry was used to measure and compare the enthalpies of solution of synthetized and purchased gold-C_8 nanoparticles, as well as gold-OH and gold-Ar nanoparticles toluene, heptane and pyridine, and deionized water. The results of the

experiments can be found on Figure 4.13 – 4.18. From Figure 4.13 it is clear that the enthalpies of solution of the purchased and synthesized gold-C_8 nanoparticles agree to within experimental error in all four solvents at 60 °C. The enthalpy of solution is sensitive to the number of ligands per unit mass, which is in turn sensitive to both the surface coverage (number of ligands/unit area) and particle size (area/unit mass). From the data, one can only suggest that the two share a common value for the number of ligands/unit mass. The enthalpies of solution at 1 g/L are positive, except for in water and possess an uncertainty of 1 J/g. A comparison between gold-C_8 and gold-C_{12} nanoparticles was made (Figure 4.14) and the results agree within the measurement uncertainty. Enthalpies of solution for synthesized gold-C_8, gold-Ar and gold-OH nanoparticles at 25 °C are presented in Figure 4.15. Results for gold-OH and gold- C_8 at 60 °C are presented in Figure 4.16. The dataset at 60°C is more restricted because ethanol boils at too low a temperature, and there was a too limited supply of the gold-Ar particles to perform the measurements.

At 25 °C, Figure 4.15, the enthalpies of solution for each particle type agree to within the experimental error in each solvent, and it can be argued that there is no difference among the solvents (toluene, heptane, ethanol, water) with the exception of gold-Ar in pyridine, which possesses a negative value ~ -1 J/g. The nominal common enthalpy of solution value for all of the other cases is ~ 1 J/g. At 60 °C the differences between gold-C_8 and gold-Ar are marked in contrast to the values at 25 °C. The values and the signs of the enthalpies of solution differ significantly. At 60°C, gold-C_8 and gold-OH show a strong endothermic behavior for non-polar solvents, while for polar solvents they show an opposite behavior. The enthalpy of solution of Gold-C_8 nanoparticles is endothermic in pyridine and exothermic in water, whereas the enthalpies of solution for gold-OH nanoparticles have an opposing trend. The similarities and differences among the nanoparticle types are attributed to the principal ligands on their surfaces but it is important to note that for gold-OH particles, the presence of ethyl chains from the salt, and for gold-Ar particles, the contaminant contributing the unexpected FTIR peak and the aggregation of particles may impact the magnitude of the calorimetric signals.

Comparison between nanoparticle and C_5-Athabasca asphaltene enthalpies of solution

The results obtained with the synthesized nanoparticles are compared with C_5-Athabasca asphaltenes at 25 °C, Figure 4.17, and at 60 °C, Figure 4.18, under comparable experimental conditions. The enthalpies of solution obtained for asphaltenes are endothermic in solvents other than water, at both temperatures. The gold-Ar nanoparticles possess a positive enthalpy of solution in water and a negative enthalpy of solution in pyridine at 25 °C and thus have a contrary qualitative behavior. The enthalpy of solution for gold-OH nanoparticles in water has the wrong sign, and the wrong trend with temperature for pyridine. The negative value at 60 °C contrasts with the positive value for asphaltenes. Only the enthalpies of solution of gold-C_8 nanoparticles possess the correct sign, within experimental uncertainty, and trends with temperature vis-à-vis asphaltenes. The gold-C_8 nanoparticles are the best mimics for C_5-Athabasca asphaltene enthalpies of solution, of the nano-particle types tested. This is an important and arguably an unexpected result depending on ones perspective on the dominance of the archipelago vs continental molecular and hence aggregate prototype. However, other untested ligands or mixes of ligands may exhibit equally good qualitative trends.

Nanoparticles exhibit possible variation in the state of aggregation in each solvent, a negligible contributor to enthalpy of solution [4.2], and variation in ligand – solvent interaction, a significant contributor to enthalpy of solution values. Enthalpies of solution of asphaltenes include these effects plus the potential for dissolution, an unknown and variable positive contributor to the enthalpy of solution. Thus, direct quantitative comparison between values for the nanoparticles and asphaltenes are precluded.

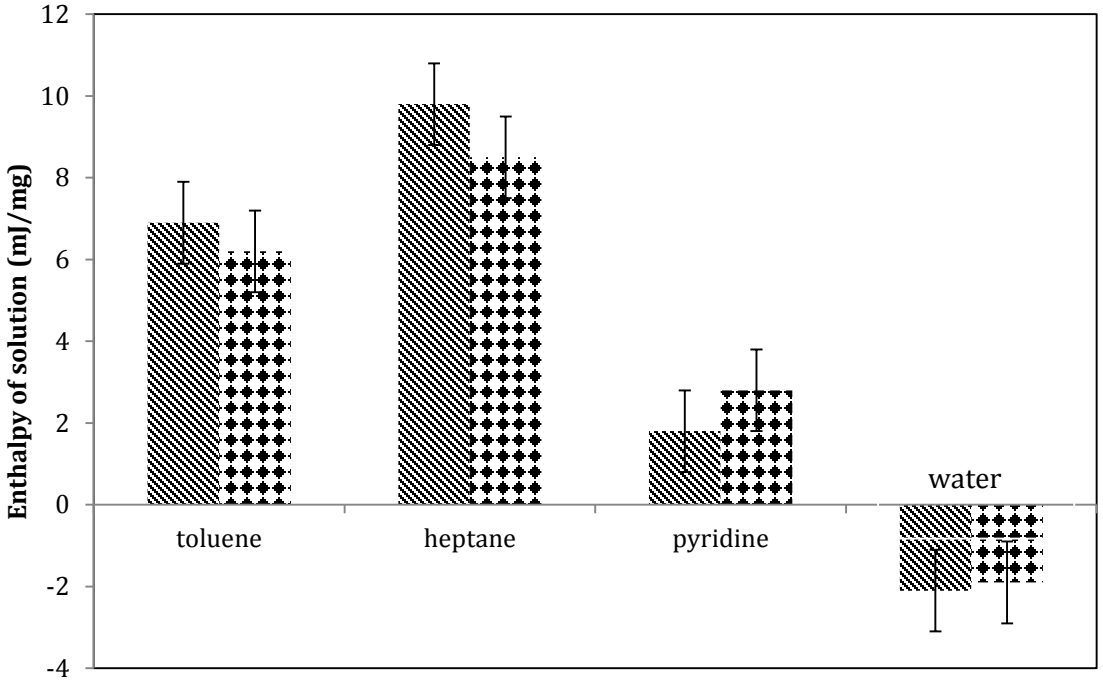

Figure 4.13: Enthalpies of solution of purchased (striped) and synthesized (gridded) gold–C_8 nanoparticles at 60 °C.

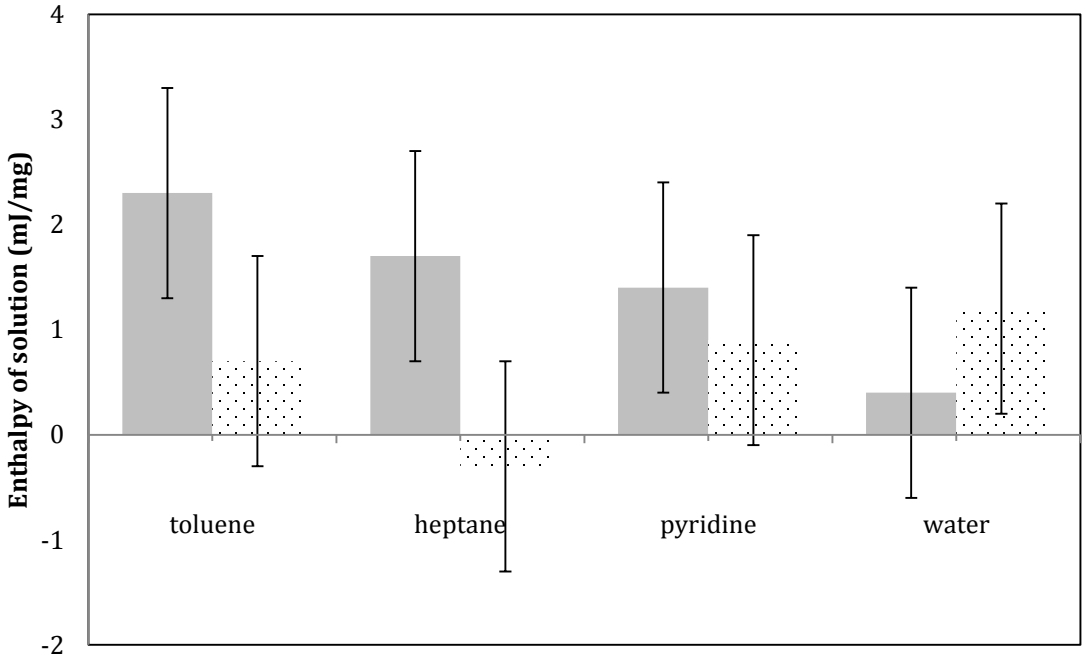

Figure 4.14: Enthalpies of solution of synthesized (grey) gold-C_8 and synthesized (dotted) gold–C_{12} nanoparticles at 25 °C.

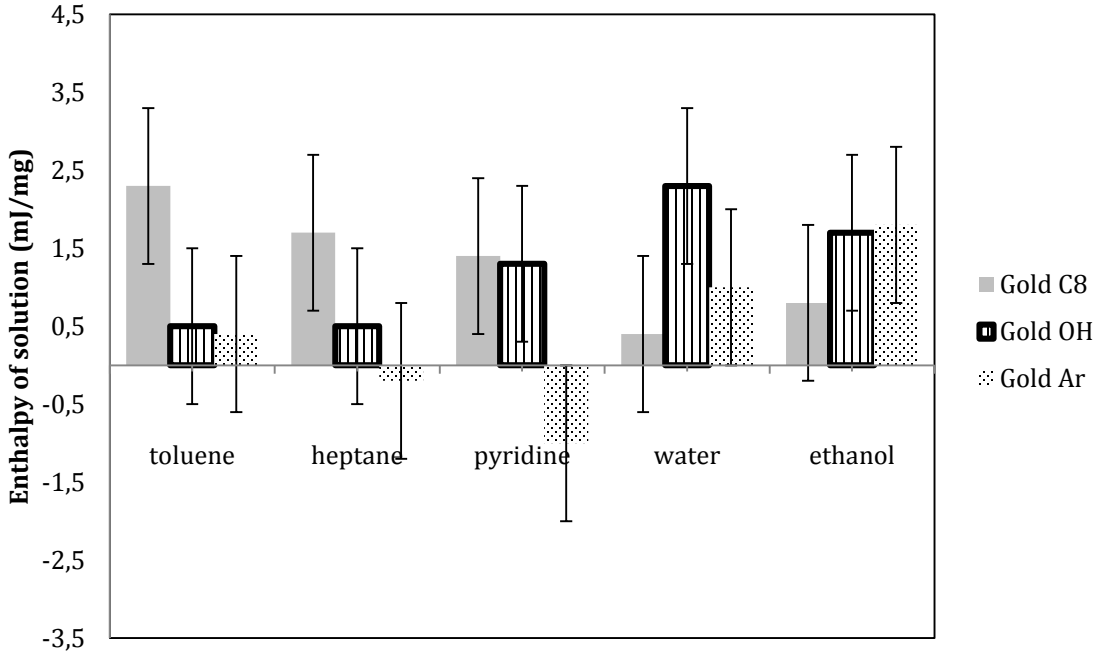

Figure 4.15: Enthalpies of solution for gold-C_8, gold-Ar and gold-OH in various solvents at 25°C.

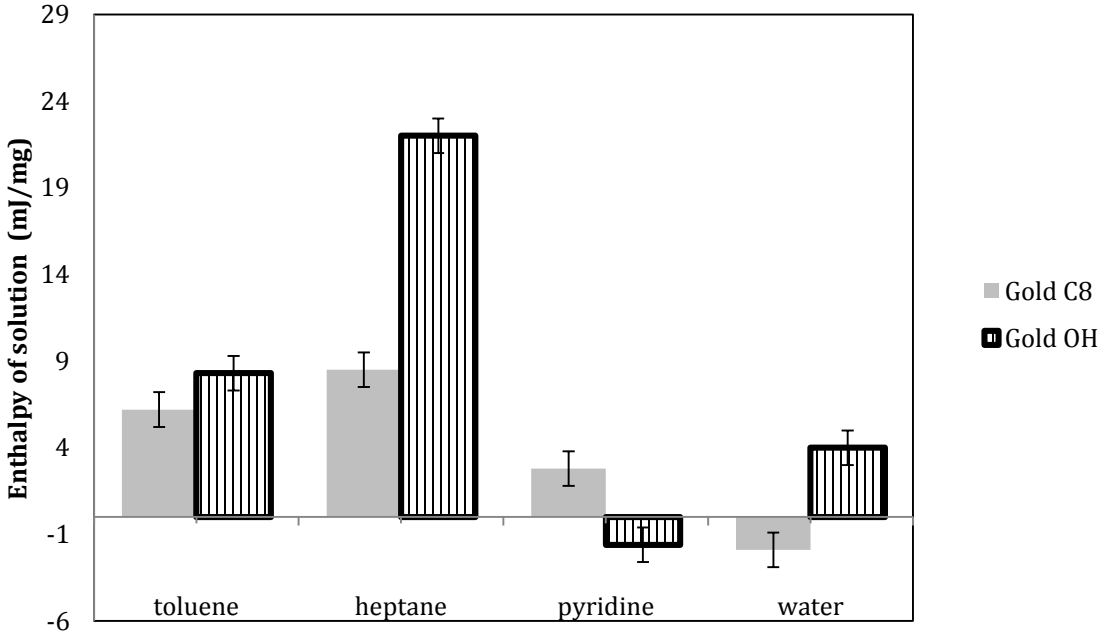

Figure 4.16: Enthalpies of solution for gold-C_8 and gold-OH in various solvents at 60°C.

.

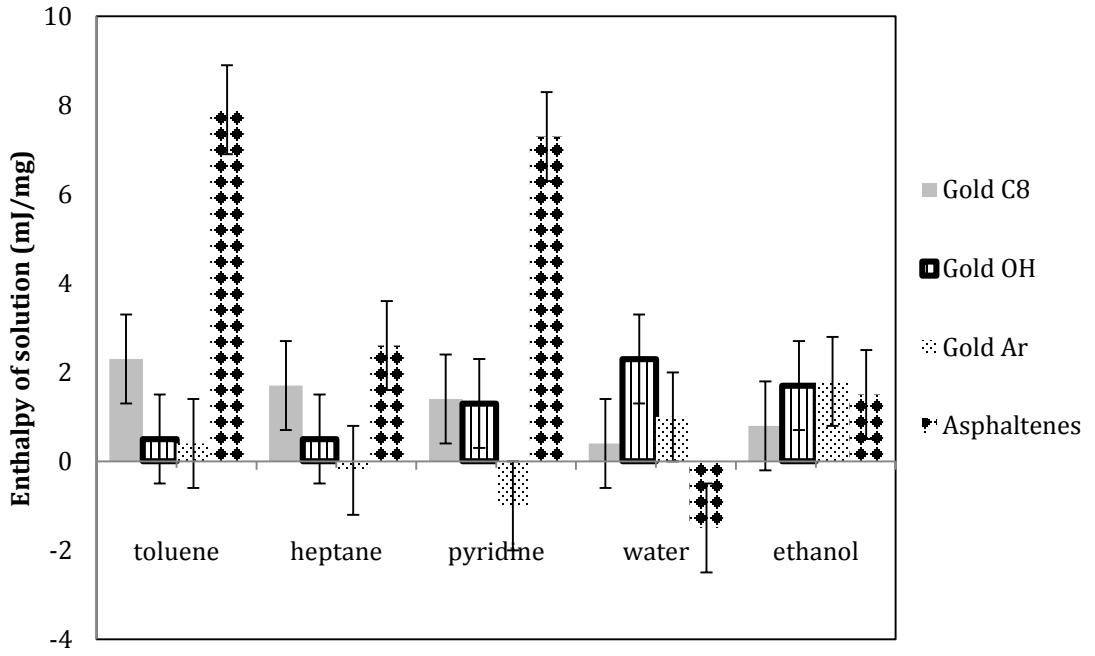

Figure 4.17: A comparison between the enthalpies of solution of gold core nanoparticles and asphaltenes in diverse solvents at 25°C.

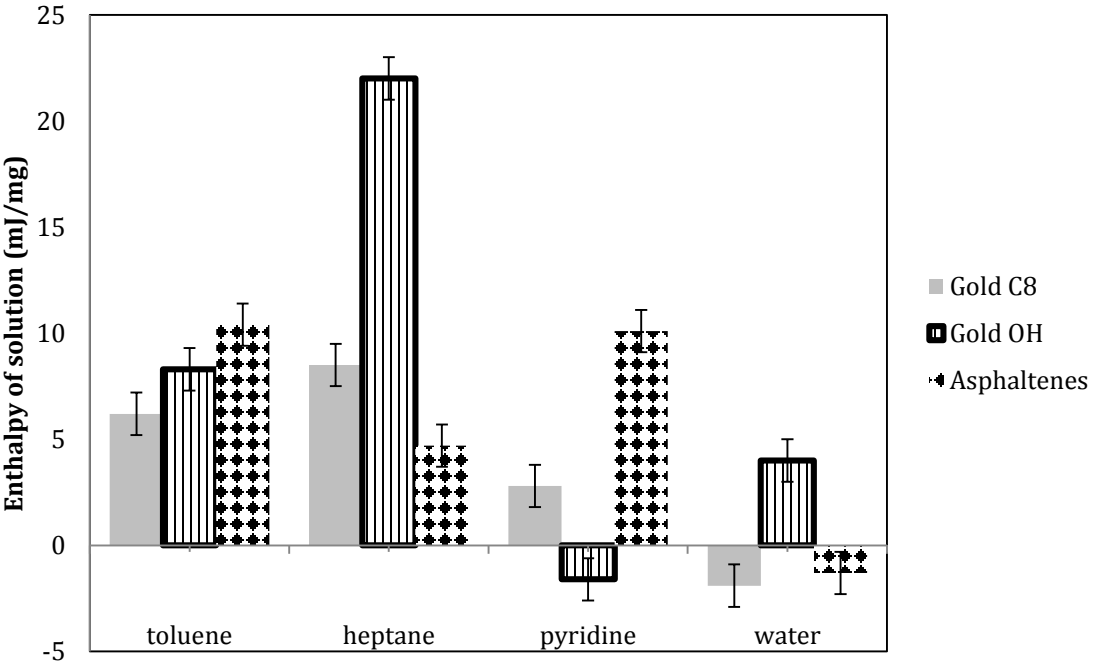

Figure 4.18: A comparison between the enthalpies of solution of gold core nanoparticles and asphaltenes in diverse solvents at 60°C.

4.3Interfacial tension measurements

The pendant drop technique is a reliable technique for interfacial tension measurement between immiscible liquids. For saturated fluids with small mutual solubilities, and in the absence of chemical impurities and small variations in drop volume uncertainties less than 0.10 mN/m can be realized. Such idealized conditions could not be achieved in a shared multiuser laboratory facility. Measurement repeatabilities (within the same experiment) of +/- 0.25 mN/m and measurement reproducibilities (between two experiments) of +/- 1 mN/m were achieved. For example, with pure toluene, drop volume variation from 30 μ L to 20 μ L led to a 1 mN/m decrease in the measured interfacial tension with water. Further, when a drop is injected into an immiscible liquid, for example toluene + nanoparticles into water, the initial value of the interfacial tension should be same as for toluene + water because diffusion of nanoparticles to the interface takes time. If the value falls outside the range of uncertainty other phenomena (impurities, aggregation) are impacting the results. Care must be taken in interpreting the absolute values of measurements, the differences among measurements, and the changes in interfacial tension measurements with time. Different uncertainties apply in each case. Repeatability uncertainties are used to interpret changes in interfacial tension over time within an experiment. Reproducibility uncertainties are necessary to compare outcomes among different experiments.

Gold-C_{12} and gold-Ar nanoparticles disperse in toluene. Their impact on the interfacial tension of toluene + water mixtures at 23°C and atmospheric pressure is shown in Figures 4.19 and 4.20 respectively. For the gold-C_{12} nanoparticles, Figure 4.19, all variations with composition and time fall at or within the relevant uncertainties and are not readily interpreted. For the gold-Ar nanoparticles, Figure 4.20, variations with composition and time fall outside the measurement reproducibility uncertainty and trends with composition and time are evident. The toluene-water interfacial tension drops significantly at less than 100 mg/L. Some interfacial tension measurements were made for gold-OH nanoparticles, see Appendix 6.B, but no solvents or mix of solvents was identified where both particles and the asphaltenes dispersed. Gold-OH nanoparticles

only dispersed in alkanols or pyridine. Some tests were made with mixtures including methanol and dodecane, but the interfacial tension (~ 3mN/m) was too low for difference measurements. Gold-OH nanoparticles do not disperse in toluene and consequently were excluded from the interfacial tension part of the study.

The toluene-water IFT values for gold-C_{12}, and gold-Ar nanoparticles and C_5-Athabasca asphaltenes are compared at 100, 500 and 1000 mg/L in Figures 4.21, 4.22 and 4.23 respectively. At all three concentrations, the IFT impact of asphaltenes falls between that of the gold-C_{12} and gold-Ar nanoparticles. At higher nanoparticle compositions it is evident that the asphaltenes more closely track the interfacial tensions of the gold-C_{12} nanoparticles than that of the gold-Ar nanoparticles in toluene. By progressively adding heptane to the toluene, as shown in the succession of Figures 4.24 to 4.27, where the ratios of toluene to heptane are 3:1, 1:1, 1:3 and pure heptane in volumic proportion respectively, the behavior of the C_5-Athabasca asphaltenes shifts toward and then beyond the track of the gold-Ar nanoparticles. Gold-C_{12} nanoparticles disperse in both toluene and heptane, and have no clear impact on the interfacial tension values vis-à-vis the solvent. By contrast, C_5-Athabasca asphaltenes and gold-Ar nanoparticles do not disperse in heptane and aggregate within minutes of sonication. Their composition in the toluene:heptane drops is uncertain, and it is likely that the aggregates accumulate at the base of drops – affecting their shape and hence the measured IFT value. Quantitative interpretation of the IFT results below at toluene: heptane ratio of 1:1 and 3:1, where significant sedimentation occurs for both gold-AR nanoparticles and asphaltenes is certainly not feasible.

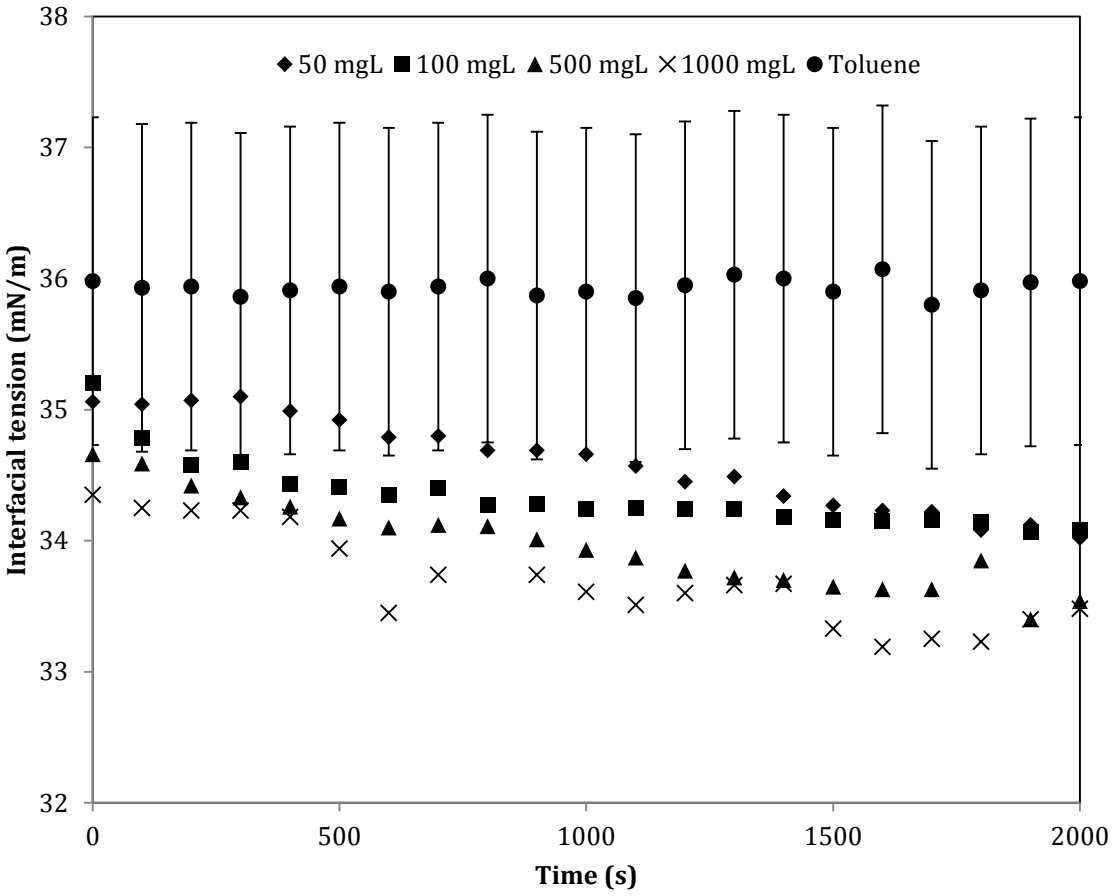

Figure 4.19: Interfacial tension water + (toluene + gold-C_{12} nanoparticle) mixture at 23°C and atmospheric pressure. Nanoparticle concentration is a parameter.

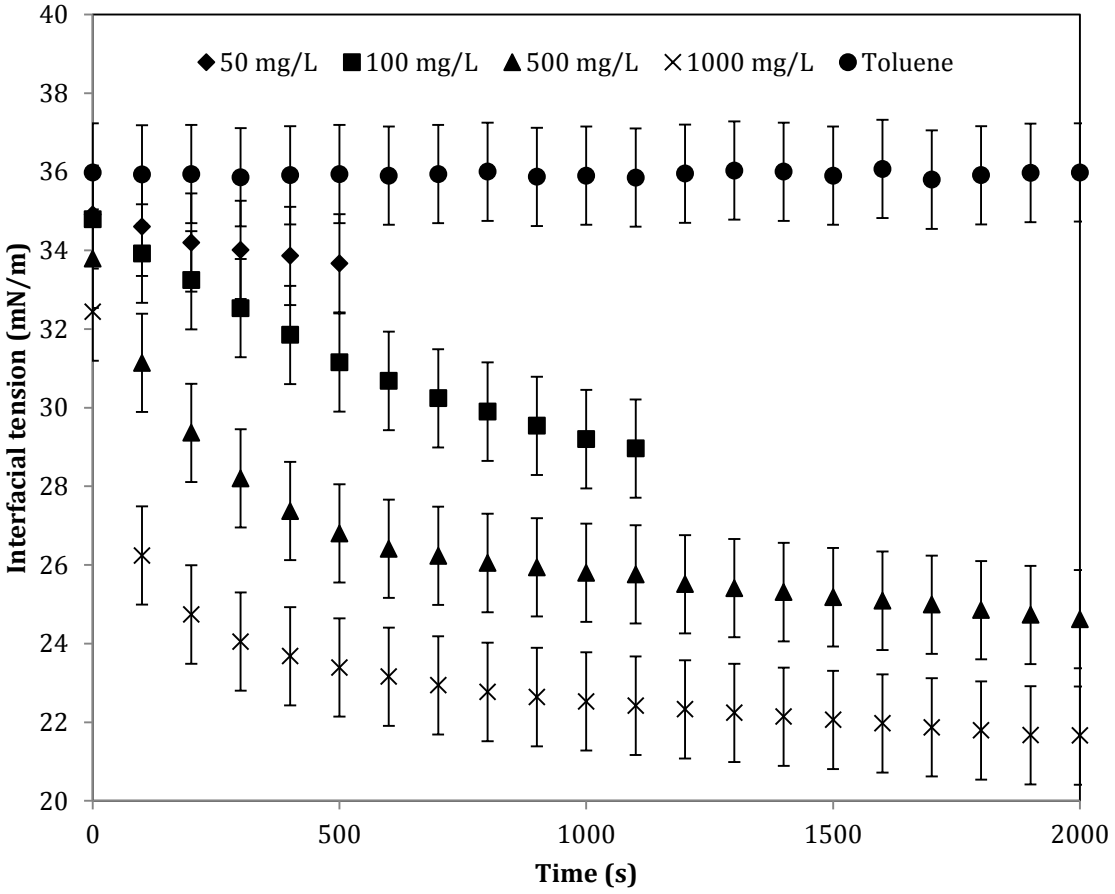

Figure 4.20: Interfacial tension water + (toluene + gold-Ar nanoparticle) mixture at 23°C and atmospheric pressure. Nanoparticle concentration is a parameter.

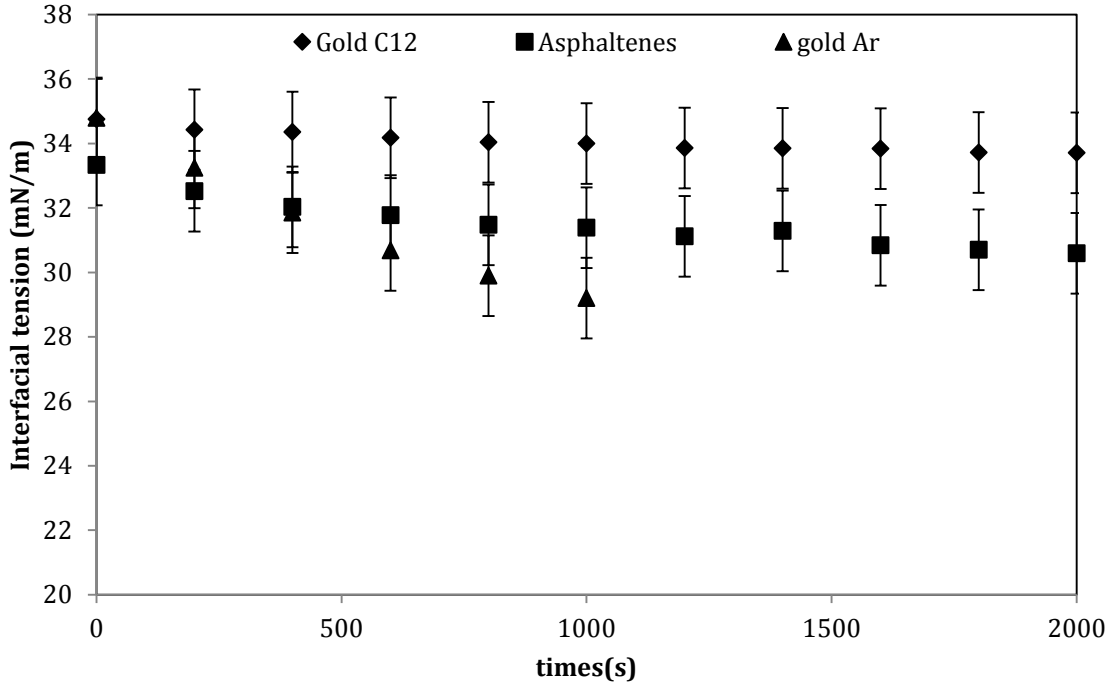

Figure 4.21: Interfacial tension measurements for (toluene + nanoparticle or asphaltene drops at 0.1 g/L) in water at 23°C.

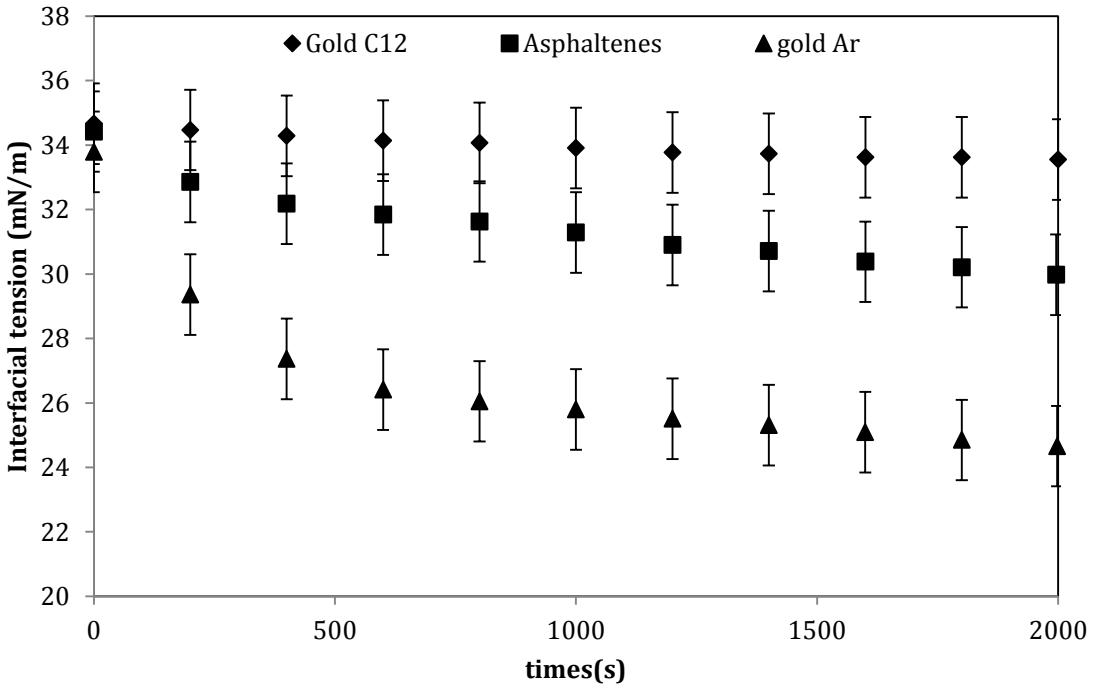

Figure 4.22: Interfacial tension measurements for (toluene + nanoparticle or asphaltene drops at 0.5 g/L) in water at 23°C..

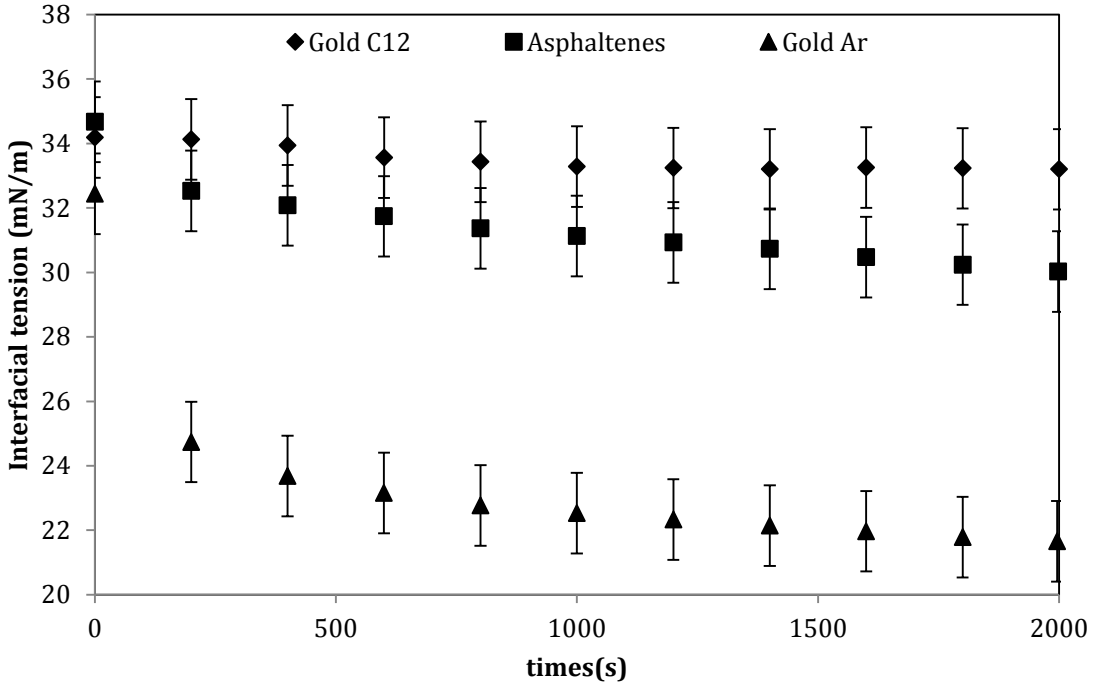

Figure 4.23: Interfacial tension measurements for (toluene + nanoparticle or asphaltene drops at 1 g/L) in water at 23°C..

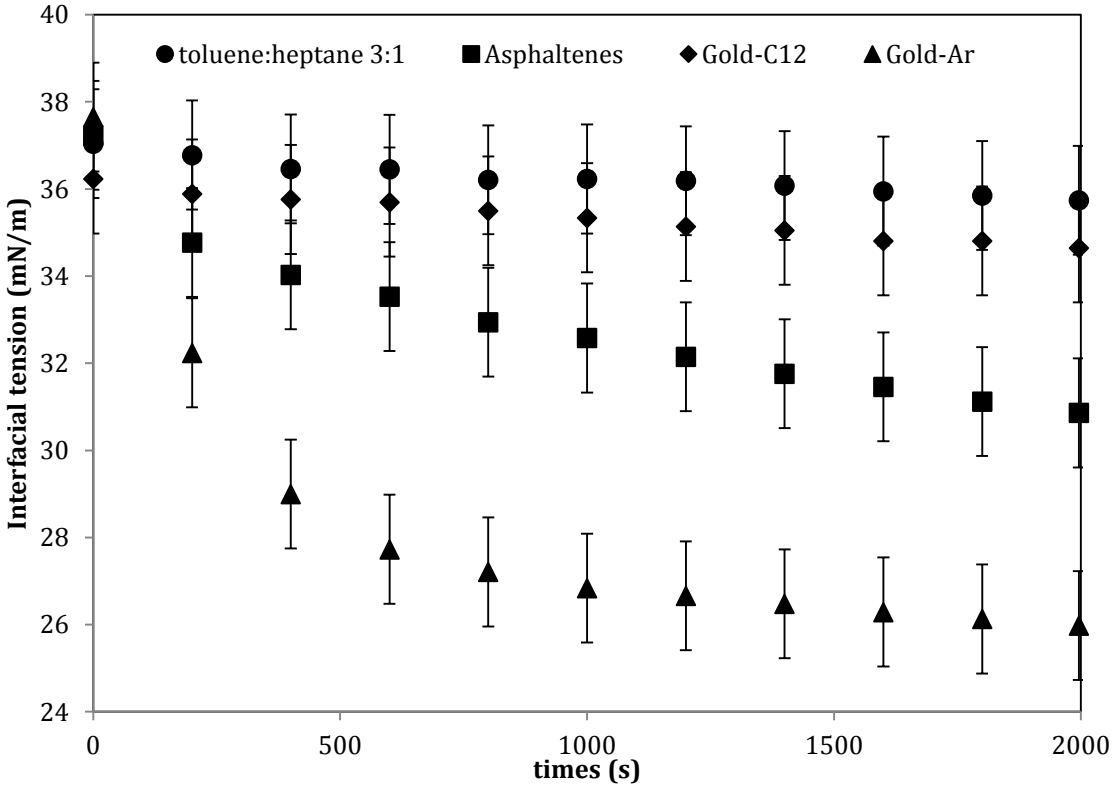

Figure 4.24: Interfacial tension measurements of gold-C_{12}, gold-Ar, Asphaltenes in toluene:heptane (3:1) by volume.

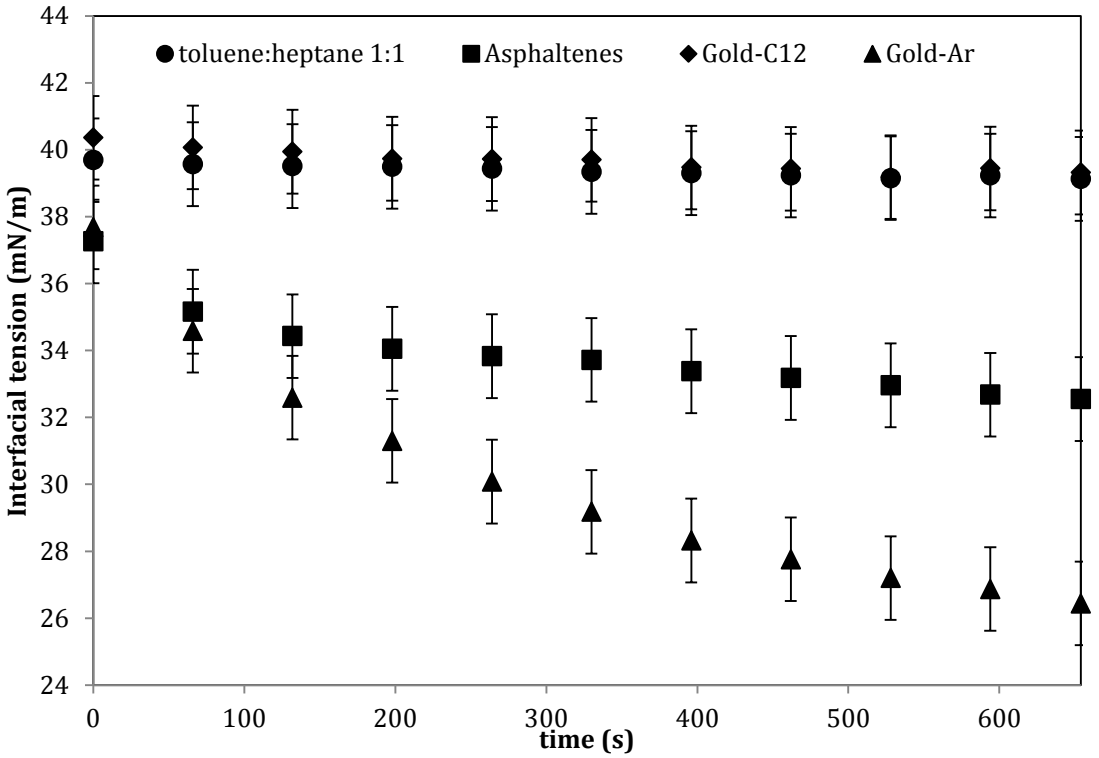

Figure 4.25: Interfacial tension measurements of gold-C_{12}, gold-Ar, Asphaltenes in toluene:heptane (1:1) by volume.

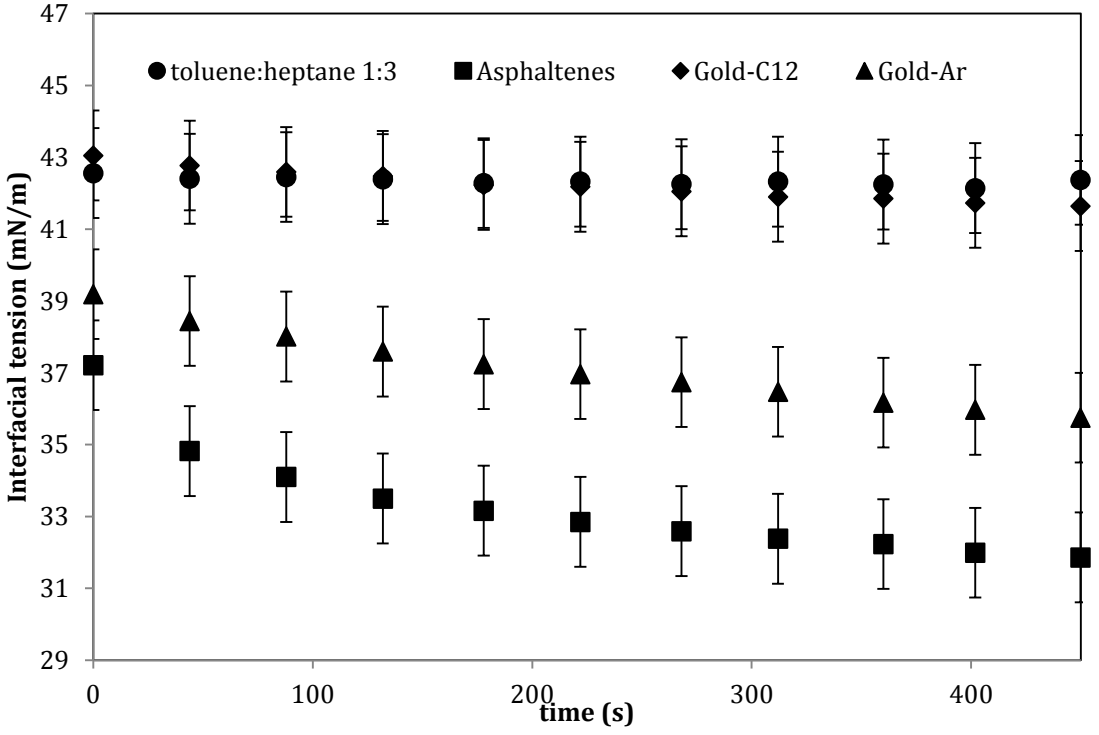

Figure 4.26: Interfacial tension measurements of gold-C_{12}, gold-Ar, Asphaltenes in toluene heptane (3:1) by volume.

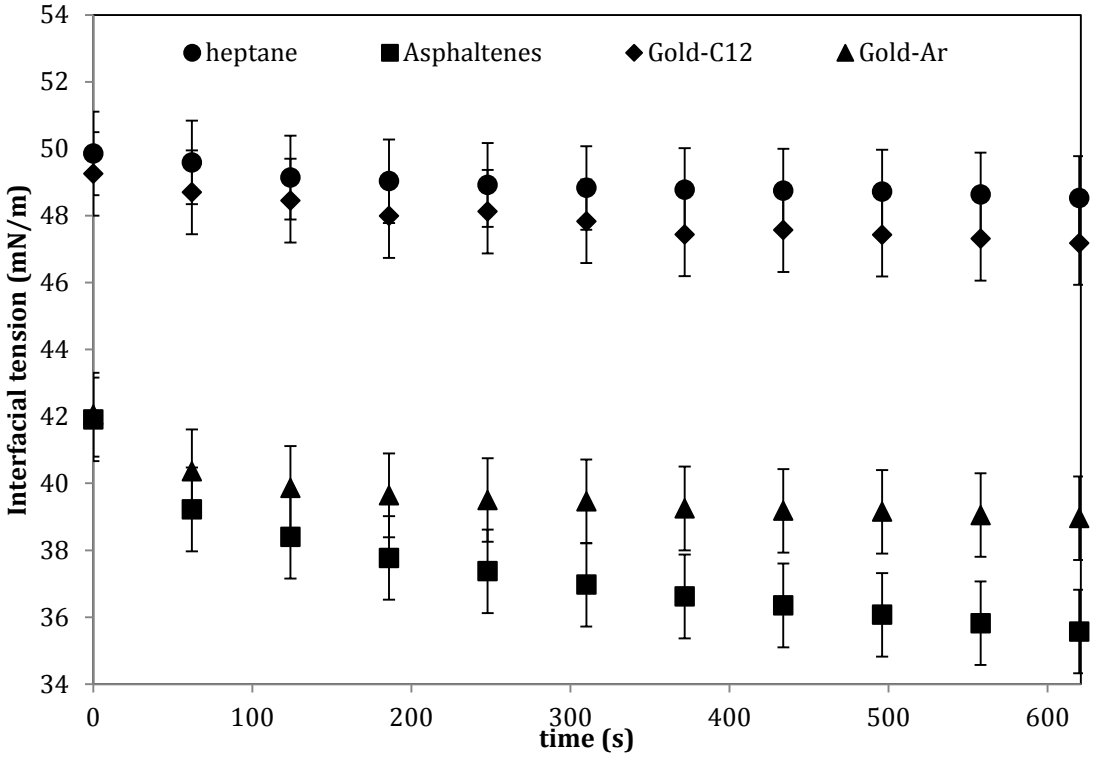

Figure 4.27: Interfacial tension measurements of gold-C_{12}, gold-Ar, Asphaltenes in Heptane.

Interfacial Tension Value Variation with time for gold-Ar and asphaltene containing mixtures.

Parity plots showing how the interfacial tensions of two species vary with time at fixed composition provide information about the relative kinetics of accumulation of species at an interface. As gold-C_{12} particles do not appear to accumulate at toluene or toluene + heptane water interfaces, parity plots are only provided for gold-Ar and asphaltenes. These plots are provided in Figure 4.28, 4.29 and 4.30 for 100, 500, 1000mg/L respectively of the asphaltenes and the gold-Ar nanoparticles; in Figure 4.31 for toluene:heptane 3:1 toluene mixtures at 500 mg/L.

In all but the case of Figure 4.28 the time dependence of sorption differs. At short times, the asphaltenes appear to sorb more quickly than the gold-Ar nanoparticles and the asphaltenes continue to sorb after the nanoparticles appear to have reached a steady state value. At intermediate times the nanoparticles appear to sorb more rapidly than the asphaltenes.

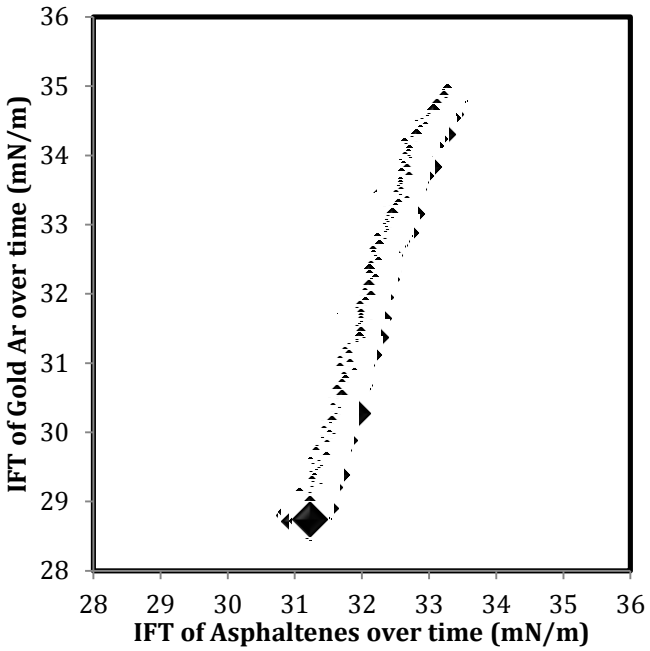

Figure 4.28: Parity plots for the variation of C_5-Athabsca asphaltenes and gold-Ar nanoparticles in toluene: 100mg/L

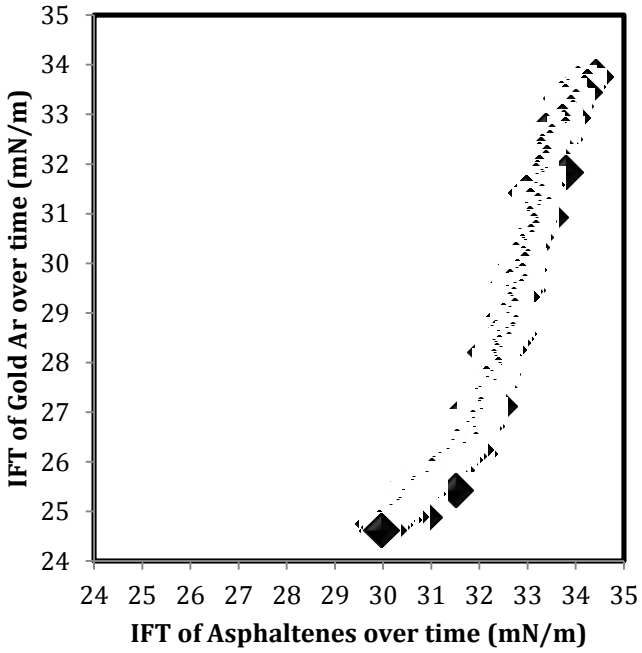

Figure 4.29: Parity plots for the variation of C5-Athabsca asphaltenes and gold-Ar nanoparticles in toluene: 500mg/L

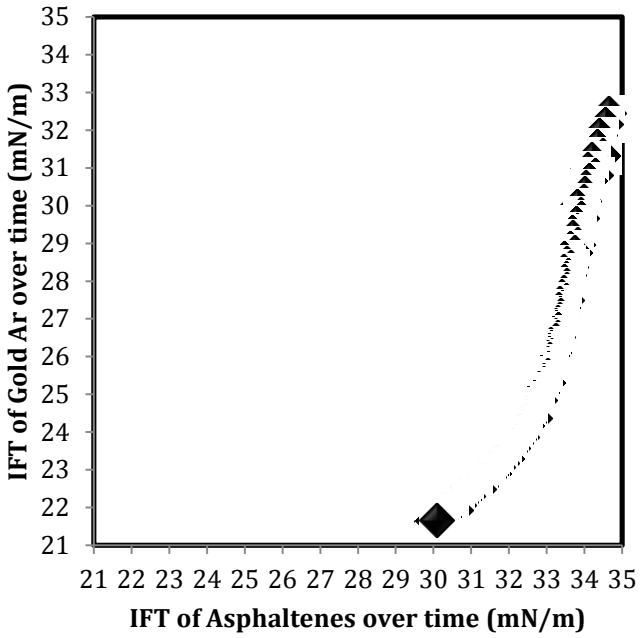

Figure 4.30: Parity plots for the variation of C_5-Athabsca asphaltenes and gold-Ar nanoparticles in toluene: 1000mg/L

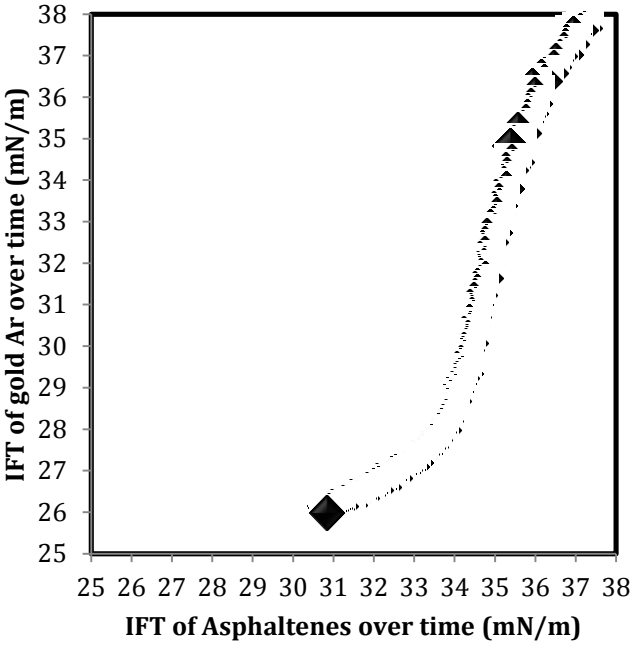

Figure 4.31: Parity plots for the variation of C_5-Athabsca asphaltenes and gold-Ar nanoparticles in toluene:heptane 3:1 : 500mg/L

4.4 Experimental Result Summary

Gold core nanoparticles with organic ligands on their outer surface were prepared and characterized. Calorimetric measurements provided information about the behavior of these nanoparticles in different solvents and these behaviors are compared to those of C_5-asphaltenes extracted from Athabasca Bitumen. The results show that the gold-alkyl nanoparticles mimic the sign of the solution behavior of the asphaltenes. By contrast, the gold-Ar nanoparticles mimic the interfacial tension behavior of the asphaltenes at water/toluene and water/toluene+heptane interfaces although there are differences in the sorption kinetics. The gold-C_{12} nanoparticles do not appear to be active at these interfaces, within the uncertainty of the measurements.

Chapter 5: Conclusions & future work

5.1 Conclusions

Three types of gold+ligand nanoparticles were synthetized and characterized. The particles, with a mean size of 3.5nm to 5nm, and three ligands dodecanethiol, 11-mercaptoundecanol and biphenyl-4-thiol include features and characteristics that are thought to be present on asphaltene nano-aggregate surfaces. The surface coverage of the desired ligand was 29%, 58% and 59% respectively. While every effort was made to minimize impurities on the particle surfaces, impurities on gold-OH nanoparticles were measured and included ethyl chains from the gold salt. Gold-Ar nanoparticles included an undetermined impurity. Gold-$C_{8/12}$ nanoparticles shared the same behaviors as purchased equivalents and no surface impurities were found for these particles during analysis.

The solution and interfacial behaviors of the three nanoparticle types are shown to differ from one another both quantitatively and qualitatively.

The signs and trends of the enthalpy of solution values for gold-C_8 nanoparticles mimic the behaviors of C_5-Athabasca asphaltenes in solution based on measurements in this work, as well as measurements in the literature [5.1]. The gold-OH and the gold-Ar nanoparticles do not mimic the solution behaviors of asphaltenes. As the nanoparticles do not dissolve and a fraction of the asphaltenes may dissolve, quantitative comparisons among the enthalpy of solution values cannot be made.

From the interfacial tension measurements, it is clear that gold-C_{12} nanoparticles are not active at toluene-water or (toluene+heptane) – water interfaces. This behavior contrasts with the behavior of asphaltenes and gold-Ar nanoparticles at the same interfaces. Both are active at these interfaces. In toluene and in toluene + heptane mixtures where asphaltenes and gold-Ar nanoparticles do not aggregate significantly, gold-Ar nanoparticles are much more surface active than asphaltenes, and the kinetics of adsorption at the interface also differ significantly from those of asphaltenes.

While it is possible that other gold core + individual ligands may prove to be better mimics for the behavior of asphaltene nanoaggregates in solution and at interfaces, it is clear from this study that asphaltene nanoaggregate behaviors can be mimicked by a combination of gold + ligand nanoparticles where alkyl ligands play a dominant role, aromatic ligands a secondary role, and hydroxyl groups a peripheral role.

5.2Recommendations for future work

This work is at a formative stage. There are numerous potential directions the work may take. Some directions are presented here.

- The solution and interfacial properties of nanoscale objects is of intrinsic interest in diverse applications. Many are removed from the focus of this work. Systematic study of the behaviours of individual gold core + ligand nanoparticles and mixtures of gold core nanoparticles with different ligands in solution and at interfaces is warranted.
- Synthesis of gold nanoparticles possessing other individual functional groups thought to be present in asphaltenes is recommended. Two examples (1-(11-Mercaptoundecyl)imidazole and 11-Mercaptoundecanoic acid are discussed in Chapter 3.
- Creation and evaluation in the present context of Janus nanoparticles (particles with different ligands covering the hemispheres of the particle) or randomly distributed bi-functional nanoparticles would permit the comparison of bi-functional particles (e.g.: alkyl groups and aromatic groups) with asphaltene interfacial and solution properties.
- Improving the quality of the synthesized nanoparticles. For example, adding a new ligand exchange step for gold-OH that would reduce the residual phosphorus content.
- Synthesis of gold core nanoparticles with ligands on their surfaces is a challenging specialty. Direct collaboration with experts is recommended.

- Reducing the reproducibility uncertainty of interfacial tension measurements would facilitate the interpretation of interfacial tension outcomes.

References

Chapter 1

[1.1] H. B, "Geochemical Studies - 4. Physical and Chemical Properties of sediments and Bitumen form some Alberta Oil Sand Deposits," Alberta Geological Survey, Open file report 1993.

[1.2] Based on publication number of web of knowledge. webofknowledge.com

[1.3] M. Ghanavati, M.-J. Shojaei, and A. R. S. A., "Effects of Asphaltene Content and Temperature on Viscosity of Iranian Heavy Crude Oil: Experimental and Modeling Study," *Energy & Fuels*, vol. 27, no. 12, pp. 7217–7232, Dec. 2013.

[1.4] P. Luo and Y. Gu, "Effects of asphaltene content on the heavy oil viscosity at different temperatures," *Fuel*, vol. 86, no. 7–8, pp. 1069–1078, May 2007.

[1.5] J. Sjöblom, P. V. Hemmingsen, and H. Kallevik, "The Role of Asphaltenes in Stabilizing Water-in-Crude Oil Emulsions," in *Asphaltenes, Heavy Oils, and Petroleomics*, O. C. Mullins, E. Y. Sheu, A. Hammami, and A. G. Marshall, Eds. Springer New York, 2007, pp. 549–587.

[1.6]J. P. Rane, D. Harbottle, V. Pauchard, A. Couzis, and S. Banerjee, "Adsorption Kinetics of Asphaltenes at the Oil–Water Interface and Nanoaggregation in the Bulk," *Langmuir*, vol. 28, no. 26, pp. 9986–9995, Jul. 2012.

[1.7] Leontaritis, K. J. "Asphaltene Deposition: A Comprehensive Description of Problem Manifestations and Modeling Approaches." *Society of Petroleum Engineers.* doi:10.2118/18892-MS Published January 1989

[1.8] F. J. A.-V. José L. Mendoza de la Cruz, "Asphaltene-Induced Precipitation and Deposition During Pressure Depletion on a Porous Medium: An Experimental Investigation and Modeling Approach," *Energy & Fuels* , vol. 23, no. 11, 2009.

[1.9] R. Martínez-Palou, M. de L. Mosqueira, B. Zapata-Rendón, E. Mar-Juárez, C. Bernal-Huicochea, J. de la Cruz Clavel-López, and J. Aburto, "Transportation of heavy and extra-heavy crude oil by pipeline: A review," *Journal of Petroleum Science and Engineering*, vol. 75, no. 3–4, pp. 274–282, Jan. 2011.

[1.10] I. Gawel, D. Bociarska, and P. Biskupski, "Effect of asphaltenes on hydroprocessing of heavy oils and residua," *Applied Catalysis A: General*, vol. 295, no. 1, pp. 89–94, Oct. 2005.

[1.11] H. W. Yarranton, D. P. Ortiz, D. M. Barrera, E. N. Baydak, L. Barré, D. Frot, J. Eyssautier, H. Zeng, Z. Xu, G. Dechaine, M. Becerra, J. M. Shaw, A. M. McKenna, M. M. Mapolelo, C. Bohne, Z. Yang, and J. Oake, "On the Size Distribution of Self-Associated Asphaltenes," *Energy & Fuels*, vol. 27, no. 9, pp. 5083–5106, Sep. 2013.

[1.12] A. E. Pomerantz, M. R. Hammond, A. L. Morrow, O. C. Mullins, and R. N. Zare, "Asphaltene Molecular-Mass Distribution Determined by Two-Step Laser Mass Spectrometry," *Energy & Fuels*, vol. 23, pp. 1162–1168, 2009.

[1.13] H. Groenzin and O. C. Mullins, "Asphaltene Molecular Size and Weight by Time-Resolved Fluorescence Depolarization," in *Asphaltenes, Heavy Oils, and Petroleomics*, O. C. Mullins, E. Y. Sheu, A. Hammami, and A. G. Marshall, Eds. Springer New York, 2007, pp. 17–62.

[1.14] J. T. Miller, R. B. Fisher, P. Thiyagarajan, R. E. Winans, and J. E. Hunt, "Subfractionation and Characterization of Mayan Asphaltene," *Energy & Fuels*, vol. 12, no. 6, pp. 1290–1298, Nov. 1998.

[1.15] S. Yoon, S. D. Bhatt, W. Lee, H. Y. Lee, S. Y. Jeong, J.-O. Baeg, and C. W. Lee, "Separation and characterization of bitumen from Athabasca oil sand," *Korean J. Chem. Eng.*, vol. 26, no. 1, pp. 64–71, Jan. 2009.

[1.16] J. D. Payzant, E. M. Lown, and O. P. Strausz, "Structural units of Athabasca asphaltene: the aromatics with a linear carbon framework," *Energy & Fuels*, vol. 5, no. 3, pp. 445–453, May 1991.

[1.17] G. C. Klein, S. Kim, R. P. Rodgers, A. G. Marshall, and A. Yen, "Mass Spectral Analysis of Asphaltenes. II. Detailed Compositional Comparison of Asphaltenes Deposit to Its Crude Oil Counterpart for Two Geographically Different Crude Oils by ESI FT-ICR MS," *Energy & Fuels*, vol. 20, no. 5, pp. 1973–1979, Sep. 2006.

[1.18] S. Wang, C. Yang, C. Xu, S. Zhao, and Q. Shi, "Separation and characterization of petroleum asphaltene fractions by ESI FT-ICR MS and UV-vis spectrometer," *Sci. China Chem.*, vol. 56, no. 7, pp. 856–862, Jun. 2013.

[1.19] John M. Shaw, Marco A. Satyro and Harvey W. Yarranton, Chapter X., The Phase Behaviour and Properties of Heavy Oils, "Practical Advances in Petroleum Production and Processing", co-edited by Chang Samuel Hsu and Paul R. Robinson. Publication expected, Fall 2015.

[1.20] A. Z. Tukhvatullina, E. E. Barskaya, V. N. Kouryakov, Y. M. Ganeeva, T. N. Yusupova, and G. V. Romanov, "Supramolecular Structures of Oil Systems as the Key to Regulation of Oil Behavior," *J Pet Environ Biotechnol*, vol. 4, no. 152, p. 2, 2013.

[1.21] O. C. Mullins, H. Sabbah, J. Eyssautier, A. E. Pomerantz, L. Barré, A. B. Andrews, Y. Ruiz-Morales, F. Mostowfi, R. McFarlane, L. Goual, R. Lepkowicz, T. Cooper, J. Orbulescu, R. M. Leblanc, J. Edwards, and R. N. Zare, "Advances in Asphaltene Science and the Yen–Mullins Model," *Energy & Fuels*, vol. 26, no. 7, pp. 3986–4003, Jul. 2012.

[1.22] H. Sabbah, A. L. Morrow, A. E. Pomerantz, and R. N. Zare, "Evidence for Island Structures as the Dominant Architecture of Asphaltenes," *Energy & Fuels*, vol. 25, no. 4, pp. 1597–1604, Apr. 2011.

[1.23] O. C. Mullins, "The Modified Yen Model†," *Energy & Fuels*, vol. 24, no. 4, pp. 2179–2207, 2010.

[1.24] F. Alvarez-Ramírez and Y. Ruiz-Morales, "Island versus archipelago architecture for asphaltenes: polycyclic aromatic hydrocarbon dimer theoretical studies," *Energy & Fuels*, vol. 27, no. 4, pp. 1791–1808, 2013.

[1.25] M. R. Gray, "Consistency of asphaltene chemical structures with pyrolysis and coking behavior," *Energy & Fuels*, vol. 17, no. 6, pp. 1566–1569, 2003.

[1.26] T. M. Jarrell, C. Jin, J. S. Riedeman, B. C. Owen, X. Tan, A. Scherer, R. R. Tykwinski, M. R. Gray, P. Slater, and H. I. Kenttämaa, "Elucidation of structural information achievable for asphaltenes via collision-activated dissociation of their molecular ions in MSn experiments: A model compound study," *Fuel*, vol. 133, pp. 106–114, Oct. 2014.

[1.27] G. Andreatta, C. C. Goncalves, G. Buffin, N. Bostrom, C. M. Quintella, F. Arteaga-Larios, E. Pérez, and O. C. Mullins, "Nanoaggregates and Structure−Function Relations in Asphaltenes†," *Energy & Fuels*, vol. 19, no. 4, pp. 1282–1289, Jul. 2005.

[1.28] A. A. Lamia Goual, "Predicting the Adsorption of Asphaltenes from Their Electrical Conductivity," *Energy & Fuels*, vol. 24, no. 1, 2009.

[1.29] E. Y. Sheu, "Petroleomics and Characterization of Asphaltene Aggregates Using Small Angle Scattering," in *Asphaltenes, Heavy Oils, and Petroleomics*, O. C. Mullins, E. Y. Sheu, A. Hammami, and A. G. Marshall, Eds. Springer New York, 2007, pp. 353–374.

[1.30] L. Barré, S. Simon, and T. Palermo, "Solution Properties of Asphaltenes," *Langmuir*, vol. 24, no. 8, pp. 3709–3717, Apr. 2008.

[1.31] E. Rogel, "Thermodynamic Modeling of Asphaltene Aggregation," *Langmuir*, vol. 20, no. 3, pp. 1003–1012, Feb. 2004.

[1.32] K. Oh and M. D. Deo, "Near Infrared Spectroscopy to Study Asphaltene Aggregation in Solvents," in *Asphaltenes, Heavy Oils, and Petroleomics*, O. C. Mullins, E. Y. Sheu, A. Hammami, and A. G. Marshall, Eds. Springer New York, 2007, pp. 469–488.

[1.33] L. Goual, M. Sedghi, H. Zeng, F. Mostowfi, R. McFarlane, and O. C. Mullins, "On the formation and properties of asphaltene nanoaggregates and clusters by DC-conductivity and centrifugation," *Fuel*, vol. 90, no. 7, pp. 2480–2490, Jul. 2011.

[1.34] J. Tsang Mui Ching, "On the Nanofiltration of Asphaltene Solutions, Crude Oils, and Emulsions," *Energy & Fuels*, 2010 24 (9), 5028-5037 2010.

[1.35] J. Tsang Mui Ching, "On the Nanofiltration of Asphaltene Solutions, Crude Oils, and Emulsions," *Energy & Fuels*, 2010 24 (9), 5028-5037 2010.

[1.36] O. C. Mullins, D. E. Freed, J. Y. Zuo, H. Elshahawi, M. E. Cribbs, V. K. Mishra, and A. Gisolf, "Downhole Fluid Analysis coupled with Asphalene Nanoscience for Reservoir Evaluation," *Perth, Australia, SPWLA*, 2010.

[1.37] I. K. Yudin and M. A. Anisimov, "Dynamic Light Scattering Monitoring of Asphaltene Aggregation in Crude Oils and Hydrocarbon Solutions," in *Asphaltenes, Heavy Oils, and Petroleomics*, O. C. Mullins, E. Y. Sheu, A. Hammami, and A. G. Marshall, Eds. Springer New York, 2007, pp. 439–468.

[1.38] J. De León, B. Hoyos, and W. Cañas-Marín, "Insights of asphaltene aggregation mechanism from molecular dynamics simulation," *system*, vol. 9, p. 10.

[1.39] M. R. Gray, R. R. Tykwinski, J. M. Stryker, and X. Tan, "Supramolecular assembly model for aggregation of petroleum asphaltenes," *Energy & Fuels*, vol. 25, no. 7, pp. 3125–3134, 2011.

[1.40] T. Maqbool, A. T. Balgoa, and H. S. Fogler, "Revisiting Asphaltene Precipitation from Crude Oils: A Case of Neglected Kinetic Effects," *Energy & Fuels*, vol. 23, no. 7, pp. 3681–3686, Jul. 2009.

[1.41] T. Maqbool, A. T. Balgoa, and H. S. Fogler, "Revisiting Asphaltene Precipitation from Crude Oils: A Case of Neglected Kinetic Effects," *Energy & Fuels*, vol. 23, no. 7, pp. 3681–3686, Jul. 2009.

[1.42] K. J. Leontaritis, "The Asphaltene and Wax Deposition Envelopes," *Fuel Science and Technology International*, vol. 14, no. 1–2, pp. 13–39, Jan. 1996.

[1.43] A. K. M. Jamaluddin, J. Creek, C. S. Kabir, J. D. McFadden, D. D'Cruz, J. Manakalathil, N. Joshi, and B. Ross, "Laboratory Techniques to Measure Thermodynamic Asphaltene Instability," *Journal of Canadian Petroleum Technology*, vol. 41, no. 07, Jul. 2002.

[1.44] J. Ancheyta, F. Trejo, and M. S. Rana, *Asphaltenes: Chemical Transformation during Hydroprocessing of Heavy Oils*. CRC Press, 2010. ISBN 9781420066302

[1.45] J. X. Wang, K. R. Brower, and J. S. Buckley, "Observation of Asphaltene Destabilization at Elevated Temperature and Pressure," *SPE Journal*, vol. 5, no. 04, pp. 420–425, Dec. 2000.

[1.46] P. Juyal, V. Ho, A. Yen, and S. J. Allenson, "Reversibility of Asphaltene Flocculation with Chemicals," *Energy & Fuels*, vol. 26, no. 5, pp. 2631–2640, May 2012.

Chapter 2

[2.1] https://apps.webofknowledge.com Search "nanoparticles" in the patent section.

[2.2] S. C. Robert A Taylor, "Small Particles, Big Impacts: A Review of the Diverse Applications of Nanofluids," *J. Phys.* vol. 113, p. 011301, 2013.

[2.3] K. L. Kelly, E. Coronado, L. L. Zhao, and G. C. Schatz, "The optical properties of metal nanoparticles: The influence of size, shape, and dielectric environment," *J. Phys. Chem. B*, vol. 107, no. 3, pp. 668–677, Jan. 2003.

[2.4] S. Eustis and M. A. El-Sayed, "Why gold nanoparticles are more precious than pretty gold: Noble metal surface plasmon resonance and its enhancement of the radiative and nonradiative properties of nanocrystals of different shapes," *Chem. Soc. Rev.*, vol. 35, no. 3, pp. 209–217, Feb. 2006.

[2.5] J. Homola, S. S. Yee, and G. Gauglitz, "Surface plasmon resonance sensors: review," *Sens. Actuator B-Chem.*, vol. 54, no. 1–2, pp. 3–15, Jan. 1999.

[2.6] S. Özerinç, S. Kakaç, and A. G. Yazıcıoğlu, "Enhanced thermal conductivity of nanofluids: a state-of-the-art review," *Microfluid Nanofluid*, vol. 8, no. 2, pp. 145–170, Nov. 2009.

[2.7] W. Yu, D. M. France, J. L. Routbort, and S. U. S. Choi, "Review and Comparison of Nanofluid Thermal Conductivity and Heat Transfer Enhancements," *Heat Transfer Engineering*, vol. 29, no. 5, pp. 432–460, May 2008.

[2.8] A. M. J. Tertsinidou Georgia, "The Apparent Thermal Conductivity of Liquids Containing Solid Particles of Nanometer Dimensions: A Critique," *International Journal of Thermophysics*, vol. 36, pp. 1367–1395, 2015.

[2.9] D. Wen, G. Lin, S. Vafaei, and K. Zhang, "Review of nanofluids for heat transfer applications," *Particuology*, vol. 7, no. 2, pp. 141–150, Apr. 2009.

[2.10] T. W. Ebbesen, H. J. Lezec, H. Hiura, J. W. Bennett, H. F. Ghaemi, and T. Thio, "Electrical conductivity of individual carbon nanotubes," *Nature*, vol. 382, no. 6586, pp. 54–56, Jul. 1996.

[2.11] M. Ferrier, A. Kasumov, R. Deblock, S. Guéron, and H. Bouchiat, "Induced and intrinsic superconductivity in carbon nanotubes," *J. Phys. D: Appl. Phys.*, vol. 43, no. 37, Sep. 2010.

[2.12] E. O. Chukwuocha, "Theoretical Studies on the Effect of Confinement on Quantum Dots Using the Brus Equation," *World Journal of Condensed Matter Physics*, vol. 02, no. 02, pp. 96–100, 2012.

[2.13] P. V. Kamat, "Quantum Dot Solar Cells. Semiconductor Nanocrystals as Light Harvesters†," *J. Phys. Chem. C*, vol. 112, no. 48, pp. 18737–18753, 2008.

[2.14] T. Prasad Yadav, R. Manohar Yadav, and D. Pratap Singh, "Mechanical Milling: a Top Down Approach for the Synthesis of Nanomaterials and Nanocomposites," *Nanoscience and Nanotechnology*, vol. 2, no. 3, pp. 22–48, Aug. 2012.

[2.15] M. Inkyo, T. Tahara, T. Iwaki, F. Iskandar, C. J. Hogan Jr., and K. Okuyama, "Experimental investigation of nanoparticle dispersion by beads milling with centrifugal bead separation," *Journal of Colloid and Interface Science*, vol. 304, no. 2, pp. 535–540, Dec. 2006.

[2.16] M. Adachi, S. Tsukui, and K. Okuyama, "Nanoparticle Formation Mechanism in CVD Reactor with Ionization of Source Vapor," *Journal of Nanoparticle Research*, vol. 5, no. 1–2, pp. 31–37, Apr. 2003.

[2.17] R. Richards and H. Bönnemann, "Synthetic approaches to metallic nanomaterials," in Nanofabrication Towards Biomedical Applications: Techniques, Tools, Applications, and Impact, Wiley, Chapter 1 Jan 2005.

[2.18] M. Faraday, "The Bakerian Lecture: Experimental Relations of Gold (and Other Metals) to Light," *Phil. Trans. R. Soc. Lond.*, vol. 147, pp. 145–181, 1857.

[2.19] S. Kumar, K. S. Gandhi, and R. Kumar, "Modeling of Formation of Gold Nanoparticles by Citrate Method†," *Ind. Eng. Chem. Res.*, vol. 46, no. 10, pp. 3128–3136, May 2007.

[2.20] J. Turkevich, P. C. Stevenson, and J. Hillier, "A study of the nucleation and growth processes in the synthesis of colloidal gold," *Discuss. Faraday Soc.*, vol. 11, pp. 55–75, Jan. 1951.

[2.21] G. Frens, "Particle size and sol stability in metal colloids," *Kolloid-Zeitschrift und Zeitschrift für Polymere*, vol. 250, no. 7, pp. 736–741, Jul. 1972.

[2.22] K. Zabetakis, W. E. Ghann, S. Kumar, and M.-C. Daniel, "Effect of high gold salt concentrations on the size and polydispersity of gold nanoparticles prepared by an extended Turkevich–Frens method," *Gold Bulletin*, vol. 45, no. 4, pp. 203–211, 2012.

[2.23] M. Brust, M. Walker, D. Bethell, D. J. Schiffrin, and R. Whyman, "Synthesis of thiol-derivatised gold nanoparticles in a two-phase Liquid–Liquid system," *J. Chem. Soc., Chem. Commun.*, no. 7, pp. 801–802, Jan. 1994.

[2.24] A. H. Pakiari and Z. Jamshidi, "Nature and Strength of M−S Bonds (M = Au, Ag, and Cu) in Binary Alloy Gold Clusters," *J. Phys. Chem. A*, vol. 114, no. 34, pp. 9212–9221, Sep. 2010.

[2.25] H. Grönbeck, A. Curioni, and W. Andreoni, "Thiols and Disulfides on the Au(111) Surface: The Headgroup−Gold Interaction," *J. Am. Chem. Soc.*, vol. 122, no. 16, pp. 3839–3842, Apr. 2000.

[2.26] M.-C. Daniel and D. Astruc, "Gold Nanoparticles: Assembly, Supramolecular Chemistry, Quantum-Size-Related Properties, and Applications toward Biology, Catalysis, and Nanotechnology," *Chem. Rev.*, vol. 104, no. 1, pp. 293–346, Jan. 2004.

[2.27] A. Kumar, S. Mandal, S. P. Mathew, P. R. Selvakannan, A. B. Mandale, R. V. Chaudhari, and M. Sastry, "Benzene- and Anthracene-Mediated Assembly of Gold Nanoparticles at the Liquid−Liquid Interface," *Langmuir*, vol. 18, no. 17, pp. 6478–6483, Aug. 2002.

[2.28] M. Schulz-Dobrick, K. V. Sarathy, and M. Jansen, "Surfactant-Free Synthesis and Functionalization of Gold Nanoparticles," *J. Am. Chem. Soc.*, vol. 127, no. 37, pp. 12816–12817, Sep. 2005.

[2.29] N. Zheng, J. Fan, and G. D. Stucky, "One-Step One-Phase Synthesis of Monodisperse Noble-Metallic Nanoparticles and Their Colloidal Crystals," *J. Am. Chem. Soc.*, vol. 128, no. 20, pp. 6550–6551, May 2006.

[2.30] R. Sardar and J. S. Shumaker-Parry, "9-BBN Induced Synthesis of Nearly Monodisperse ω-Functionalized Alkylthiol Stabilized Gold Nanoparticles," *Chem. Mater.*, vol. 21, no. 7, pp. 1167–1169, Apr. 2009.

[2.31] H.-J. Butt, K. Graf, and M. Kappl, "Surfactants, Micelles, Emulsions, and Foams," in *Physics and Chemistry of Interfaces*, Wiley-VCH Verlag GmbH & Co. KGaA, 2003, pp. 246–279.

[2.32] Smoluchowski, Marian "Drei Vorträge über Diffusion, Brownsche Molekularbewegung und Koagulation von Kolloidteilchen". *Physik. Z.* (in German) **17**: 557–571, 585–599. 1916. Partly available in ref [2.29]

[2.33] Hitchon, B. Physical and Chemical Properties of Sediments and Bitumen from Some Alberta Oil Sands Deposits. *Open File Report 1993-25 Geochemical Studies*

[2.34] Kokal, S. "Crude Oil Emulsions: Everything You Wanted to Know but Were Afraid to Ask. Society of Petroleum Engineers" *Society of Petroleum Engineers*. SPE Distinguished lecture 2007/2008 published on 1rst January 2008

[2.35] Alajmi, A. F. F., Algharaib, M. K., & Gharbi, R. C. "Experimental Evaluation of Heavy Oil Recovery by Hot Water Injection in a Middle Eastern Reservoir". *Society of Petroleum Engineers*. (2009, January 1). doi:10.2118/120089-MS

[2.36] Laurier L. Schramm, "Petroleum Emulsions," in *Emulsions*, vol. 231, American Chemical Society, 1992, pp. 1–49.

[2.37] D. Lin "Water treatment complicates heavy oil production" *Oil & Gas Journal,* vol 97, issue 38, Sep 1999

[2.38] L. Xia, S. Lu, and G. Cao, "Stability and demulsification of emulsions stabilized by asphaltenes or resins," *J Colloid Interface Sci*, vol. 271, no. 2, pp. 504–506, Mar. 2004.

[2.39] X. R. Xu, J. Y. Yang, B. L. Zhang, and J. S. Gao, "Demulsification of Extra Heavy Crude Oil," *Petroleum Science and Technology*, vol. 25, no. 11, pp. 1375–1390, Nov. 2007.

[2.40] Y. H. Kim, D. T. Wasan, and P. J. Breen, "A study of dynamic interfacial mechanisms for demulsification of water-in-oil emulsions," *Colloids and Surfaces A: Physicochemical and Engineering Aspects*, vol. 95, no. 2–3, pp. 235–247, Feb. 1995.

[2.41] K. K. Salam, A. O. Alade, A. O. Arinkoola, and A. Opawale, "Improving the Demulsification Process of Heavy Crude Oil Emulsion through Blending with Diluent," *Journal of Petroleum Engineering*, vol. 2013, pp. 1–6, 2013.

[2.42] M. Kukizaki and M. Goto, "Demulsification of water-in-oil emulsions by permeation through Shirasu-porous-glass (SPG) membranes," *Journal of Membrane Science*, vol. 322, no. 1, pp. 196–203, Sep. 2008.

[2.43] N. M. Kocherginsky, C. L. Tan, and W. F. Lu, "Demulsification of water-in-oil emulsions via filtration through a hydrophilic polymer membrane," *Journal of Membrane Science*, vol. 220, no. 1–2, pp. 117–128, Aug. 2003.

[2.44] C. W. Angle, T. Dabros, and H. A. Hamza, "Demulsifier Effectiveness in Treating Heavy Oil Emulsion in the Presence of Fine Sands in the Production Fluids†," *Energy & Fuels*, vol. 21, no. 2, pp. 912–919, Mar. 2007.

[2.45] J. D. McLean and P. K. Kilpatrick, "Effects of asphaltene solvency on stability of water-in-crude-oil emulsions," *Journal of Colloid and Interface Science*, vol. 189, no. 2, pp. 242–253, 1997.

[2.46] X. Wu, "Investigating the Stability Mechanism of Water-in-Diluted Bitumen Emulsions through Isolation and Characterization of the Stabilizing Materials at the Interface," *Energy & Fuels*, vol. 17, no. 1, pp. 179–190, Jan. 2003.

[2.47] J. Czarnecki, P. Tchoukov, and T. Dabros, "Possible Role of Asphaltenes in the Stabilization of Water-in-Crude Oil Emulsions," *Energy & Fuels*, vol. 26, no. 9, pp. 5782–5786, Sep. 2012.

[2.48] J. P. Rane, V. Pauchard, A. Couzis, and S. Banerjee, "Interfacial Rheology of Asphaltenes at Oil–Water Interfaces and Interpretation of the Equation of State," *Langmuir*, vol. 29, no. 15, pp. 4750–4759, Apr. 2013.

[2.49] A. B. Andrews, A. McClelland, O. Korkeila, A. Demidov, A. Krummel, O. C. Mullins, and Z. Chen, "Molecular Orientation of Asphaltenes and PAH Model Compounds in Langmuir−Blodgett Films Using Sum Frequency Generation Spectroscopy," *Langmuir*, vol. 27, no. 10, pp. 6049–6058, May 2011.

[2.50] J. P. Rane, D. Harbottle, V. Pauchard, A. Couzis, and S. Banerjee, "Adsorption Kinetics of Asphaltenes at the Oil–Water Interface and Nanoaggregation in the Bulk," *Langmuir*, vol. 28, no. 26, pp. 9986–9995, Jul. 2012.

[2.51] Y. Xu, T. Dabros, H. Hamza, and W. Shefantook, "Destabilization of Water in Bitumen Emulsion by Washing with Water," *Petroleum Science and Technology*, vol. 17, no. 9–10, pp. 1051–1070, Oct. 1999.

[2.52] A. Bhardwaj and S. Hartland, "Dynamics of Emulsification and Demulsification of Water in Crude Oil Emulsions," *Ind. Eng. Chem. Res.*, vol. 33, no. 5, pp. 1271–1279, May 1994.

[2.53] M. Jeribi, B. Almir-Assad, D. Langevin, I. Hénaut, and J. F. Argillier, "Adsorption Kinetics of Asphaltenes at Liquid Interfaces," *Journal of Colloid and Interface Science*, vol. 256, no. 2, pp. 268–272, Dec. 2002.

[2.54] V. Pauchard, J. P. Rane, S. Zarkar, A. Couzis, and S. Banerjee, "Long-term adsorption kinetics of asphaltenes at the oil-water interface: a random sequential adsorption perspective," *Langmuir*, vol. 30, no. 28, pp. 8381–8390, Jul. 2014.

[2.55] O. A. Alomair and A. S. Almusallam, "Heavy Crude Oil Viscosity Reduction and the Impact of Asphaltene Precipitation," *Energy & Fuels*, vol. 27, no. 12, pp. 7267–7276, Dec. 2013.

[2.56] S. I. Andersen and E. I. Stenby, "Thermodynamics of Asphaltene Precipitation and Dissolution Investigation of Temperature and Solvent Effects," *Fuel Science and Technology International*, vol. 14, no. 1–2, pp. 261–287, Jan. 1996.

[2.57] K. Nikooyeh "Phase behavior of asphaltenes in organic media," Published Ph.D. thesis University of Alberta, 2012.

[2.58] G. Andreatta, C. C. Goncalves, G. Buffin, N. Bostrom, C. M. Quintella, F. Arteaga-Larios, E. Pérez, and O. C. Mullins, "Nanoaggregates and Structure−Function Relations in Asphaltenes†," *Energy & Fuels*, vol. 19, no. 4, pp. 1282–1289, Jul. 2005.

[2.59] A. A. Lamia Goual, "Predicting the Adsorption of Asphaltenes from Their Electrical Conductivity," *Energy & Fuels*, vol. 24, no. 1, 2009.

[2.60] O. C. Mullins, H. Sabbah, J. Eyssautier, A. E. Pomerantz, L. Barré, A. B. Andrews, Y. Ruiz-Morales, F. Mostowfi, R. McFarlane, L. Goual, R. Lepkowicz, T. Cooper, J. Orbulescu, R. M. Leblanc, J. Edwards, and R. N. Zare, "Advances in Asphaltene Science and the Yen–Mullins Model," *Energy & Fuels*, vol. 26, no. 7, pp. 3986–4003, Jul. 2012.

[2.61] O. C. Mullins, "The Modified Yen Model†," *Energy & Fuels*, vol. 24, no. 4, pp. 2179–2207, 2010.

[2.62] S. Verdier, F. Plantier, D. Bessières, S. I. Andersen, E. H. Stenby, and H. Carrier, "Study of Asphaltene Precipitation by Calorimetry," *Energy & Fuels*, vol. 21, no. 6, pp. 3583–3587, Nov. 2007.

[2.63] D. Merino-Garcia and S. I. Andersen, "Application of Isothermal Titration Calorimetry in the Investigation of Asphaltene Association," in *Asphaltenes, Heavy Oils, and Petroleomics*, O. C. Mullins, E. Y. Sheu, A. Hammami, and A. G. Marshall, Eds. Springer New York, 2007, pp. 329–352.

[2.64] S. I. Andersen and S. D. Christensen, "The Critical Micelle Concentration of Asphaltenes As Measured by Calorimetry," *Energy & Fuels*, vol. 14, no. 1, pp. 38–42, Jan. 2000.

[2.65] Y. Zhang, T. Takanohashi, S. Sato, T. Kondo, I. Saito, and R. Tanaka, "Dissolution and Dilution of Asphaltenes in Organic Solvents," *Energy & Fuels*, vol. 17, no. 1, pp. 101–106, Jan. 2003.

[2.66] K. Nikooyeh and J. M. Shaw, "On Enthalpies of Solution of Athabasca Pentane Asphaltenes and Asphaltene Fractions," *Energy & Fuels*, vol. 27, no. 1, pp. 66–74, Jan. 2013.

[2.67] K. Nikooyeh, S. R. Bagheri, and J. M. Shaw, "Interactions Between Athabasca Pentane Asphaltenes and n-Alkanes at Low Concentrations," *Energy & Fuels*, vol. 26, no. 3, pp. 1756–1766, Mar. 2012.

Chapter 3

[3.1] U. Bergmann, O. C. Mullins, and S. P. Cramer, "X-ray Raman Spectroscopy of Carbon in Asphaltene: Light Element Characterization with Bulk Sensitivity," *Anal. Chem.*, vol. 72, no. 11, pp. 2609–2612, Jun. 2000.

[3.2] R. C. Silva, P. R. Seidl, S. M. C. Menezes, and M. A. G. Teixeira, "1H and 13 C NMR for Determining Average Molecular Parameters of Asphaltene from Vacuum Residue Distillation," *Ann. Magn. Reson*, vol. 3, pp. 63–67, 2004.

[3.3] S. Mitra-Kirtley, O. C. Mullins, J. Van Elp, S. J. George, J. Chen, and S. P. Cramer, "Determination of the nitrogen chemical structures in petroleum asphaltenes using XANES spectroscopy," *Journal of the American Chemical society*, vol. 115, no. 1, pp. 252–258, 1993.

[3.4] B. Bennett and G. D. Love, "Release of organic nitrogen compounds from Kerogen via catalytic hydropyrolysis," *Geochemical Transactions*, vol. 1, no. 1, p. 61, Dec. 2000.

[3.5] G. S. Waldo, R. M. K. Carlson, J. M. Moldowan, K. E. Peters, and J. E. Penner-hahn, "Sulfur speciation in heavy petroleums: Information from X-ray absorption near-edge structure," *Geochimica et Cosmochimica Acta*, vol. 55, no. 3, pp. 801–814, Mar. 1991.

[3.6]A. E. Pomerantz, D. J. Seifert, K. D. Bake, P. R. Craddock, O. C. Mullins, B. G. Kodalen, S. Mitra-Kirtley, and T. B. Bolin, "Sulfur Chemistry of Asphaltenes from a Highly Compositionally Graded Oil Column," *Energy & Fuels*, vol. 27, no. 8, pp. 4604–4608, Aug. 2013.

[3.7] M. A. Desando and J. A. Ripmeester, "Chemical derivatization of Athabasca oil sand asphaltene for analysis of hydroxyl and carboxyl groups via nuclear magnetic resonance spectroscopy," *Fuel*, vol. 81, no. 10, pp. 1305–1319, Jul. 2002.

[3.8] S. E. Moschopedis and J. G. Speight, "Oxygen functions in asphaltenes," *Fuel*, vol. 55, no. 4, pp. 334–336, Oct. 1976.

[3.9] P. I. Premović, T. Allard, N. D. Nikolić, I. R. Tonsa, and M. S. Pavlović, "Estimation of vanadyl porphyrin concentration in sedimentary kerogens and asphaltenes," *Fuel*, vol. 79, no. 7, pp. 813–819, May 2000.

[3.10] G. P. Dechaine, "Solubility and diffusion of vanadium compounds and asphaltene

aggregates," Published Ph.D Thesis, University of Alberta, 2010.

[3.11] O. C. Mullins, "The Modified Yen Model" *Energy & Fuels*, vol. 24, no. 4, pp. 2179–2207, 2010

[3.12] N. Zheng, J. Fan, and G. D. Stucky, "One-Step One-Phase Synthesis of Monodisperse Noble-Metallic Nanoparticles and Their Colloidal Crystals," *J. Am. Chem. Soc.*, vol. 128, no. 20, pp. 6550–6551, May 2006.

[3.13] M. Schulz-Dobrick, K. V. Sarathy, and M. Jansen, "Surfactant-Free Synthesis and Functionalization of Gold Nanoparticles," *J. Am. Chem. Soc.*, vol. 127, no. 37, pp. 12816–12817, Sep. 2005.

[3.14] R. Sardar and J. S. Shumaker-Parry, "9-BBN Induced Synthesis of Nearly Monodisperse ω-Functionalized Alkylthiol Stabilized Gold Nanoparticles," *Chem. Mater.*, vol. 21, no. 7, pp. 1167–1169, Apr. 2009.

[3.15] P. M. Shem, R. Sardar, and J. S. Shumaker-Parry, "One-Step Synthesis of Phosphine-Stabilized Gold Nanoparticles Using the Mild Reducing Agent 9-BBN," *Langmuir*, vol. 25, no. 23, pp. 13279–13283, Dec. 2009.

[3.16] G. H. Woehrle, L. O. Brown, and J. E. Hutchison, "Thiol-Functionalized, 1.5-nm Gold Nanoparticles through Ligand Exchange Reactions: Scope and Mechanism of Ligand Exchange," *J. Am. Chem. Soc.*, vol. 127, no. 7, pp. 2172–2183, Feb. 2005.

[3.17] S. Eustis and M. A. El-Sayed, "Why gold nanoparticles are more precious than pretty gold: Noble metal surface plasmon resonance and its enhancement of the radiative and nonradiative properties of nanocrystals of different shapes," *Chem. Soc. Rev.*, vol. 35, no. 3, pp. 209–217, Feb. 2006.

[3.18] IFT Ramé-Mart Goniometer manual http://folk.uio.no/fhansen/dropbroc.html

Chapter 4

[4.1] S. K. Ghosh and T. Pal, "Interparticle Coupling Effect on the Surface Plasmon Resonance of Gold Nanoparticles: From Theory to Applications," *Chem. Rev.*, vol. 107, no. 11, pp. 4797–4862, Nov. 2007.

[4.2] K. Nikooyeh and J. M. Shaw, "On Enthalpies of Solution of Athabasca Pentane Asphaltenes and Asphaltene Fractions," *Energy & Fuels*, vol. 27, no. 1, pp. 66–74, Jan. 2013.

Chapter 5

[5.1] K. Nikooyeh "Phase behavior of asphaltenes in organic media," Published Ph.D thesis University of Alberta, 2012.

Appendices

A) Data Tables

Table 6.1: Enthalpies of solution of gold core nanoparticles and asphaltenes in diverse solvents at 25°C in mJ/mg. (+/- 1mJ/mg)

	Gold-$C_{8/12}$		Gold-OH	Gold-Ar	Asphaltenes
Toluene	2.3	0.7	0.5	0.4	7.9
Heptane	1.7	-0.3	0.5	-0.2	2.6
Pyridine	1.4	0.9	1.3	-1	7.3
Water	0.4	1.2	2.3	1	-1.5
Ethanol	0.8	/	1.7	1.8	1.5

Table 6.2: Enthalpies of solution of gold core nanoparticles and asphaltenes in diverse solvents at 60°C in mg/mJ. (+/- 1mg/mJ)

	Gold-C_8	Gold-OH	Gold-Ar	Asphaltenes
Toluene	6.2	8.3	/	10.4
Heptane	8.5	22	/	4.7
Pyridine	2.8	-1.6	/	10.1
Water	-1.9	4	/	-1.3
Ethanol	/	/	/	/

B) Interfacial tension measurements for of (methanol+Gold-OH) in dodecane

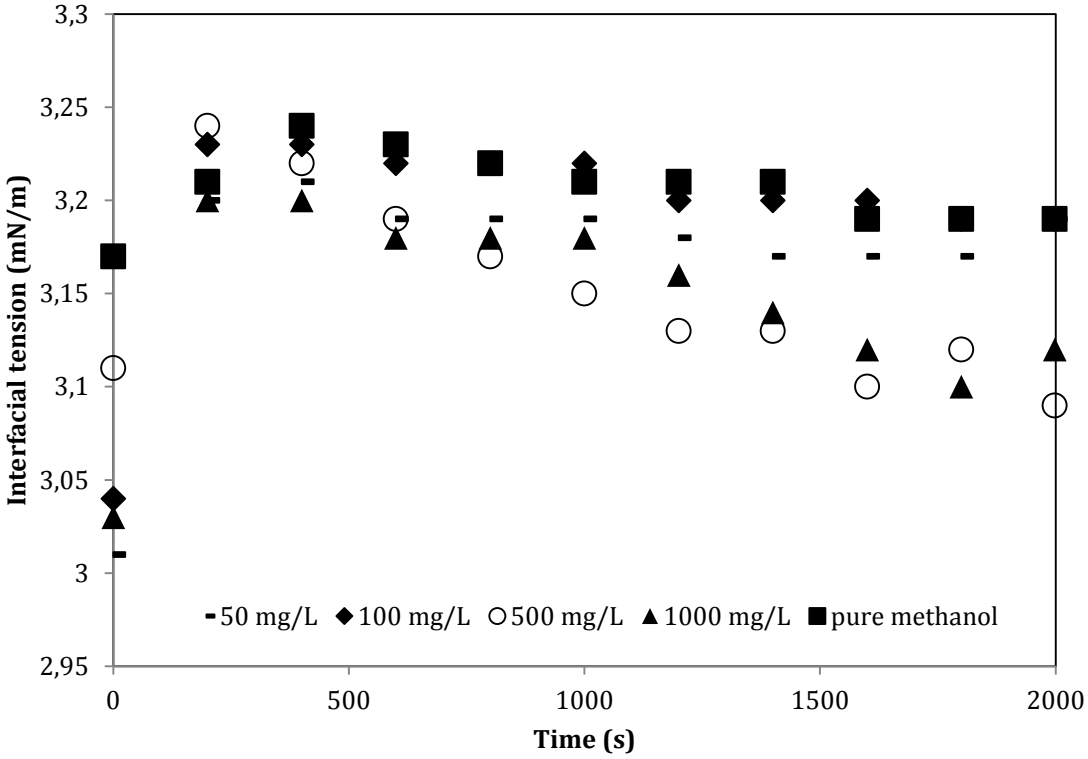

Figure 6.1: Interfacial tension of dodecane + (methanol + gold-OH nanoparticle) mixtures at 23°C and atmospheric pressure. Nanoparticle concentration is a parameter. All measurements are within the error margins of +/- 1.25mN/m